CHALMERS
UNIVERSITY OF TECHNOLOGY

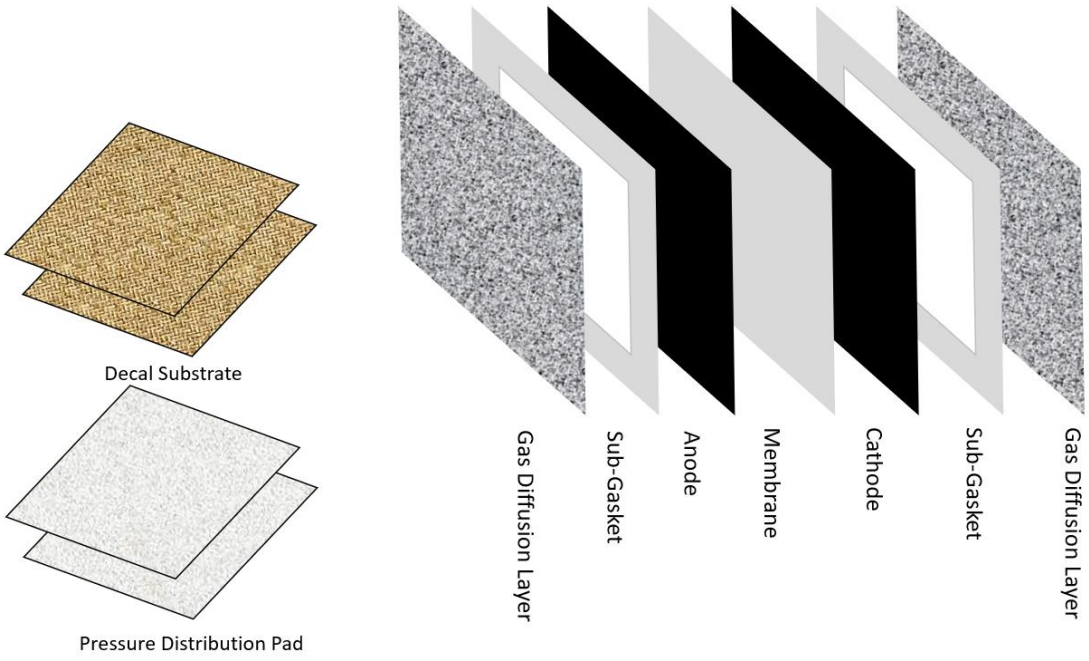

Exploring the process design and parameters for a fuel cell membrane electrode assembly by decal transfer

Master's thesis in Innovative and Sustainable Chemical Engineering

Dylan Schulz

DEPARTMENT OF PHYSCIS
CHALMERS UNIVERSITY OF TECHNOLOGY

Gothenburg, Sweden 2023
www.chalmers.se

Abstract

Proton exchange membrane fuel cells (PEM FCs) are a promising key component in a renewable energy infrastructure. At their heart is the membrane electrode assembly (MEA), where both the hydrogen oxidation and oxygen reduction reactions occur. Decal transfer is an effective method for fabricating MEAs, as it is highly scalable and noted for its low interfacial resistance. In this thesis, the main processing parameters for the decal transfer – temperature, pressure and transfer time – are varied to explore the parameter space available for MEA production. Based on these results, in-situ performance tests using polarization curves and high frequency resistance (HFR) measurements are performed in a 2^k experiment matrix to study the effects of these parameters on the MEA performance. Further experiments are conducted for different proton exchange membranes and for in-house produced cathodes to understand the effects of these materials on the performance and processing parameter space. Further studies are performed to explore the glass transition temperatures of the membranes, to understand the real temperature profiles of the MEA during the transfer, and to explore the morphological changes undergone by the electrode during transfer. The results of this thesis most notably illustrate the sets of parameters that can result in a good transfer, demonstrate the effects of these parameters on the transfer quality and MEA performance.

Acknowledgements

No project of significance is undertaken alone, and this thesis is no exception. I would like to take this opportunity to thank those who have helped me during my thesis.

At PowerCell, Parinaz Mikaeili has been a wonderful supervisor, helping me with everything from using equipment to discussing experiment designs and results. Gabor Toth has been instrumental in understanding results and helped me to learn about theory and how to evaluate measurements. Lukas Hansen and Kalle Genheden enabled me to conduct the performance measurements integral to this thesis. Felix Ernst and Marika Männikkö helped me with the onboarding and getting to know the lab, equipment and transfer process in the first stages of my thesis. Emma Ulberstad helped me with the preparation of in-house electrodes for my experiments.

At Chalmers, Björn Wickman, my examiner, facilitated all contact with the university and helped connect me to colleagues with a DSC machine. These colleagues are Jan Svensson and Mikael Käll, without whom I could not have obtained glass transition temperature measurements for my membranes.

A huge thanks goes to all these wonderful people, without whom I could not have achieved nearly as much in my thesis.

List of Figures

List of Tables

Abbreviations

CCM	Catalyst coated membrane
DSC	Differential scanning calorimetry
ECSA	Effective catalyst surface area
EIS	Electrochemical impedance spectroscopy
FC	Fuel cell
GDL	Gas diffusion layer
HC	Hydrocarbon
HFR	High frequency resistance
LSC	Long side chain
MEA	Membrane electrode assembly
MPL	Microporous layer
MSC	Medium side chain
OCV	Open circuit voltage
PEM	Proton exchange membrane / polymer electrolyte membrane
PFSA	Perfluorosulfonic acid
SSC	Short side chain
Tg	Glass transition temperature

Symbols and Operators

Symbol	Description	Units
$\dot{Q}$	Heat flux	W
$\dot{q}$	Specific heat flux	W/m^2
m	Mass	kg
c_p	Specific heat capacity	J/kgK
T	Temperature	K, °C
A	Area	m^2
R_t	Thermal resistance	W/K
k_i	Thermal conductivity of a material	W/mK
l	Length	m
Δ	Difference operator, eg. ΔT	
I/Pt	Ratio of ionomer to (platinum) catalyst	
C/Pt	Ratio of carbon to (platinum catalyst	
σ	Standard deviation	

Contents

1 Introduction

Climate change stands as one of the greatest challenges facing human civilization in the 21st century. According to the Intergovernmental Panel on Climate Change (IPCC)'s sixth assessment report, human activities have already caused a 1.1 °C increase in global surface temperatures from pre-20th-century levels, emphasizing the urgent need to secure a livable and sustainable future [1]. Unsustainable energy use, a key driver of climate change, continues to persist, with energy demand projected to grow as economies develop [2]. Additionally, the finite nature of fossil fuel resources necessitates the adoption of alternative technologies well before depletion occurs. Hence, renewable energy sources play a critical role not only in preserving favorable climatic conditions but also in enabling future economic prosperity. Efficient energy storage solutions are essential due to the intermittent nature of many renewables, and hydrogen holds significant promise in this regard. It can be produced through electrolysis, stored, and converted back to energy via fuel cells, offering advantages in mobility, scalability, and grid regulation potential.

The concept of a hydrogen-powered future has captivated the imagination for decades. As far back as 1874, Jules Verne envisioned in his book The Mysterious Island that water could serve as a fuel source, with hydrogen and oxygen providing an inexhaustible source of heat and light [3]. Verne's visionary ideas about hydrogen as a fuel source are particularly relevant today as we explore the potential of hydrogen-powered technologies. Despite this longstanding fascination, the availability and production of hydrogen have posed significant challenges. However, with the increasing scale of renewable power generation, the feasibility of periods with abundant and inexpensive energy for electrolysis is becoming more attainable.

Proton exchange membrane fuel cells (PEM FCs) have emerged as a promising technology for achieving high-efficiency, low-emission energy conversion, particularly in decentralized and mobile applications such as vehicles. At the heart of PEM FCs lies the membrane electrode assembly (MEA), where the hydrogen oxidation and oxygen reduction reactions occur. The two main methods of MEA production are by direct coating of a catalyst ink onto a PEM, and by decal transfer where the electrode is coated onto a decal substrate as a carrier and then transferred onto the membrane. This thesis aims to address the crucial aspects of MEA production by decal transfer by systematically investigating the effects of temperature, pressure, and transfer time on MEA performance. Through a comprehensive experimental approach, the transfer quality will be evaluated across a range of processing parameters, and in-situ performance tests will be conducted using a 2k experiment matrix. By elucidating the impact of these processing parameters, valuable insights can be gained into the electrochemical performance of the resulting MEAs. Furthermore, this research explores the influence of different proton exchange membranes and in-house produced cathodes on MEA performance and processing parameter space. Supplementary experiments will shed light on the effects of these materials on the overall performance of PEM FCs. Attention is also devoted to understanding the glass transition temperatures of the membranes and the real temperature profiles experienced by the MEAs during the transfer process. These investigations provide a foundation for optimizing the transfer process and offer insights into the morphological changes occurring within the electrode.

Chapter 2 will discuss the background of this thesis, including analytic methods and relevant materials. Chapter 3 will discuss glass transition temperature measurements made for different membranes. Chapter 4 will describe the decal transfer process, including modifications made during this thesis as well as a novel 'series stacking' approach which promises greatly increased production capacity. Chapter 5 discusses the temperature driven annealing behavior of electrodes observed during the

decal transfer. Chapter 6 describes the observed set of parameters available for a complete transfer to occur for different materials. Chapter 7 shows and discussed the in-situ performance measurements made in this thesis for MEAs produced with different processing parameters and materials. Chapter 8 provides a conclusion to the thesis, and chapter 9 provides an outlook based on the results and conclusions from this thesis and further ideas that merit investigation.

The findings obtained from this study contribute to advancing MEA production knowledge, specifically focusing on the effects of processing parameters and materials on the performance of PEM FCs through decal transfer. The insights gained from exploring the parameter space, investigating glass transition temperatures, temperature profiles, and morphological changes hold the potential to inform future optimization strategies. As this research progresses, advancements in catalyst and MEA production may be achieved, potentially enhancing PowerCell's in-house capabilities. Furthermore, these findings have broader implications for the academic and renewable energy communities, offering valuable insights towards the development of more efficient and sustainable energy solutions.

2 Background

This section describes in brief the technical background of fuel cells and membrane electrode assemblies, as well as the situation at PowerCell that is the impetus for this thesis.

2.1 Proton Exchange Membrane Fuel Cells (PEM FC)

Polymer Electrolyte Membrane Fuel Cells (PEM FC) have long been among the most promising if challenging energy systems to be developed. They represent a clean energy storage system with the potential for indefinite scalability. While several fuels, including syngas, methanol and biogas, can be considered for use in fuel cells, and each presents its own challenges, hydrogen/air is the most widely developed fuel source mixture. This includes the research at PowerCell. The chemical reactions in a hydrogen fuel cell can be broken down into two half-cell redox reactions:

Anode (oxidation): $2\,H_2 \rightarrow 4\,H^+ + 4\,e^-$

Cathode (reduction): $4\,H^+ + 4\,e^- + O_2 \rightarrow 2\,H_2O$

Figure 1 shows the schematic operation of a hydrogen PEM FC. Hydrogen gas flows via a gas diffusion layer to the anode, where the oxidation reaction occurs. Hydrogen ions flow through the polymer electrolyte to the cathode, while electrons pass through a load, giving electrical power, before flowing to the cathode. Oxygen flows through a gas diffusion layer to the cathode, where together with the electrons and hydrogen ions it forms water, which flows out of the cell.

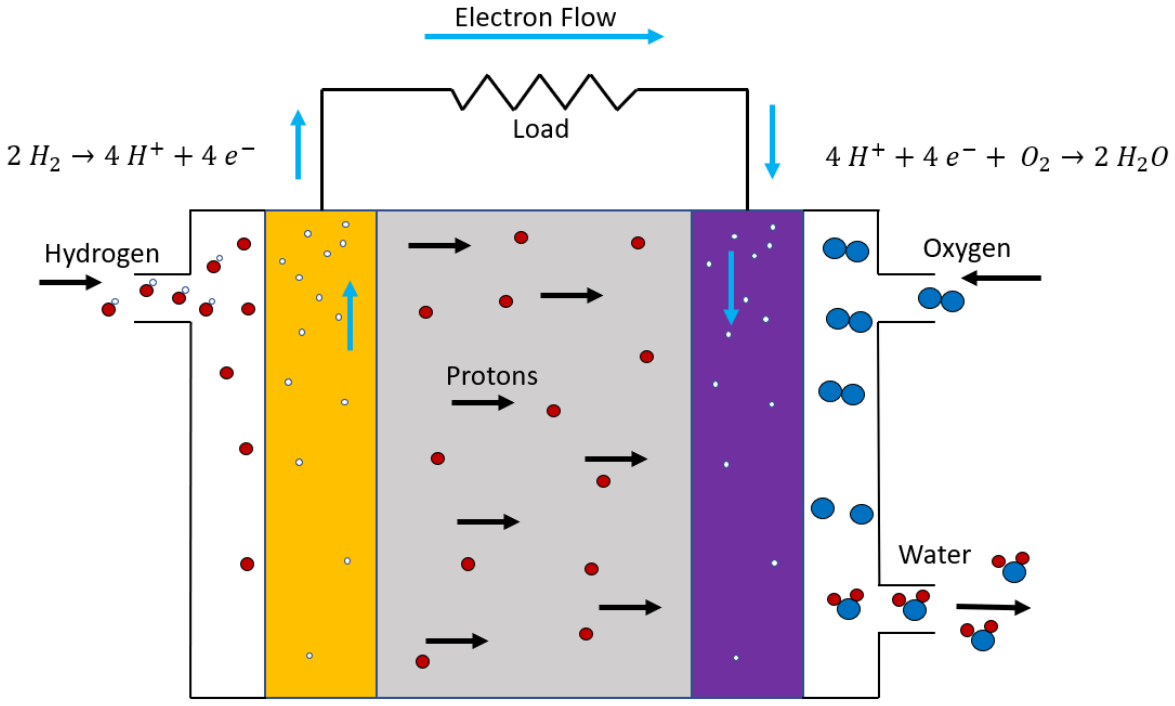

Figure 1: Schematic diagram of a PEM FC.

2.2 The Membrane Electrode Assembly (MEA)

The heart of the fuel cell is the membrane electrode assembly (MEA). This is where the cell reactions and mass transport all take place in a fuel cell, and an MEA design needs to carefully balance the needs of mass transport to the electrodes, mass transport to the membrane and within the membrane, electrical conductivity to the electrodes, electrical resistance between the electrodes, catalyst availability, degradation resistance, mechanical stability and so on.

In this work, an MEA refers to an anode, membrane and cathode assembly. This is a 3-layer MEA, as opposed to a 5-layer MEA which has additional sub gaskets, or a 7-layer MEA which also has gas diffusion layers added on either side (Figure 2).

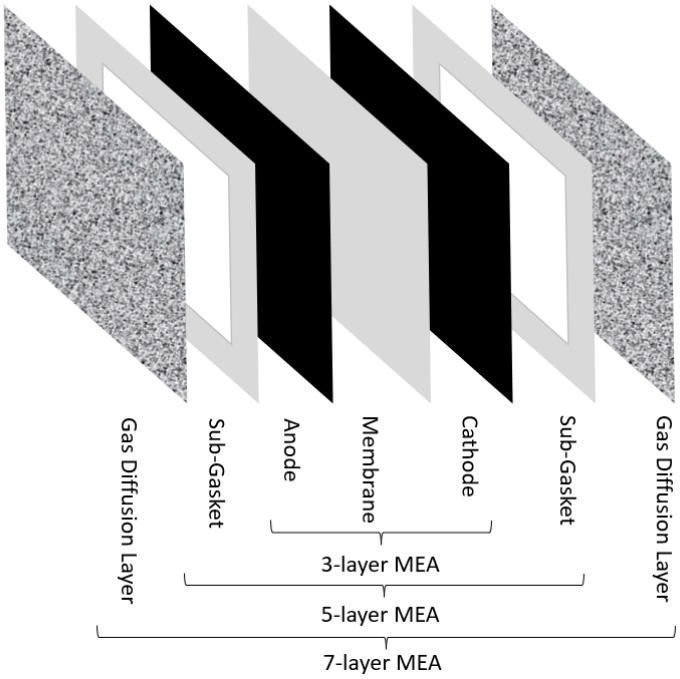

Figure 2: Schematic overview of 3-, 5- and 7-layer MEAs.

The MEAs at PowerCell are prepared using a decal transfer procedure. In this method, electrodes are prepared by spreading an electrode ink onto a decal substrate, which functions as an easily removable carrier material. The anode, membrane and cathode are then laminated together under controlled temperature, pressure and time. This method is one of the most common for preparing MEAs and is particularly interesting for its potential to be scaled up as a roll-to-roll process. Another major method of MEA fabrication is to directly coat catalyst ink onto the membrane; however, that will not be focused on in this thesis.

2.3 Significance to PowerCell

PowerCell wishes to produce the MEAs needed for the company's fuel cell products in-house via a decal transfer hot pressing method. The company primarily intends to use in-house electrodes for this process. Previous work at PowerCell by S. A. Ogu-Egege [4] has established a general method for producing these MEAs, but little work has been done to explore the process parameters, particularly pressure, temperature and time in the hot-pressing stage. In addition, it is critical that proper design of the hot-pressing step is understood for different materials. New membrane ionomers such as hydrocarbon PEMs present new opportunities for performance and 'tunability' that need to be explored, as well as presenting the chance to move away from fluorinated ionomers. This requires increased understanding of the MEA assembly procedure. Furthermore, the company aims to produce fuel cells for the aviation sector, which requires the use of catalysts with very high loadings. Exploring the assembly process for such catalysts is therefore of enormous and immediate importance to PowerCell.

2.4 Analysis Methods and Conditions

It is important to describe what means of evaluation are used and what information they can deliver. Different means of evaluation have different strengths and different purposes, ranging from quick and simple methods to more in-depth methods capable of providing large amounts of detailed information.

2.4.1 Visual Inspection

A direct, visual inspection is among the most useful and undervalued analysis methods. It is particularly useful as a means of quality control and as a preliminary observation of results. It is notably useful for inspecting electrodes, especially in conjunction with backlighting via a light board, to determine the quality and consistency of the coating as well as the location of defects and damaged areas where a coating is not useable. A visual inspection of an assembled MEA is useful for identifying defects such as pinholes where light can shine through, and the removed decals can be analyzed to ascertain the completeness of the transfer. When laminating sub gaskets onto a 3-layer MEA, a visual inspection allows for the early detection of leaks that may make the MEA unusable. In chapter 6, visual inspection is the primary means by which the quality of the transfer is evaluated.

2.4.2 Differential Scanning Calorimetry

Differential Scanning Calorimetry (DSC) is done by slowly heating a small sample of a substance and measuring the heat flux through the sample as a function of temperature, relative to a known reference. Here, DSC is performed with samples of 10 ±1 mg in sealed aluminum pans under a nitrogen atmosphere at a temperature increase rate of 10 K/min, in order to evaluate the glass transition temperatures of polymer electrolyte membranes. The glass transition temperature can be seen graphically in the DSC by way of a diagram of specific heat flux versus temperature, where the curve experiences a decrease [5]. In this thesis, the midpoint glass transition temperature is used. An example of a DSC curve is shown in Figure 3.

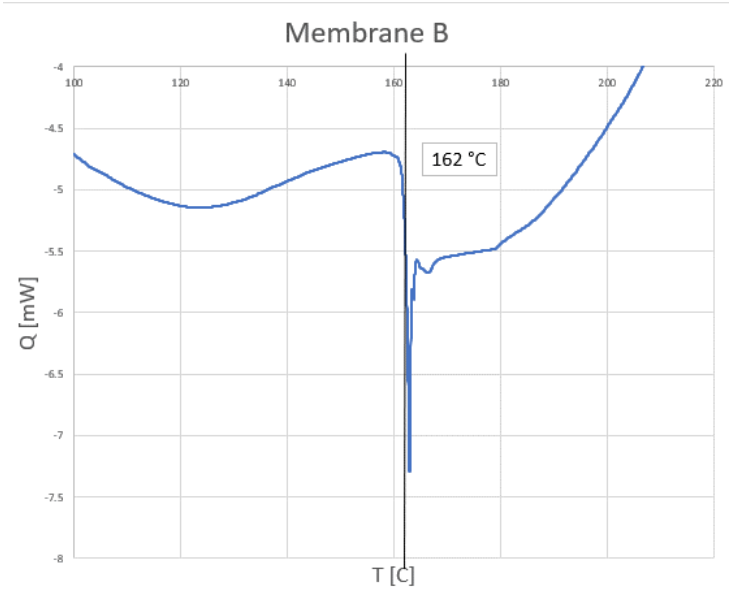

Figure 3: Example of a DSC graph for measuring the glass transition temperature of a membrane.

2.4.3 In-Situ Testing Conditions

The resistance properties of the MEA are measured in-situ using a single cell testing approach. An MEA is prepared and placed into the testing setup. Figure 4 shows the circuit diagram for in-situ testing. The setup is current controlled at the load bank, and the voltage is measured directly from the bipolar plates. The hydrogen and air flow within the cell is in excess of the reaction stoichiometry. In-situ tests in this thesis are done as 12 cm^2 subscale tests under normal operating conditions (NOC) with a cell temperature of 65 °C and 60 % relative humidity. The reactant inflow is in excess of the required reaction stoichiometry by a factor of 12.5 and 15 at the anode and cathode respectively.

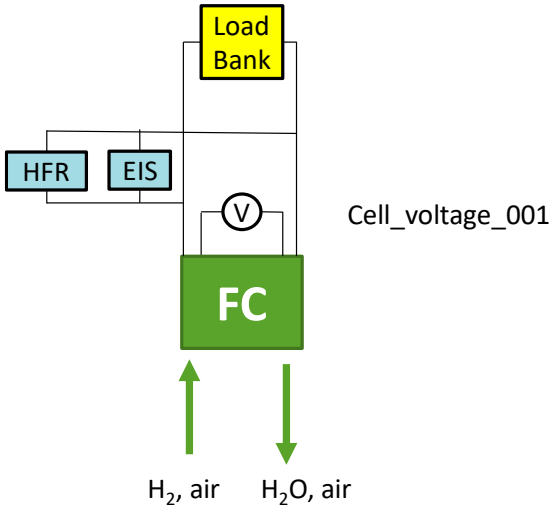

Figure 4: General circuit diagram for in-situ subscale testing.

2.4.4 Conditioning Data

Before in-situ testing, the MEA must be conditioned, as the membrane and catalyst ionomer is not fully hydrated. This is done by operating the fuel cell for up to 12 hours under a constant current of 1.5 A/cm^2 at a high relative humidity of 80%, during which the water generated by the reaction activates the ionomer. The resulting voltage graph gives information on the water uptake of the membrane from the slope of the voltage curve in the beginning once constant current has been reached. Some information on the MEA interface can be read from the final, stable voltage and HFR. Should these values not reach a constant value, this can indicate a malfunction of the MEA or a minor leak in the membrane. The conditioning data is especially useful for such troubleshooting.

Figure 5 shows the conditioning data for a well-functioning MEA, while Figure 6 shows the conditioning data for a poorly functioning MEA. The poorly functioning MEA shows a decreasing voltage and an increasing resistance while the well-functioning MEA shows the opposite; moreover the poorly functioning MEA also fails to reach a constant steady value. It is likely that a fiber from the GDL or something similar caused damage to the membrane.

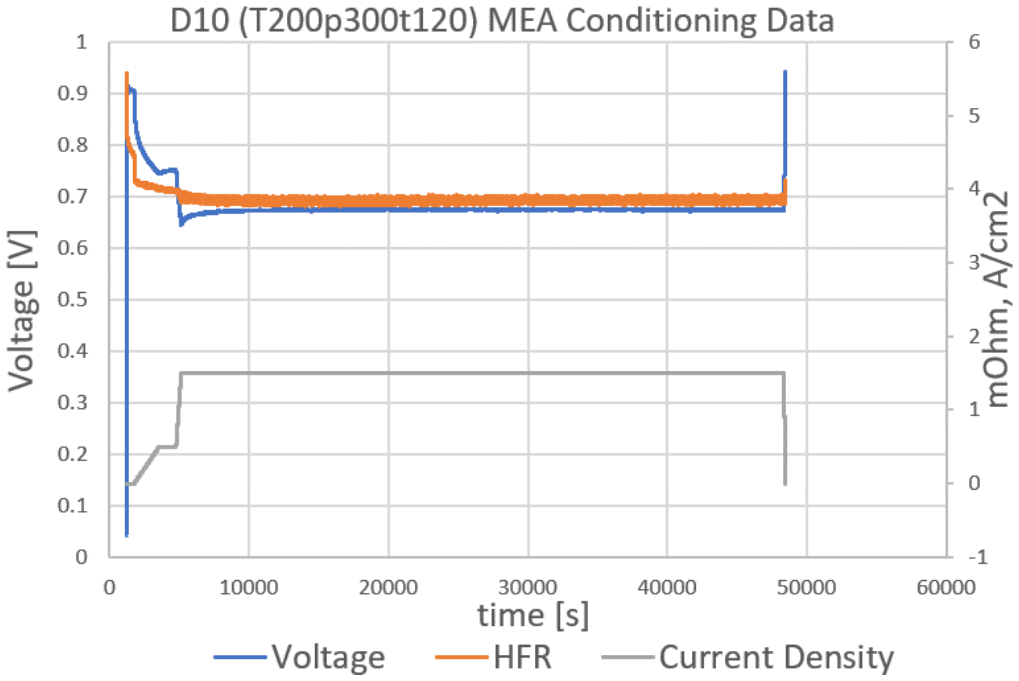

Figure 5: Example of conditioning data for a well-functioning MEA, from MEA D10 manufactured under T=200C and p=300 N/cm2 for t=300 s

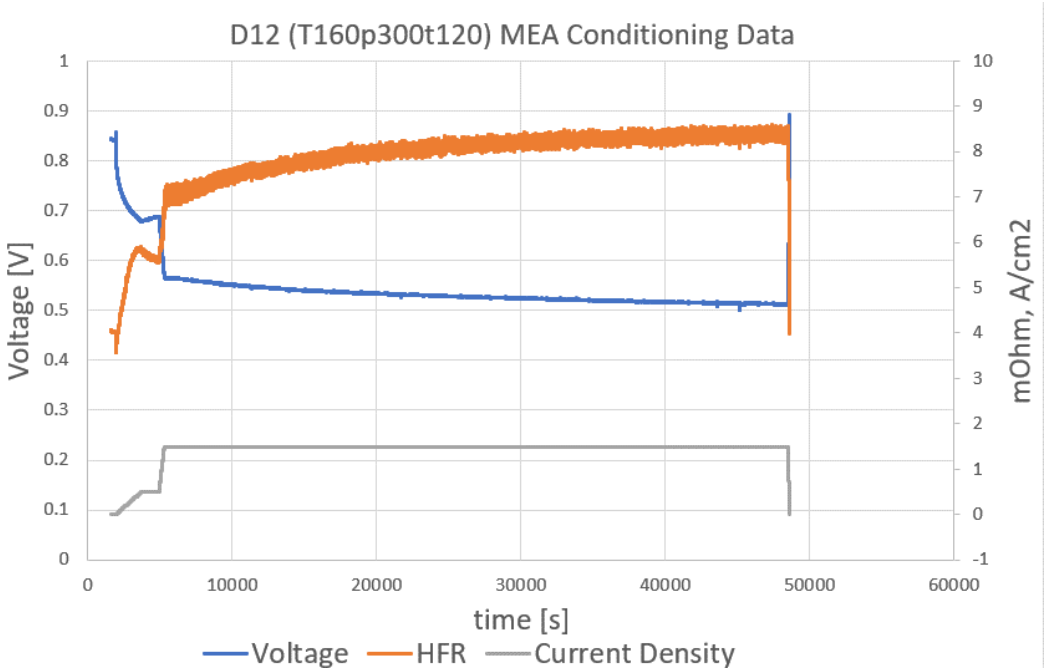

Figure 6: Example of conditioning data for a poorly functioning MEA, from MEA D12 manufactured under T=160C and p=300 N/cm2 for t=300 s.

2.4.5 Polarization Curve

The polarization curve of a fuel cell is obtained by measuring the voltage of the cell while varying the current density. It can be divided into three regions, where kinetic, ohmic and mass transport effects are respectively dominant. Also significant is the open circuit voltage (OCV) of the fuel cell. A polarization curve with the kinetic, ohmic and mass transport dominated regions marked is shown in Figure 7.

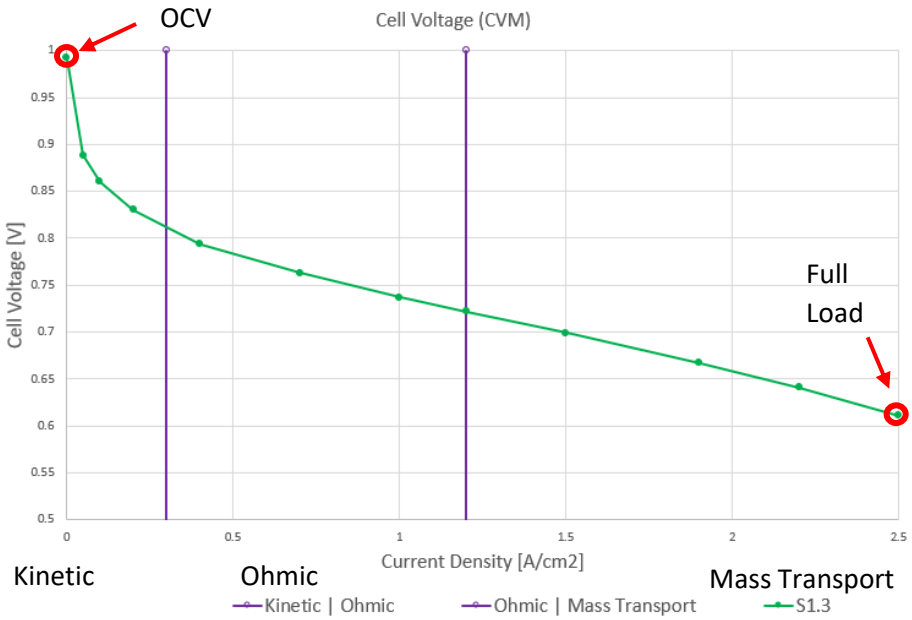

Figure 7: Example of a polarization curve with the OCV and the kinetic, ohmic and mass transport regions marked.

The theoretical OCV of a fuel cell, given from the electrochemical potentials of hydrogen and oxygen, is 1.23 V; however, since no fuel cell is perfectly tight and some hydrogen crossover diffusion always occurs, this value cannot be reached in practice and the OCV of a well performing fuel cell using hydrogen and air as fuel is generally around 0.9 to 1.0 V. An OCV below 0.9 indicates a 'tightness' issue in the MEA with a greater amount of fuel crossover. An OCV below 0.8 generally indicates a hole in the membrane.

In the kinetic region of the fuel cell, losses are dominated by reaction kinetics. Specifically, the oxygen reduction at the cathode is dominant, as the hydrogen oxidation reaction at the anode is very fast. This is also the reason why the cathode generally has a higher catalyst loading than the anode in a fuel cell. Of particular interest is the 'kinetic point' at 0.1 A/cm^2, as this provides information on the reaction kinetics and the effective catalyst surface area (ECSA). The main information here is about the catalyst behavior rather than the interfaces between PEM and electrodes.

The losses in the ohmic region are dominated by resistance effects to the flow of charged species during the reaction. Generally, the resistance to the flow of electrons is negligible compared to the resistance to the flow of protons due to the large difference in mass and mobility between the two. It is thus the ionic conductivity of the protons in the electrodes and membrane as well the resistance at the interfaces between the membrane and the electrodes that are significant here, meaning that the PEM and interface dominate this region. If the PEM is the same between two tests, then the interface dominates any differences, and the interface is determined by the decal transfer conditions. To analyze the ohmic region, polarization curves can be normalized in the kinetic point, i.e. shifted so that the kinetic points overlap. The quasi-linear slope in the ohmic region is of particular interest as it provides information about the cell resistance, which is strongly affected by the MEA transfer conditions.

In the mass transport region, the current density is so high that mass transport within the cell becomes the limiting factor. It is common in this region that not enough reactant can be supplied to the electrodes – mainly to the cathode, since hydrogen diffusion is very fast - through normal background diffusion from the bulk gas phase. This results in a concentration gradient as the transport of the reactant species becomes a significant source of resistance. When comparing the mass transport regions of two polarization curves, the degree of divergence is of note alongside the full-load point at 2.5 A/cm^2. For a well-functioning MEA, this point should be at or above 0.6 V.

2.4.6 High Frequency Resistance (HFR) and Electrochemical Impedance Spectroscopy (EIS)

High frequency resistance is measured by applying a perturbation current of at least 1 kHz to the fuel cell and measuring the resulting resistance. Because many resistance sources are frequency dependent [6], the HFR value ignores most resistance sources and (in the ohmic region) mainly shows the ion conduction resistance through the electrodes, membrane and at the interfaces [7]. HFR is particularly useful because it can be performed continuously throughout the testing without interfering in other measurements or operations. It can also provide information about the hydration of the membrane during conditioning, as the hydration state of the membrane is a significant contributor to the ionic resistance in the PEM.

Electrochemical impedance spectroscopy (EIS) obtains a complex resistance from the fuel cell by inducing a sinusoidal perturbation and measuring the phase shift delay of the response [8]. This

complex resistance is measured across a spectrum of different frequencies, forming a Nyquist plot (Figure 8). In this thesis, the real component of the EIS is desired, and so EIS resistance values are taken as the Y-axis intercept of the Nyquist plot. This is considered a very high-accuracy method of obtaining the internal resistance of the fuel cell, as any remaining complex portion of the resistance that may remain in the HFR is resolved.

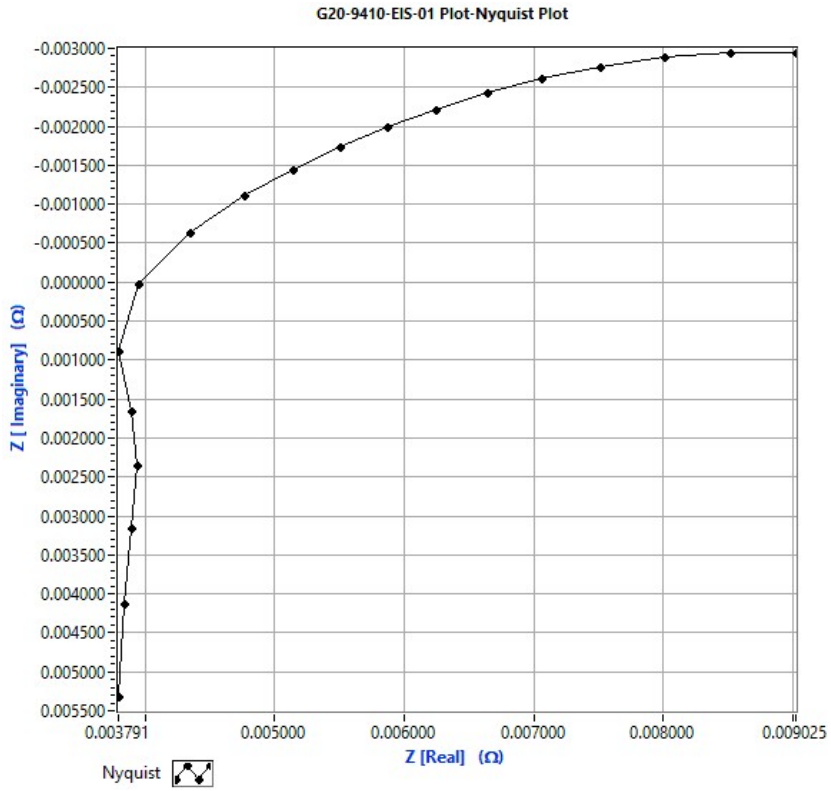

Figure 8: A Nyquist plot, obtained by measuring the complex EIS resistance between 5000 and 100 Hz.

In this thesis, two methods of finding the resistance are employed: EIS, and a steady-HFR, which takes the resistance at a 1 kHz steady perturbation frequency. While the steady HFR and EIS are both high-frequency resistance methods, in this thesis references to “HFR” refer to the steady 1 kHz HFR specifically while “EIS” values refer to the real portion of a complex EIS measurement between 5000 and 100 Hz.

Note also that while the EIS value is more exact due to being able to eliminate the imaginary component of the Nyquist plot entirely, it cannot be measured at the same time as the polarization curve. Because of this, the MEA has a different testing history when the EIS is measured compared to when the HFR and polarization curves are measured, which can affect results.

2.5 Materials

This chapter describes the different materials relevant to the production of MEAs by the decal transfer process. This includes the components of the MEA, the electrodes, the proton exchange membrane, the sub gaskets and the gas diffusion layer, as well as materials in the assembly process that affect the transfer, the pressure distribution pads and the decal substrate.

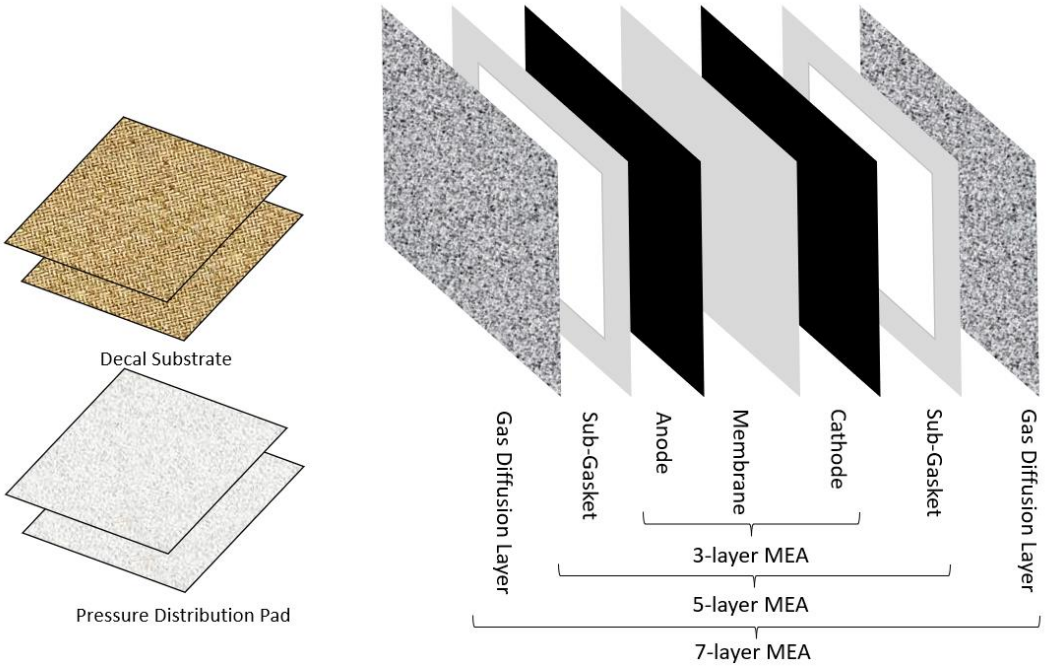

Figure 9: Schematic overview of the materials in the MEA, as well as supplementary materials for the decal transfer.

2.5.1 Proton Exchange Membrane (PEM)

The proton exchange membrane separates the two electrodes, and thereby the two half-cell reactions. It must be electrically insulating, yet conductive to protons. To achieve this, the membrane is composed of a thin sheet of ionomer, which is electrically insulating, yet forms conductive channels from polar $-SO_3H$ groups. Most state-of-the-art PEMs have a thickness between 10 and 20 µm.

An ionomer is a thermoplastic polymer which is stabilized by ionic cross-linkages. Generally, an ionomer has a main backbone polymer chain, and various side chains branching off from it which contain the ionic group ($-SO_3H$). The structure of an ionomer is shown in Figure 10.

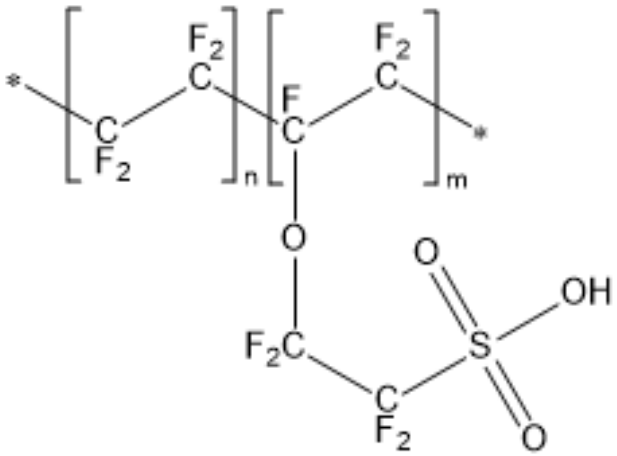

Figure 10: Structure of an Ionomer (Nafion).

The hydrophilic ion groups tend to orient themselves together, which on a very small thickness scale creates channels with inward facing ion groups. These ion groups attract water due to their polarity, and as they are acidic form a highly protonated electrolyte within the channels. Whenever a new proton is introduced on one side of the channel, another proton is ejected from the other side of the channel to maintain charge neutrality, and by this method the channel can be used to conduct protons (or other cations).

Most membranes use a perfluoro sulfonic acid (PFSA) ionomer, with hydrocarbon (HC) PEMs more recently emerging into focus for commercial application. In this work, four membranes are studied. PFSA ionomers are broadly categorized by the length of their side chain.

Membrane A is a PFSA membrane with a medium side chain (MSC) length that is 12 microns thick.

Membrane B is a PFSA membrane with a long side chain (LSC) length that is 15 microns thick.

Membrane C is a PFSA membrane with a short side chain (SSC) length that is 12 microns thick.

Membrane D is a HC membrane that is 7 microns thick.

Short side chain ionomers offer a lower proton conductivity resistance than long side chain ionomers as the density of ion groups in the structure is greater.

2.5.2 Electrodes

Within this thesis, a fuel cell electrode consists of a catalyst (Pt on carbon) in a highly dispersed form mixed with an ionomer. The reaction takes place at a 3-phase boundary, where the catalyst has access to an electrical connection (via the carbon support) for the electrons to flow to/from, and an ionic connection (through the ionomer) for protons to flow. This is the case for both anode and cathode, though the difference in the reaction rates means that the cathode requires a higher catalyst loading. In this thesis, electrodes are either sourced from Supplier A or produced in-house.

2.5.2.1 In-House Electrodes

In general, to prepare an electrode ink, the catalyst (Pt on carbon) is mixed with ionomer and a solvent consisting of water and various alcohols. This is left to mix overnight, either by use of ceramic milling balls or a stirring bar.

Then, the mixture is dispersed via ultrasonic dispersion. Depending on the recipe, this may occur in multiple steps with additional stirring in between. Once this catalyst ink is finished, rheological measurements are taken for quality control.

A decal substrate material is selected, and a doctor blade is used to distribute the ink over the decal substrate. Once the decal has been coated, it is left to dry under its own atmosphere. Then, a quality control of the electrodes is carried out. Here the electrodes are examined using a light board to assess the evenness of the coating and under a microscope to assess whether the electrodes show significant cracks or agglomerates. If the electrode passes muster, it is ready for the MEA transfer process. The electrode preparation follows the work of E. Ulberstad in the context of her master's thesis [9].

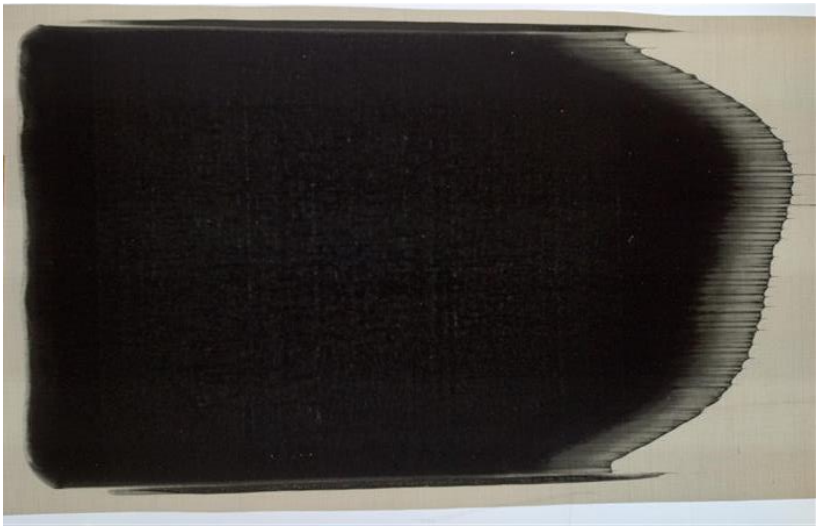

Figure 11: An In-house prepared cathode, visual inspection using a light board.

In this thesis, the in-house electrode materials were supplied by the catalyst lab with an I/Pt ionomer to catalyst ratio of 1.0 in each case. The inks were produced from catalyst material (high or low surface area Pt/C) with a carbon support to catalyst ratio of 1.0, a dry content of 12.6 % by mass, and a 60:40 solvent matrix of water and 1-propanol.

Cathode 1 used a high surface area Pt/C catalyst and ionomer 1. The ink was dispersed up to a total energy of 200 kWs in 50 kWs cycles interspersed by 30 minute resting periods. The average loading of the produced decals was measured at 0.262 mgPt/cm^2 with a standard deviation of 0.014 mgPt/cm^2 across six measurements with a sample size of 25 cm^2.

Anode 1 used a low surface area Pt/C catalyst and ionomer 2. The ink was dispersed up to a total energy of 200 kWs in 50 kWs cycles interspersed by 30 minute resting periods. The given loading of the electrode was 0.1 mgPt/cm^2.

Cathode 2 used a high surface area Pt/C catalyst and ionomer 2. The ink was dispersed up to a total energy of 200 kWs in 50 kWs cycles interspersed by 30 minute resting periods. The given loading of the electrode was 0.25 mgPt/cm^2.

Cathode 3 used a high surface area Pt/C catalyst and ionomer 2. The ink was dispersed up to a total energy of 50 kWs. The given loading of the electrode was 0.25 mgPt/cm^2.

Cathode 4 used a high surface area Pt/C catalyst and ionomer 2. The ink was dispersed up to a total energy of 10 kWs. The given loading of the electrode was 0.25 mgPt/cm^2.

2.5.2.2 Supplier Electrodes

All externally supplied electrodes came from Supplier A. Two batches each of anode and cathode were available, and each pair had the same specifications. The anode electrodes had an I/Pt ionomer to catalyst ratio of 0.7, with a target loading of 0.05 and a measured loading of 0.06 mgPt/cm^2 for each batch. The cathode electrodes had an I/Pt ratio of 0.9, with a target loading of 0.25 and a measured loading of 0.24 and 0.27 mgPt/cm2 respectively for the two batches. In each case, the C/Pt carbon support to catalyst ratio was 1.0.

At outset of the thesis, a thorough visual inspection of the supplier electrodes was conducted. This showed several issues that had to be considered when using the electrodes. These issues were most visible when backlit by a light board, and include pinholes, dry regions, coating waves and smudges (see Figure 12). Such problem areas were marked and avoided when selecting material to work with.

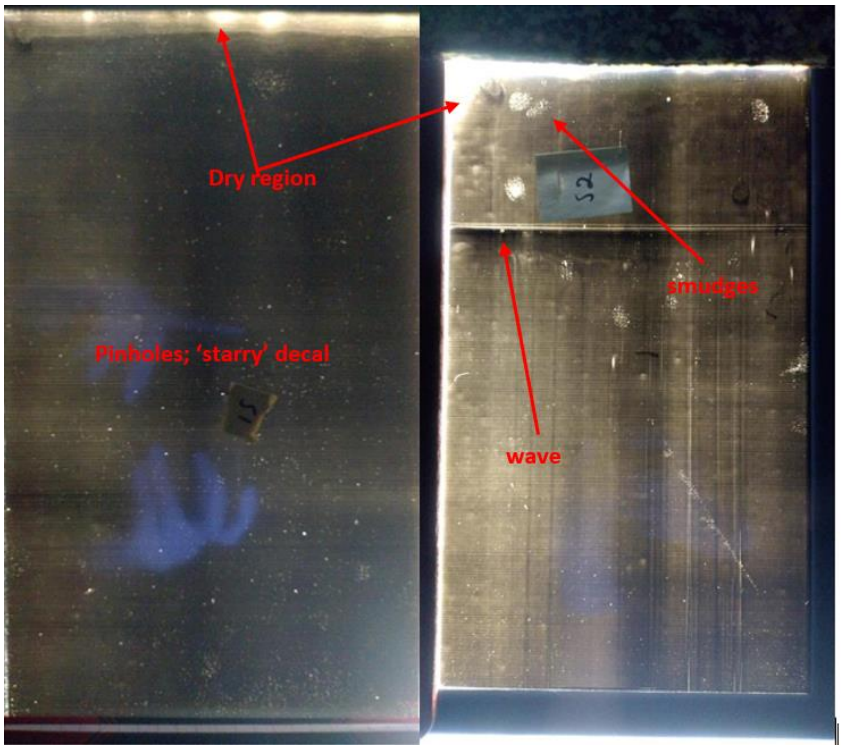

Figure 12: Supplier A electrode decals with visible defects.

Coating waves and dry regions are problems that stem from the coating process. Pinholes and smudges are more likely to occur during the storage and transportation of decals, though pinholes can also be a result of an incomplete dispersion or a local agglomeration of the catalyst particles. Prior to hot pressing, during which the ionomer in the electrodes helps bind the material together similar to an annealing process, the electrodes are extremely fragile, and at present no good solution to their storage and transport is available. Fortunately, these issues are easily detectable via visual inspection.

Other parameters, such as agglomeration or dispersion, are harder to detect visually; this is a major research focus for the catalyst lab.

Even while avoiding the problematic areas, some variance in quality was noted. This variance was present between different batches and different electrode sheets within each batch. Therefore, the Mx experiments mix batches in the four-cell array, such that each batch of cathode has one sample with each batch of anode. In chapter 7 resistance measurements are carried out on MEAs prepared from different sheets and batches in order to establish a statistical error margin for electrical measurements. A significant part of this variance likely stems from these differences in electrode quality.

2.5.3 Sub-gaskets

The sub-gaskets consist of a polymer base film and a heat activated adhesive. They are mounted on the MEA such that the adhesive side is facing inwards and a window with a defined area is left free for the reaction to take place. Their function is to enable the mounting of the MEA into a testing cell without any leaks across the cell. The assembly of the sub-gasket is a lamination procedure which requires moderate heat and pressure applied using an appropriate hand tool.

2.5.4 Gas Diffusion Layer

The gas diffusion layer is a thin layer of a porous material which serves the purpose of enabling an even spread of the gases across the electrodes. In this thesis, carbon paper is used for this purpose.

2.5.5 Decal Substrates

The decal substrate is the carrier material for the electrodes before and during the decal transfer. They must be chemically inert, thermally stable across the operating conditions of the hot press and have excellent release properties. Here, glass fiber reinforced Teflon is used as a decal substrate.

2.5.6 Pressure Distribution Pads

The use of pressure distribution pads is a recent addition to the MEA assembly procedure at PowerCell, introduced by S. A. Ogu-Egege [4]. At present, disposable pressure distribution pads made of cellulose are used. Their function is to ensure an even distribution of pressure across the MEA during the transfer process.

3 Glass Transition Temperature

A phenomenon of amorphous polymers, including ionomers, is the glass transition temperature, where the material undergoes a change from a rigid glassy state to a more malleable rubbery state. This change comes with significant differences in the physical and mechanical properties of the ionomer. In the decal transfer process, the malleable state is significant for the transfer behavior and MEA properties.

While an investigation of the glass transition behavior of ionomers is not the purpose of this thesis, it is important to consider the glass transition temperature of the membranes in order to understand the effects of temperature on both transferability and performance of the MEA in other experiments. Thus, glass transition temperature measurements are conducted using DSC. In future work, a more in-depth study of the glass transition behavior may be needed; these measurements are not repeated, are only performed on the ionomers in the membranes A, B, C and D, and are only performed in one direction, i.e., heating up the sample rather than cooling it down. The mechanical properties of the ionomers above and below the glass transition temperature are also not measured. These measurements should serve to support later experiments by giving context to the glass transition temperatures of relevant materials.

3.1 Initial Experiments

The glass transition temperatures of membranes A, B, C and D are measured by DSC as described in section 2.4.2. Figure 13 shows the DSC graphs for membranes A, B, C an D.

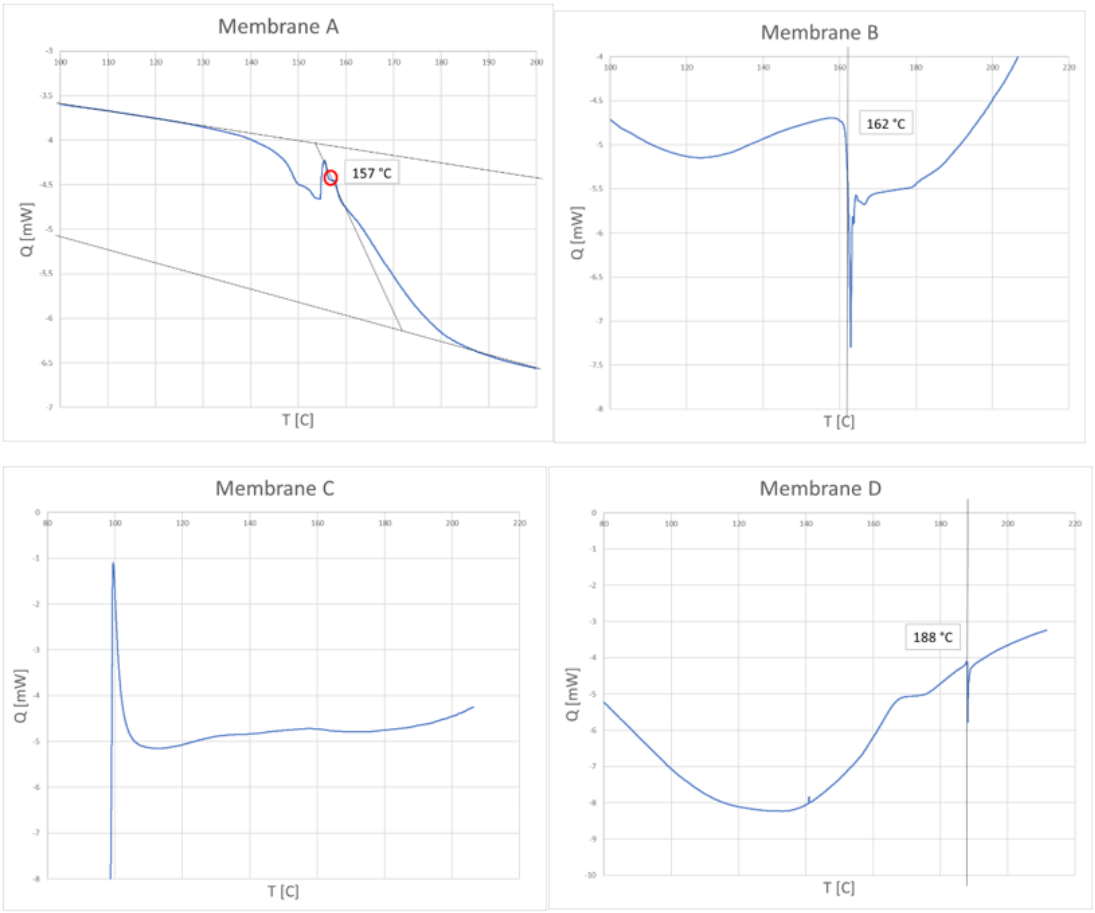

Figure 13: DSC results for membranes A, B, C and D.

Membrane A shows a (midpoint) glass transition temperature at 157 °C, membrane B at 162 °C, and membrane D, which is a hydrocarbon ionomer, shows a glass transition at 188 °C. Membrane C shows no glass transition. Most likely the sample was not compressed sufficiently in the pan, leading to poor contact with the aluminum and obscuring the specific heat transport relative to the (empty) reference pan.

It is important to note that these measurements are single measurements conducted in only one direction (heating the sample, not cooling the sample). They are intended to provide general values for the glass transition temperature to inform the discussion around other results. There are many effects and observations around the glass transition, such as the different observed shapes of the DSC graphs and the annealing behavior described in chapter 5, which warrant further investigation than is possible in this thesis.

3.2 Discussion

While the Tg measurement failed for membrane C, the results show a Tg at 157 and 162 °C respectively for membranes A and B. Such a low difference is expected, as both are PFSA membranes which mainly deviate in the length and frequency of their side chains, and it is likely that a successful measurement of membrane C would also show a Tg near 160 °C. Membrane D showed a significantly higher Tg at 188 °C, which correlates to the significant difference of a HC ionomer to a PFSA ionomer.

While this is a sufficient investigation of the glass transition temperature for this thesis, there remain many questions. The shape of the graphs varies significantly, and the greatest variance is between the two successful tests of PFSA membranes (A and B), which are expected to have similar structures and morphology. It may also be worthwhile, in future work, to test the degradation temperature of the ionomers. In this thesis, the glass transition is mainly interesting as context for the temperature-driven behavior in other tests, so these measurements should be sufficient. Further work may need to investigate the glass transition in greater detail.

4 The Decal Transfer Process

At PowerCell, the membrane electrode assembly is produced using a decal transfer process. In this method the anode, the membrane and the cathode are laminated into an MEA at elevated temperature and pressure in a single processing step. The electrodes are provided on a decal substrate, a chemically inert carrier material with good release properties and high thermal stability, and this process transfers them onto the membrane while also 'annealing' each electrode from a homogenized mix of ionomer and catalyst powder into a solid material.

The decal transfer process is done using a programmable hot press. The MEA sample is placed on a suspended steel tray within the press where it remains until the top and bottom plates of the press have reached their desired temperature. The bottom plate then closes towards the top plate, lifting the suspended tray and sample in the process. The pressing commences for the defined time at the defined pressure, following which the top and bottom plates open, and cooling cassettes are used for 120 seconds to return the sample and tray to room temperature.

At the outset of work on this thesis, a functional operating point for the successful transfer of the electrodes was known from previous work at PowerCell [4] at 160 °C pressing temperature, 300 seconds of pressing time, at a pressure of 300 N/cm^2 (operating point D4 in this thesis). The same work introduced pressure distribution pads consisting of cellulose in order to ensure an even distribution of pressure within the MEA.

During this thesis, the following alterations were made to the basic process:

- 'Fitting' the cellulose pressure distribution pads, membrane and electrodes to the same size to better control the distribution of pressure

- Introducing assembly plates to streamline MEA preparation outside the press and allow for the simultaneous preparation of multiple samples

Furthermore, the temperatures within the MEA during pressing were examined, as opposed to the temperatures of the top and bottom plates of the press, and the possibility of pressing multiple MEAs simultaneously in series as a stack was explored.

4.1 Assembly Plates

Assembly plates were introduced to the process primarily in order to facilitate the rapid production of MEA samples of varying sizes in large quantities, as is necessary for the 'Mx matrix' form of experiments used in this thesis. The assembly plates consist of two flat steel plates, one of which has placement markings on it, upon which samples are arranged. It is then possible to arrange samples outside of the hot press and, by switching between different sets of plates, maximize the use time of the hot press. Sample arrangement is then far simpler and can be accomplished while the previous MEA is being produced. Figure 14 shows two sets of assembly plates with samples.

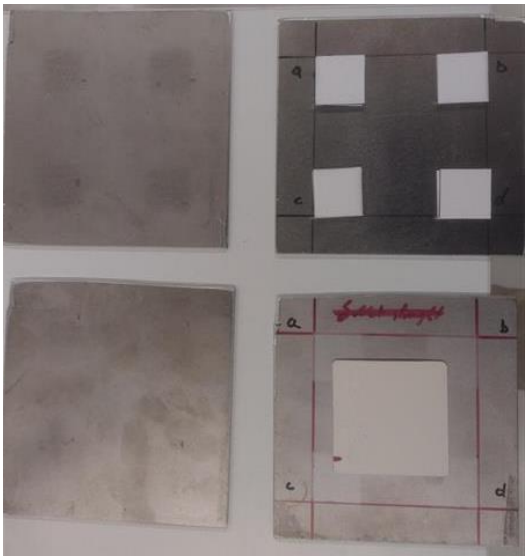

Figure 14: Assembly plates.

Beyond simplifying the sample arrangement and increasing the efficiency with which the press can be used, these plates also avoid a problem whereby slightly misaligned samples may have sections of membrane 'poke out' from underneath the cellulose and can stick to the hot press. Further, they can serve to protect the hot press from damage, as was the case during an attempt to measure the internal temperature of the MEA during pressing in absence of the cellulose pressure distribution pads (Figure 15).

Figure 15: Assembly plate damaged instead of the hot press.

In future work at PowerCell, it may be feasible to expand this concept to accommodate larger MEA samples needed for full scale prototyping or commercial production, possibly including integration with the current suspended tray setup.

4.2 Pressure Distribution and Fitting the Components

As determined by S. A. Ogu-Egege [4], a pressure distribution pad is required to ensure an even distribution of pressure across the MEA during the transfer, and single use cellulose pads provide a good and economical solution. With the size of this pad exceeding the size of the membrane, which in turn exceeds the size of the electrodes, it is necessary to better understand the distribution of pressure between areas of the sample with different materials.

An experiment was set up in which a sample was pressed together with a layer of pressure sensitive film (FujiFilm Prescale LW). Figure 16 shows the general setup of the experiment.

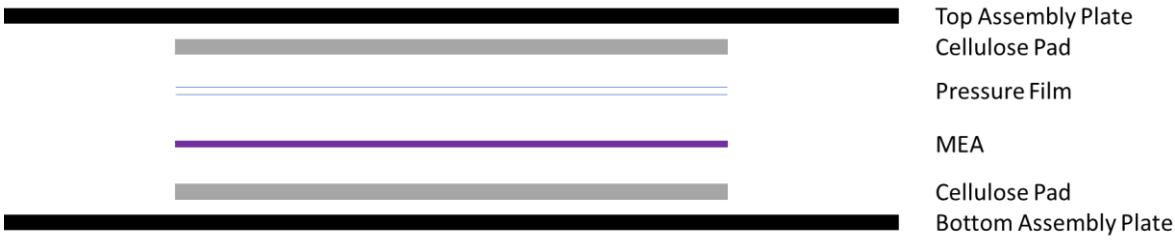

Figure 16: Pressure distribution measurement general setup.

Between the assembly plates is first a layer of the cellulose pressure distribution pad, upon which is the MEA, upon which is the pressure sensitive film. The experiment was carried out using cellulose pads with dimensions of 7 x 7 cm, a commensurate area for the pressure film, and four MEA samples with dimensions of 2 x 2 cm arranged in a grid pattern. The experiment was run at a pressure of 300 N/cm^2 relative to the area of the cellulose, a pressing time of 300 s, and a temperature of 30 °C to accommodate the pressure sensitive film. The MEA used Supplier A anode and cathode material and membrane A. Figure 17 shows the results of the experiment.

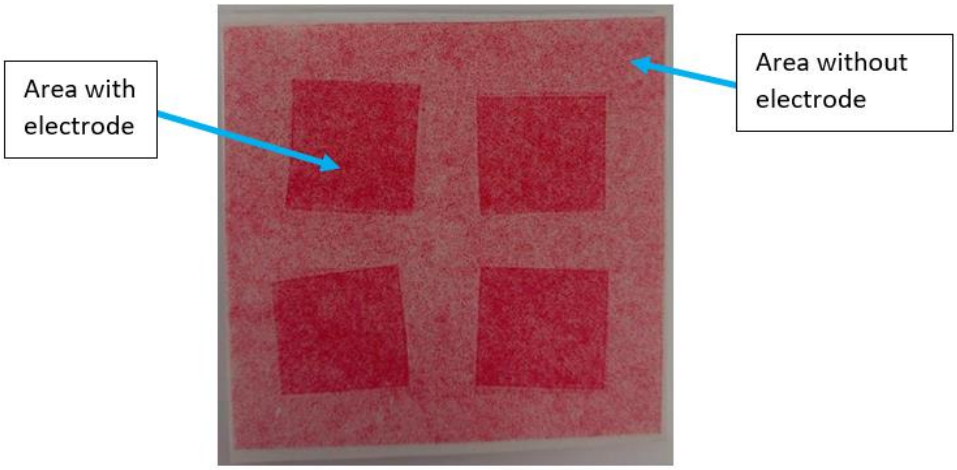

Figure 17: Initial prescale pressing test including cellulose pressure distribution layers, with four 2x2 MEA samples, showing areas with and without electrodes.

Clearly visible is an imbalance between areas of the cellulose with and without MEA, with the areas with the MEA seeing a higher pressure. The distribution of this pressure is very even for each MEA and between the four samples. However, the actual pressure upon the MEA remains unknown, which somewhat complicates efforts to characterize and control the effects of pressure on the transfer process.

Interestingly, the edge of the electrode experiences greater pressure than the rest of the electrode. It may be that when the electrode is cut, the blade pushes electrode or decal material to the side, creating a localized increase in the height of the electrode. Fortunately, the change appears to be too localized to be a significant contributor to MEA performance.

A 'fitting' approach is used to resolve the pressure distribution problem. In this method, cutting die are used to prepare membranes, electrodes and cellulose pads such that all possess the same dimensions. This avoids having different 'zones' with different actual pressures.

Testing fitted cellulose with four 2.5x2.5 cells and a 33 cm^2 configuration that can be cut down for the BFC 12 gives the following results:

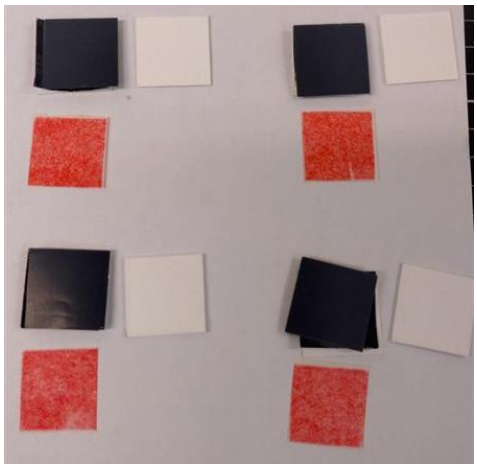

Figure 18: pressure distribution in the hot press for the four-cell array.

Figure 19: Pressure distribution in the hot press for a 33 cm^2 sample.

In both images, there is an even pressure distribution, which shows the viability of the fitted cellulose configuration. Further, in Figure 18 we see that the pressure distribution is also even between separated samples, which shows the viability of pressing multiple samples simultaneously if their materials and the process parameters are the same. Going forward, all samples are prepared using cutting die, with electrodes, membrane and cellulose pressure pads all of the same dimensions.

4.3 Temperature within the MEA

The decal transfer process takes place at an elevated temperature. In previous work [4], 160 °C was established as a good operating temperature for achieving a good quality decal transfer with Membrane A and both select in-house electrodes and electrodes from Supplier A. The MEA, as well as surrounding materials including the decal substrates and pressure distribution pads, must all reach this temperature. For this to occur, heat must be supplied.

$$\dot{Q} = m \cdot c_p \cdot \Delta T$$

The heat source is the heated plates of the hot press. For each layer in between these plates and the MEA the transfer of heat becomes slower because the heat transport resistance increases. For a series of solid layers, this can be described as

$$Q = \dot{q} \cdot A = \frac{\dot{T}_{plate} - T_{MEA}}{R_t} \qquad R_t = \frac{l_1}{k_1 \cdot A} + \frac{l_2}{k_2 \cdot A} + \cdots$$

It is clear, then, that the introduction of additional layers between the MEA and the hot plates of the press must increase the thermal resistance of the assembly and that the MEA will therefore take a longer time to reach the required temperature. For each layer, this effect increases proportionally to the thickness l_i of the materials and decreases proportionally to the thermal conductivity of the requisite material k_i.

With the introduction of several layers beyond the decal substrate of the electrodes – specifically the assembly plates and cellulose pads - it is necessary to characterize the course of the temperature within the MEA during the transfer. To this end, an experiment is conducted to measure the temperature of the hot plates of the press and the MEA during a transfer. Temperature readings from the plates are taken directly from the press, while the internal temperature of the MEA is taken via a type T thermocouple added to the sample in between the top electrode decal and cellulose pad. The transfer is conducted at the 'D4' operating point at 160 °C, 300 N/cm^2 and with 300 s of pressing time.

Figure 20: Internal temperature measurement during a decal transfer.

The temperatures of the hot press plates and the internal temperature of the MEA during the pressing are presented in Figure 21.

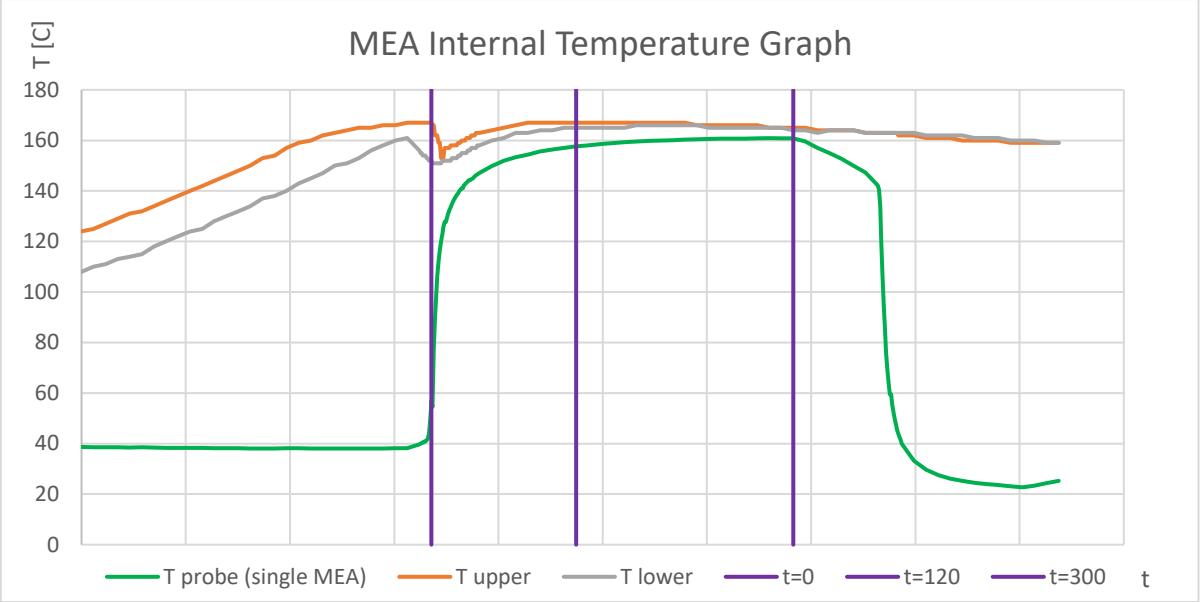

Figure 21: Temperature course of the MEA and hot plates during a decal transfer.

During the warmup of the press, the temperature of the MEA naturally remains constant at room temperature. Following the warmup, the press closes. This begins with the lower plate of the press lifting up and carrying the suspended tray with the MEA with it. This is why the temperature of the lower plate drops before t=0, as heat begins to flow from the lower plate to the suspended tray and the sample. The MEA temperature, T probe, begins to increase at this point as well.

At t=0 s, the hot press is closed; as heat flows from both the upper and lower plates to the sample, the temperature of the upper plate is decreased and the temperature of the MEA increases rapidly. Shortly thereafter, the temperatures of the plates begin to stabilize as the hot press adjusts their internal heating. Meanwhile, the heating of the sample slows down as the temperature difference between plate and sample, which is the driving force for the heat transfer, decreases.

At t=120 s, the internal temperature of the MEA has reached the desired temperature of 160 ± 5 °C, and the temperatures of the hot plates have stabilized. The various temperature profiles remain steady until t=300 s, when the press opens. The MEA at first cools down slowly, then rapidly as the press closes again with cooling cassettes in place.

These results generally follow expectations. The interesting unknown that they reveal is what manner of time characteristic is needed, at minimum, for the internal temperature to approach the set temperature. At 120 s, the gap closes to within ca. 5 °C, and continues to increase logarithmically towards the set temperature. At t=300 s, the difference between the internal temperature of the MEA and the set temperature of the press is negligible.

4.4 Series stacking

In order to support eventual commercial production, it is important for the decal transfer process to be upscaled considerably. Decreasing the time seems to have stark limits, and so a better approach would be to increase the MEA production volume with each pressing. As demonstrated in section 4.2,

the use of pressure distribution pads makes a parallel pressing of multiple samples viable. What about stacking multiple MEAs in series?

Towards this end, it is necessary to verify that the pressure distribution remains even and find the temperature curve in the center of such an MEA stack. In these investigations 8 MEAs are used, with membrane A electrodes from Supplier A.

In order to investigate the pressure distribution in the stack, an experiment is set up with pressure sensitive film (Fujifilm Prescale LW) every 2 MEAs. The setup can be seen in Figure 22 and is operated in the same manner as the pressure distribution experiment in section 4.2.

Figure 22: Pressure distribution experiment setup for multiple MEAs.

The results of this experiment are shown in Figure 23. To the left is the result while lit from above; to the right the result is backlit using a light board.

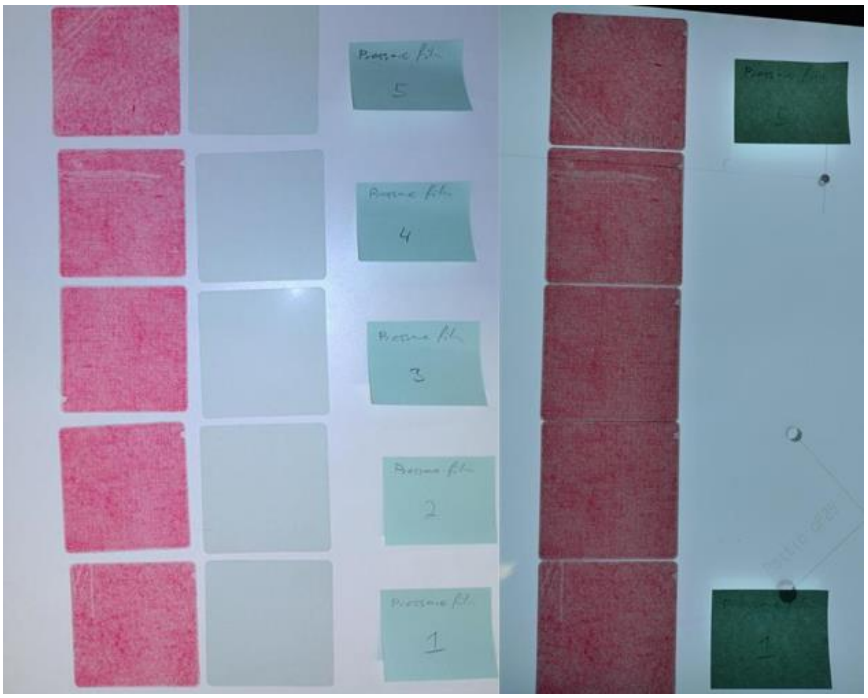

Figure 23: The pressure distribution during transfer in a stack of multiple MEAs.

The pressure distribution is mostly even, with some notable, localized inconsistencies. A closer inspection of the electrodes in these locations shows equivalent defects, such that this localized difference seems to speak more to the electrode quality than an inherent imbalance in the distribution of pressure (Figure 24). The electrode quality varies here because these MEAs were produced from rejected electrode material on account of them not being required to undergo resistance testing.

Figure 24: Localized electrode defects appear on the pressure film.

Aside from these localized defect areas the pressure distribution is even across the MEA, and across the stack. This suggests that transferring multiple MEAs simultaneously and in series is, from a pressure perspective, viable even without the introduction of further intermediate pressure distribution layers.

It remains necessary to explore the temperature curve inside the MEAs during transfer. With a hot plate above and below, the greatest thermal resistance is to the center of the stack. An experiment is conducted in the same manner as the temperature curve measurement in section 4.3, but with a stack of 8 MEAs rather than one, and with the temperature probe located at the center of the stack, between MEAs 4 and 5. The results are shown in Figure 25 alongside the initial temperature curve for a single MEA.

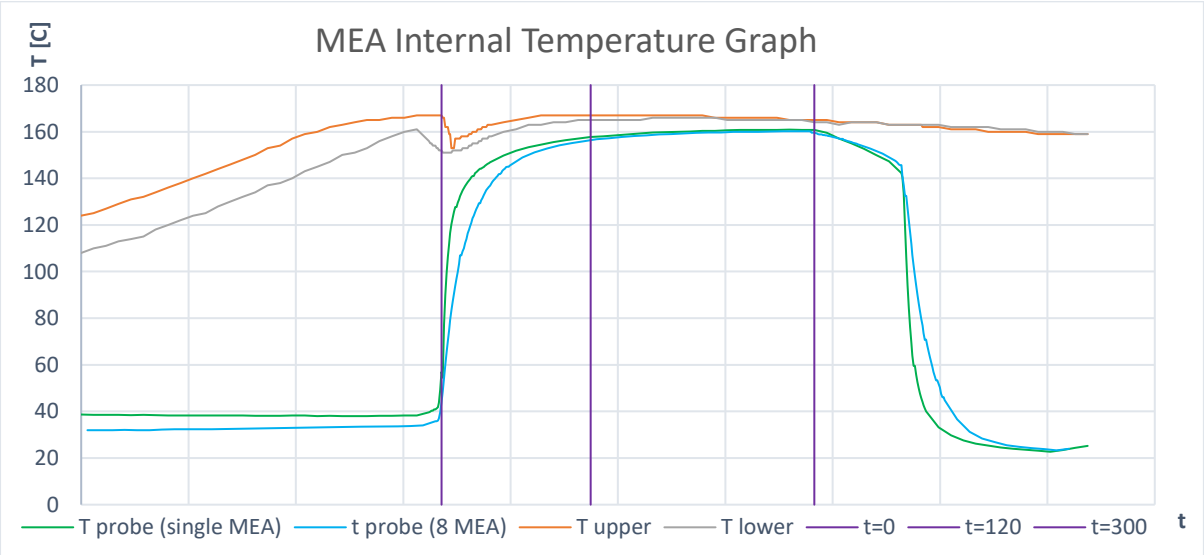

Figure 25: Internal temperature course during transfer for one MEA and 8 MEAs.

The temperature curve within the stack of 8 MEAs is qualitatively similar to that of the sample with only one MEA. What is apparent is the effects of the increased distance – and therefore thermal resistance – on the change in temperature, as the temperature curve is delayed during the heating and cooling sections. By t=120 s, the temperature curve of the 8 MEA stack is comparable to the curve for one MEA. Together with the pressure distribution, this suggests that a series stacking approach to increasing the production volume of MEAs is viable, and that the number of MEAs could be increased beyond the 8 used in this experiment, so long as the pressing time is sufficiently long.

This provides a very promising outlook for future MEA production on a large scale. The hot press is large enough to accommodate a small number of commercial scales MEAs in parallel. With appropriate logistical preparation, it should be possible to complete and switch the stacks within 15 minutes. Should four stacks of 8 MEAs be pressed simultaneously, this suggests a possible throughput of 128 MEAs per hour, which, if implemented, would be sufficient to sustain commercial production at PowerCell for the foreseeable future.

The in-situ performance is evaluated in chapter 7.3. A stack of 9 MEAs is used for this to maintain symmetry around the central MEA.

5 Electrodes: Quasi-Annealing Behavior

During transfer, the electrode material undergoes a significant change. The 'raw' electrode before the transfer is more matte in texture and is very vulnerable to physical damage such as being smudged, while the 'annealed' electrode after the transfer has a shinier texture and feels like a plastic film which is much more resistant to physical damage. This behavior is likely due to the ionomer softening and binding the catalyst particles together, and takes place for both in-house produced electrodes and the electrodes from Supplier A.

This annealing behavior is a poorly understood effect with significant implications which cannot be thoroughly explored in this thesis due to time constraints. Here, some initial tests to explore this phenomenon are done, and some of the possible applications, implications, and experiments surrounding this behavior are discussed. Future work at PowerCell should explore this phenomenon further.

5.1 Initial Experiments

Some initial tests are conducted to observe the annealing behavior. Time constraints limit the amount of testing that can be done, so these are preliminary experiments aimed at providing a general overview and understanding of the behavior so that a more comprehensive test plan can be performed in future work.

Three tests are used to gain a qualitative understanding of the annealing behavior - 'observing reflection', 'smudging' and 'wiping' the electrode. The raw electrode is matte black with very little 'reflection'; during annealing the electrode gains a shiny appearance comparable to a black plastic film, which can be used to characterize the annealing. The annealed electrode is also much more resistant to 'smudging', and a qualitative assessment of the normal and shear forces required to smudge the electrode is used to characterize the annealing process. A 'wiping' test is performed, in which a solvent-laced cloth is used to remove the electrode from the decal. This occurs even for a fully developed MEA, however the force required is considerably greater for an annealed electrode.

Three annealed electrodes are prepared. This is done in a similar manner to the transfer method for an MEA described in chapter 4 with the difference that instead of an MEA assembly of anode, membrane and cathode only an electrode is used, which is covered by a layer of decal substrate on its exposed side. In each case, cathode material from supplier A is used. The first sample is prepared at T = 160 °C, p = 300 N/cm^2, and t = 300 s (p300 sample). From observations in chapter 5 it is expected that the annealing behavior is temperature driven rather than pressure driven, and so the second and third samples are prepared with the same time and temperature, but at pressures of p = 0 N/cm^2 (p0) and p = 5 N/cm^2 (p5). These points are selected because it may be useful to introduce an annealing step during the preparation of in-house electrodes after the drying step so that the electrodes are less fragile in storage and in case there may be advantages for layering multiple electrode coatings. In this case it may be simpler to use a hot plate with low downforce rather than a hot press.

The reflexion behavior of the raw, p0 annealed electrode and p300 annealed electrode is shown in Figure 26.

Figure 26: Reflexion behavior for (a) the raw electrode, (b) the p0 annealed electrode and (c) the p300 annealed electrode.

The reflexion of the raw electrode is very low, and indeed almost non-existent, the reflection of the p300 annealed electrode is comparable to that of well transferred MEAs, and the reflection of the p0 annealed electrode is in between, certainly present but not nearly as developed. The reflection of the p5 annealed electrode was observed to be shinier than the p0, but not as shiny as the p300 annealed electrode.

The raw electrode is very easily smudged with little to no downforce required, which is highly problematic for electrode storage. The p0, p5 and p300 electrodes all required far more force to be damaged, with increasing pressure leading to improved smudging resistance. Of note is that even with no pressure, the smudging resistance was sufficient to prevent most accidental damage, and that the difference between the behavior of the p5 and p300 annealed electrodes was comparable to the difference between the p0 and p5, suggesting greatly diminishing returns with increasing pressure.

The wiping test had very similar results to the smudging test, with the difference that even a fully transferred MEA is vulnerable to such an attack. In this case, considerable downforce and multiple passes are required to remove the electrode. Of note is that for the annealed electrodes, larger sections tended to break off together when sufficient force was applied, which confirms the improved internal cohesion due to the annealing.

Upon conclusion of the reflection, smudging and wiping tests, an MEA transfer using annealed electrodes was performed. Anode and cathode were annealed with the same protocol as the p300 annealed electrode using supplier A materials, and membrane A was used. The transfer occurred at operating point D4 (T = 160 °C, p = 300 N/cm^2, and t = 300 s). This resulted in a successful MEA transfer without residue on the decals, as seen in Figure 27, indicating that pre-annealing the electrodes does not interfere with the decal transfer behavior.

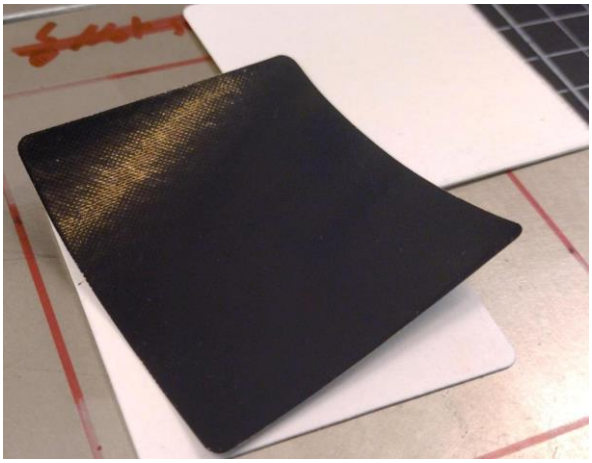

Figure 27: MEA transfer result using p300 annealed electrodes.

5.2 Discussion

Temperature seems to be the greatest driver of the observed annealing behavior, with pressure playing a supplementary role. Some pressure seems to be advantageous to the annealing process, but this may be simply due to the pressure facilitating a better interface for heat transfer in the hot press. This could be examined further using heated plates without cellulose pressure distribution pads. The effect of time is yet an unknown, though results from chapters 6 and 7 suggest it may be relevant. Of great significance is that a pre annealing step does not appear to challenge the transferability of the electrode. This could be explored further in an experiment like the matrix experiments in chapter 6. For further experiments, it would be useful to establish a quantitative way of assessing annealing behavior.

The observed annealing behavior appears to have a major impact on the morphology and structure of the electrodes. It is unclear how the difference in the electrode surface may impact interactions with other components, such as the GDL. When pre-annealing the electrode there may be an effect on the interface between electrode and membrane which needs to be explored. It may also be possible to use such a step to 'heal' cracky electrodes, a phenomenon explored by S. A. Ogu-Egege [4]. A pre annealing step could be used for such crack healing while being optimized separately from the decal transfer step. It may also be of use in the pursuit of electrodes with higher catalyst loadings, as the more robust, annealed electrode might lend itself to being produced in multiple layers. Such an approach risks creating additional interface effects, but may provide other opportunities, such as controlling the gradient of ionomer across the height of an electrode. If different ionomers are used in the membrane and electrode, it may be useful to expose the electrode to a higher temperature in the pre-annealing step than the membrane can support. It may then be useful to consider the glass transition temperatures of the ionomer used in the electrode in future work.

6 Processing Parameter Matrix: What Works?

In this chapter, an experiment matrix is set up in order to analyze, by visual inspection, the range of parameters available to achieve a successful decal transfer for the MEA. This should provide insight into the design rules for a successful MEA transfer and inform the usable operating points for later experiments.

The most significant processing parameters for the decal transfer of the MEA are temperature T, pressure p and the time t the MEA is exposed to these factors. At outset of work on this thesis, only select operating points were known to transfer reliably. By varying these parameters, an experiment matrix can be set up to explore the processing parameters available for a complete transfer.

The completeness of the transfer can be confirmed visually by the residual electrode left on the decal substrate after transfer. There is a dependency on the decal substrate used. However, this is not varied within the bounds of this thesis. The parameters explored are the set parameters on the hot press; for pressure and transfer time, this corresponds directly to the conditions of the MEA; for the temperature this is not the case for the entire pressing time, as discussed in section 4.3, which must be taken into account during the analysis of this data.

6.1 Experiment Description

Prior to this thesis, the operating point at T = 160 °C, p = 300 N/cm^2 and t = 300 s had been used to achieve a successful transfer with membrane A and both supplier A and in-house electrodes. This operating point was, therefore, used to inform the experiment matrix for this exploration of the available processing parameters.

Five temperature levels were selected, 120, 140, 160, 180 and 200 °C, around the temperature of the known operating point. The distance of 20 °C was chosen because the regulatory behavior of the hot press results in temperatures of ± 5 °C, and so differences of 20 °C should always be significant.

Five pressure levels were selected, 50, 150, 300, 450 and 600 N/cm^2, around the pressure of the known operating point with the lowest pressure adjusted upwards to maintain some compression of the MEA. 600 N/cm^2 was taken as an upper bound on account of literature showing greatly diminishing returns from increasing the pressure beyond this point [10].

Two time levels were selected, 120 and 300 s. The upper time is the pressing time used for the known operating point; the lower time was selected at the point where the set temperature of the press is reached by the MEA within reasonable deviation (see section 4.3).

The experiment design matrix is shown in Figure 28 below. The cell designations form a useful shorthand for their respective processing parameters. The known operating point at T = 160 °C, p = 300 N/cm^2 and t = 300 s is assigned to cell D4 by this method.

	A	B	C	D	E	F	G
1	T [C]			t = 300 s			
2	200						
3	180						
4	160						
5	140						
6	120						
7		50	150	300	450	600	p [N/cm^2]
8							
9	T [C]			t = 120 s			
10	200						
11	180						
12	160						
13	140						
14	120						
15		50	150	300	450	600	p [N/cm^2]

Figure 28: Experiment design matrix for exploring the space of available processing parameters.

As seen in section 224.2, the pressure distribution remains the same even when multiple samples are being transferred in parallel. For these parameter matrix experiments, an array of four 2.5 x 2.5 cm samples was used for each test. This was done so that the anode and cathode materials can be varied. For each array, material from two sheets of anode and two sheets of cathode was used, and this material was distributed between the four cells so that each cathode material was paired with each anode material. In this way, some of the variance between different electrode sheets and batches can be counteracted, and the array was better able to show whether a transfer behavior was consistent.

Table 1: Color designations for rating the transfer result.

Dark Green	Successful transfer with no residual
Light Green	Successful transfer with some residual
Yellow	Inconsistent success of transfer, or high residual
Red	Failed transfer

The transfer was observed visually by the residual of the electrode on the decal and given a color based rating. Dark green (Figure 29) represents a full, successful transfer on all samples in the array. Light green (Figure 30) represents a successful transfer with minor residual of electrode left on the decal, either as individual points or in the texture of the decal. Yellow (Figure 31) represents a successful transfer with significant residual or an inconsistently successful transfer where most samples transfer successfully but some fail. Red (Figure 32) represents an array with major failures. Dark green represents the preferred operating points, light green is generally still acceptable; yellow and red are not.

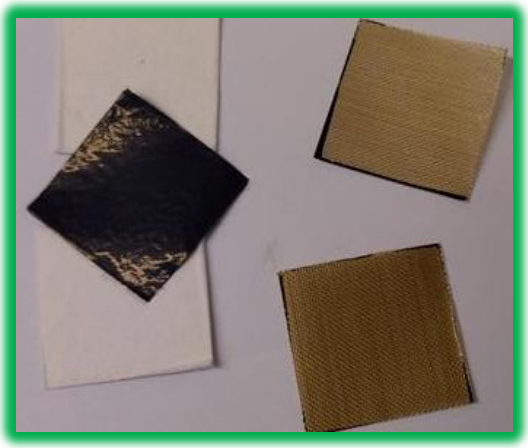

Figure 29: Dark Green: A successful transfer with no residual.

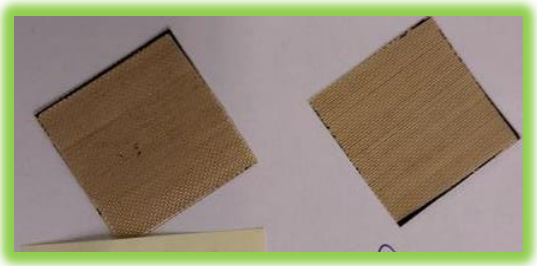

Figure 30: Light Green: A successful transfer with some residual.

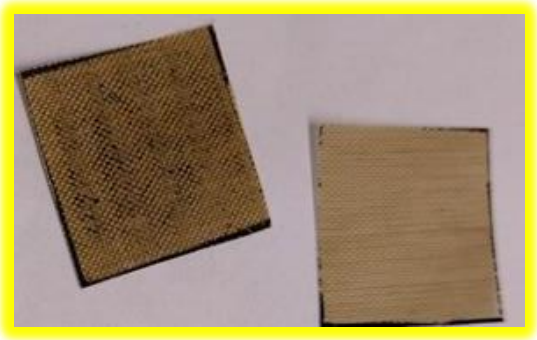

Figure 31: Yellow: A transfer with high residual.

Figure 32: Red: A failed transfer.

This experiment was carried out with several different material combinations, described in Table 2. In M2, supplier A electrodes and membrane A were used to find the general trends for the parameter space. In M3, M4 and M5 the experiment was repeated with the same electrode materials and membranes B, C and D respectively in order to understand the impact of using membranes with different ionomers. Note that the ionomer was only varied in the membrane, not the electrode. In M6 the same membrane and anode as in M2 were used, but with the in-house produced cathode 1.

Table 2: Description of the experiments for finding the parameter space for the decal transfer process.

Experiment Designation	Materials	Description
M1	Waste Material	Test matrix to refine the experiment method and setup
M2	Membrane A, Supplier A anode and cathode	Finding trends and a baseline parameter space
M3	Membrane B, Supplier A anode and cathode	Varying the membrane
M4	Membrane C, Supplier A anode and cathode	Varying the membrane
M5	Membrane D, Supplier A anode and cathode	Varying the membrane (HC PEM)
M6	Membrane A, Supplier A anode, in-house cathode 1	Varying the cathode (relative to M2)

Because M2 shows the general trends for the process parameters, some assumptions were made for the tests in experiments M3 to M6. First, when a transfer fails (red or yellow), conditions with lower temperature or pressure are also unsuccessful. Second, if the operating conditions above and below or to both sides of a cell transfer successfully, that cell is also considered successful. These assumptions lowered the number of experiments required for a matrix by as much as 2/3.

6.2 Results

The results for the M2 experiment matrix, with supplier A anode and cathode and membrane A, are shown in Figure 33.

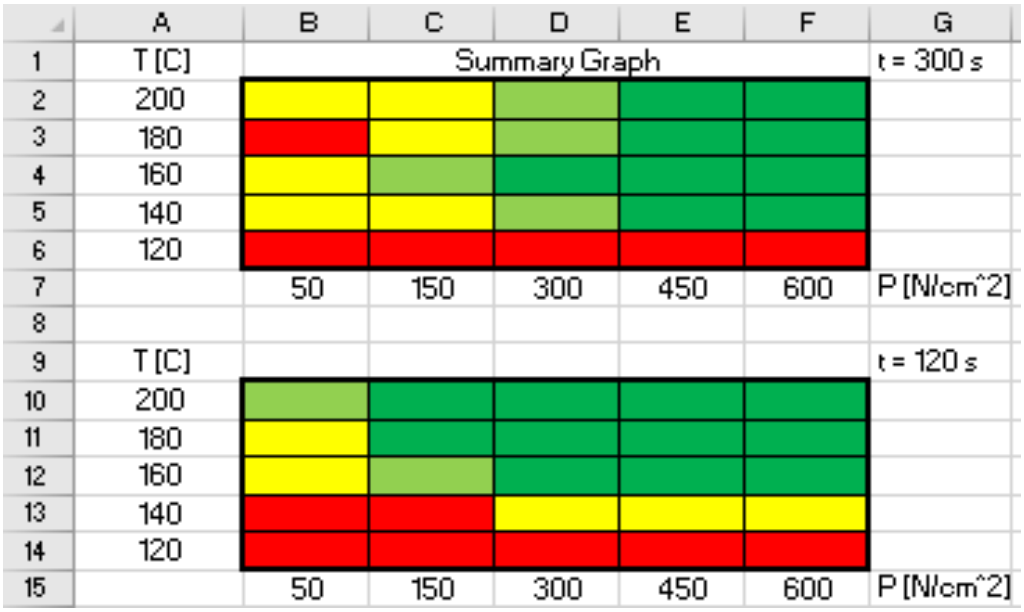

Figure 33: Process parameter space for M2: Supplier A anode and cathode with membrane A.

There appears to be a minimum pressing temperature which is one step higher at the lower time level. The temperatures in question are 140 and 160 °C, compared to the measured midpoint glass transition temperature of 157 °C for this membrane (see chapter 3). At the higher time level, there also appears to be a minimum pressure that is required, though the C4 operating point with T=160 °C, p=150 N/cm^2 and t=300 s seems to be an exception. At the lower time level, lower pressures enable a good transfer as well if the temperature is sufficiently high.

The results for the M3 experiment matrix, with supplier A anode and cathode and membrane B, are shown in Figure 34.

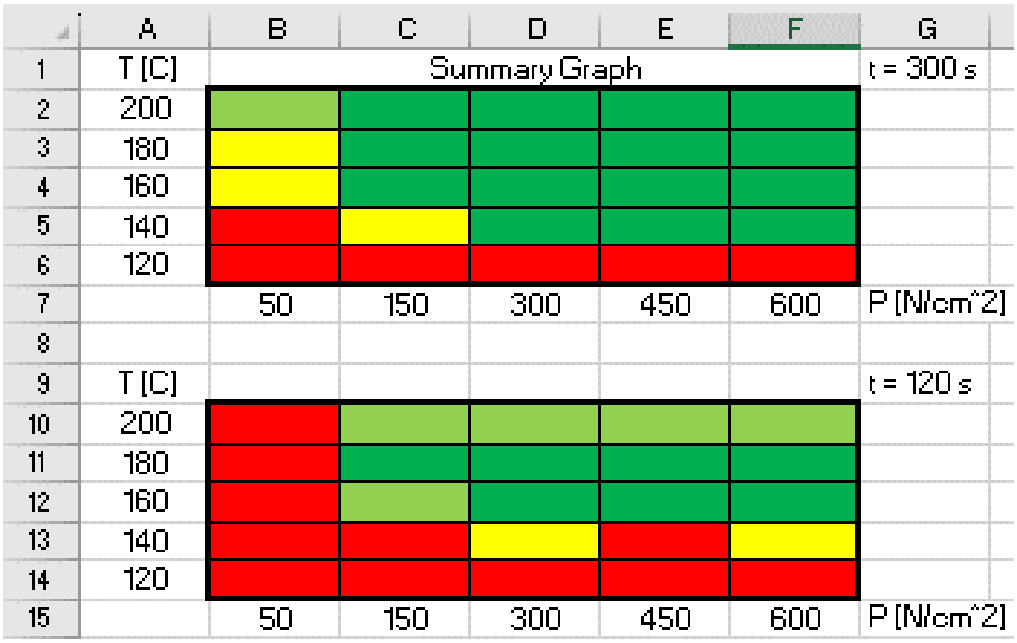

Figure 34: Process parameter space for M3: Supplier A anode and cathode with membrane B.

Once again, the results indicate a minimum temperature requirement which is at 140 to 160 °C. The membrane B used here has a glass transition temperature comparable to membrane A at 162 °C. Unlike the previous matrix, the pressure boundary is much more similar between the two time levels, with the longer time level achieving slightly better transfers at low pressure than the higher time level. Another point of interest is that at very high temperatures in the lower time level the transfer worsens slightly, although not enough to fully fail.

The results for the M4 experiment matrix, with supplier A anode and cathode and membrane C, are shown in Figure 35.

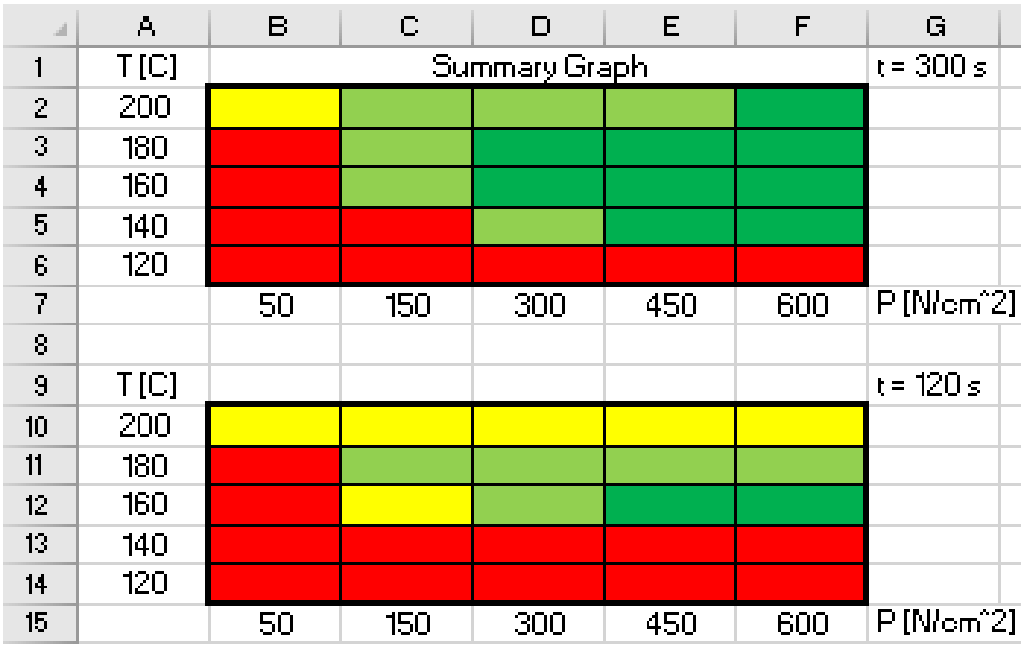

Figure 35: Process parameter space for M4: Supplier A anode and cathode with membrane C.

The lower bounds for temperature are similar here as for the previous two membranes. The Tg for this membrane is not known, as the measurement was unsuccessful (see section 3.1), but is likely

comparable to the Tgs for membranes A and B. At the higher time level, the lower bound for pressure is like the previous test with membrane B. At the lower time level, the temperature range for a successful transfer is significantly reduced, however, with high temperatures transferring in the yellow region.

The results for the M5 experiment matrix, with supplier A anode and cathode and membrane C, are shown in Figure 36.

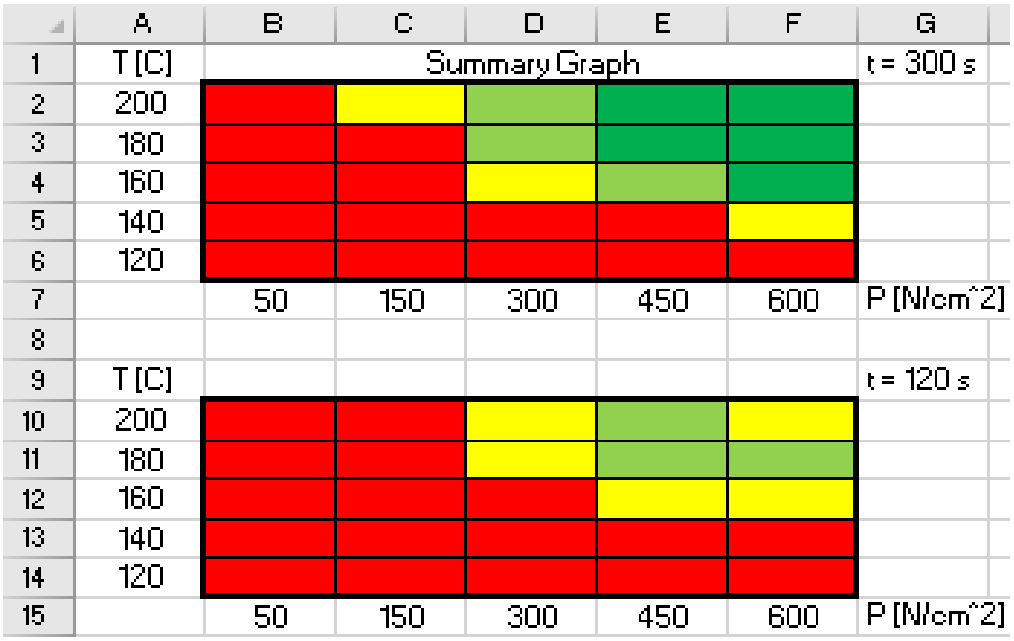

Figure 36: Process parameter space for M5: Supplier A anode and cathode with membrane D.

The membrane in this test is a hydrocarbon PEM, with a significantly different structure from PFSA PEMs and a measured glass transition at 188 °C. The minimum required temperature is correspondingly higher than for the other membranes. The pressure requirement also seems to be higher, and at the higher time level seems to be affected by the pressing temperature. At the lower time level, the transfer space is significantly smaller than for the higher time level.

The results for the M6 experiment, with membrane A and supplier A anode material but in-house produced cathode 1 material, are shown in Figure 37.

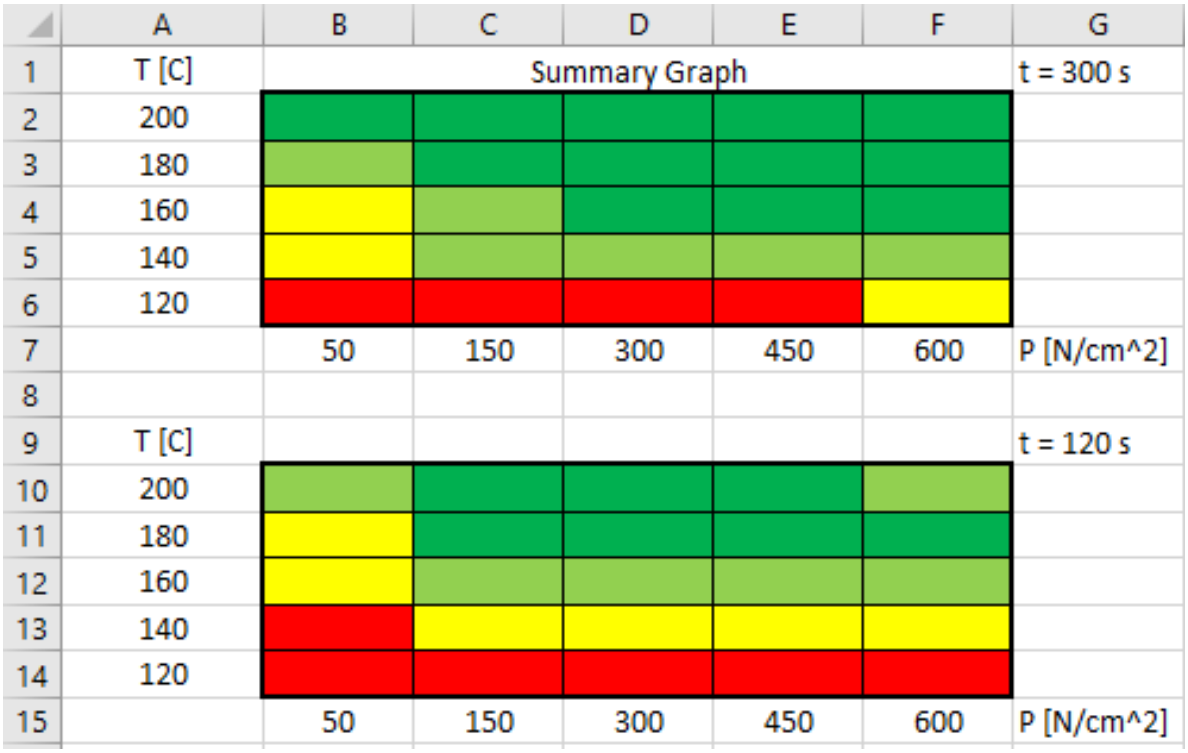

Figure 37: Process parameter space for M6: Supplier A anode and membrane A with in-house cathode 1.

The available processing parameters are like what was initially expected, with a minimum temperature requirement, which is lower for the lower time level, and a pressure requirement that is lowered with increasing temperature in both time levels.

6.3 Discussion

The expected results are as follows: It is expected that there is a minimum required temperature to achieve a successful transfer which is related to the glass transition temperature of the ionomer in the membrane. It is expected that below a minimum pressure, the compression force on the MEA will be too low and the transfer will either fail or be inconsistent. This pressure may be lower at higher temperatures as it may relate to the degree of softening of the membrane. The results from section 4.3 show that at the lower time level (t=120 s) most of the pressing time is spent below the set temperature and there should be a correlation between temperature and time whereby a longer time may allow for a lower temperature.

For the lower limit on the temperature, these expectations are met. Each matrix shows a hard limit temperature below which the transfer is unsuccessful, with the higher time level having this limit one step lower than the lower time. This makes sense, as the section 4.3 results indicate that at the lower time level, the MEA only barely reaches the desired temperature. There also seems to be a correlation with the glass transition temperature as expected. The test matrices with membrane A (Tg = 157 °C), membrane B (Tg = 162 °C) and membrane C – also a PFSA membrane which is expected to have a comparable Tg – all have the lowest transfer temperature at 140 °C for the longer time level and 160 °C for the shorter time. It does not, then, appear necessary to cross the glass transition temperature, though it does seem like the transfer temperature must approach the glass transition temperature for a successful result. The membrane seems to be softening sufficiently while somewhat below the Tg.

Also interesting is that some of the matrices, particularly M4, show a worse transfer at very high temperatures than at more moderate temperatures. This is especially clear at the lower time level. This could be a result of thermal ionomer degradation, but in that case the longer time level should show this behavior even more strongly than the lower time level. Another reason might be the decal substrate softening and having a stronger adhesion to the electrode, though this should also affect both temperature levels. The thermal-mechanical behavior of the membrane may warrant further investigation.

In most of the matrices, the pressure performed as expected, with very low pressures rarely performing well, and higher pressures performing better, so some pressure seems to be required. The limit of the pressure seems to be temperature dependent, though the higher time limit in the M2 experiment matrix is an exception, with higher temperatures enabling lower transfer pressures. This makes sense if the degree to which the ionomer softening increases with temperature. The link between the required pressure and the transfer time is considerably opaquer, however. M4 and M6 show little to no difference in the required pressure between the different time levels; M3 and M5 suggest that a longer transfer time may allow for lower pressures to function; and M2 suggests that having a shorter transfer time enables lower pressures. This last trend is particularly inexplicable. These contradictory trends are hard to parse, but overall, it seems that lower pressures are less consistent, and that the link between pressure and time is less pronounced compared to the link between pressure and temperature or temperature and time.

Time generally performs as expected. The shorter time level generally indicates a smaller available parameter space, and the transfer time is strongly linked to the transfer temperature. A time level near or above the glass transition seems to be a significant requirement for a successful transfer, and if it becomes necessary to reduce the time it takes to produce an MEA, it may be worthwhile to consider times between the values of 120 s and 300 s used here. If a more thermally conductive material is used for the pressure distribution pads, this would allow the temperature to more rapidly reach the set operating point. Another point of note is that many of the matrices at the lower time level had more light green results than the matrices at the longer time level – a longer pressing time seems to give more stable and consistent results.

There is a strong link between the available parameters and the materials used in the transfer. Both M2 and M6 use membrane A and supplier A anodes, but for M2 the cathode also comes from supplier A while for M6 the cathode was the in-house produced cathode 1. At the lower time level, the matrix is nearly identical, and the minimum temperature at the higher and lower time levels respectively is also the same. At the higher time level, the higher pressure regions of the graph are also very similar. At the lower pressure region, the transfer behavior of the M2 matrix with the supplier A cathode, was worse. The in-house cathode achieved better transfer results at low pressure and a long transfer time, which is very unexpected. This may be because the M2 matrix is unusual – none of the other matrices show a behavior where the low-pressure transfer is worse at the longer transfer time. Another possibility is that the in-house cathode had characteristics that favored the transfer at lower pressures, such as a rougher dispersion or catalyst particle size distribution. A more likely cause is that the higher I/Pt ratio of ionomer to catalyst in the in-house fabricated cathode (I/Pt = 1.0) compared to the supplier A cathode (I/Pt = 0.9) enabled these low-pressure transfers. In this case, it may be worth investigating in more detail the effects of I/Pt on the available transfer space.

M2, M3 and M4 all use supplier A anode and cathode, but different PFSA membranes (A, B and C respectively). We have already seen how the similar glass transition temperatures of the PFSA membranes explain the similar lower temperature bounds. Except for the longer time level of M2, they show a similar pressure limit that increases with temperature. Of note is that M3 and particularly

M4 show a worse performance at very high temperatures, particularly at the lower time level. This behavior does not seem to be related to the side chain length of the membrane's ionomer or to the thickness of the membrane, as in these cases matrix M2 (using membrane A) should show worse transfer at very high temperatures than M3 (using membrane B) which is not the case. It is possible this may be a result of different thermomechanical behavior or due to differences in the membrane's reinforcement material. Different materials seem to have different requirements for their transfer time, which may be a result of them softening to different degrees.

M5 uses a membrane D, a hydrocarbon PEM with a glass transition temperature at 188 °C. The lower bounds for the temperature are accordingly higher than for the test matrices with PFSA membranes, at 160 and 180 °C for the higher and lower time levels respectively. The membrane also requires higher pressures than the PFSA membranes to transfer well. Such significant differences are expected, as the HC ionomer has a fundamentally different structure compared to PFSA ionomers. The higher temperature required may make it difficult to pair with PFSA ionomer catalysts if those catalysts have low degradation temperatures.

6.4 Conclusion

The materials used in the decal transfer, particularly the membrane, play a significant role in determining what operating points are favorable. Of particular importance seem to be the I/Pt ratios of the catalyst and the glass transition temperature of the membrane. The glass transition of the ionomer in the catalyst layers is also likely to be significant, but is not examined closely here.

Some general trends can also be established for the influence of the transfer parameters. The temperature has a minimum value which must be met for a successful transfer. If the transfer time is only barely enough for the temperature to be met, then the required temperature will be higher. Very high temperatures can result in worse transfers, however. Higher pressures favor a complete, successful transfer, though higher temperatures can allow for lower pressures. This is very dependent on the material configuration, and it may be that, within reason, more pressure is better. The transfer time must, of course, be sufficient for the actual MEA temperature to reach the necessary levels, which is influenced by factors such as the thermal resistance of the pressure distribution pads, but more consistent results can be achieved with sufficiently long pressing time.

Overall, an understanding of the available parameter space within which a successful transfer can be consistently achieved has been reached, and some of the design rules for MEA production illuminated. This should serve as a good foundation for in-situ performance measurements.

7 Performance of the MEAs

It is crucial to understand the effects of the decal transfer processing parameters and the materials the MEA is made of on cell performance. The results from chapter 6, which show the available transfer space for the different materials, are used to inform the operating points at which MEAs are produced for in-situ testing.

As it is necessary to have a general understanding of the variance for these tests, a qualitative statistical evaluation with five repeats is performed. The results from this should give an indication of what overall variance can be expected from all sources of error.

In-situ measurements are also done for the series stacking experiment described in chapter 4.4, which should identify any trends across the stack. As the nominal operating conditions used in this test correspond to the operating point used in the statistical repeats, a comparison may be useful here.

The effects of the processing parameters are evaluated in the form of a 2^3 experimental matrix for the processing parameters (temperature, pressure and time) based on the processing parameters that provide a good transfer result found in chapter 6.

A single operating point was chosen for a comparison of the different materials based on those processing parameters.

7.1 Experiment Description

The in-situ measurements were performed as described in chapter 2.4.3, with each test beginning with a membrane conditioning step at high relative humidity before the EIS and polarization curves were measured at normal operating conditions. HFR was used continuously during the conditioning and polarization curve measuring. In order to more efficiently use testing resources, a reduced polarization curve with five current densities was measured for the statistical repeats. The series stacking tests do not include an EIS measurement for the same reason.

The statistical evaluation was performed at the operating point D4 (T = 160 °C, p = 300 N/cm^2, t = 300 s) using membrane A and supplier A anode and cathode material (‘M2’ material). Five independent repeats were made, each using different sheets of anode and cathode. This should give a variance that encompasses most sources of error, including differences in the electrode material, variations in the processing conditions such as the ambient, weather-driven humidity and any variance in the testing conditions. Variation by season was not considered but is expected to be negligible.

The series stacking experiment described in chapter 4.4 was performed for a stack of nine MEAs, numbered 1-9 from the bottom to the top of the stack as shown in Figure 38. In-situ measurements are run on MEAs 1, 3, 5, 7 and 9, however the measurement of MEA 7 failed due to a leak in the sub gasket. The MEAs all used membrane A and supplier A anode and cathode material. The electrode material was taken from the same sheet for each MEA in the series stack.

Figure 38: Experimental setup of the MEAs in the series stacking experiment for in-situ performance testing.

The 2^3 experiment matrix of measurements to investigate the effects of processing parameters was developed from the M2 matrix result, and the MEAs in question correspondingly use membrane A and supplier A anode and cathode material. The 2^3 experiment uses temperature levels of 160 and 200 °C, pressure levels of 300 and 600 N/cm^2, and transfer time levels of 120 and 300 s respectively. Figure 39 shows the operating points at which measurements were conducted. Operating point D4 has five measurements because this is the operating point at which measurements for the statistical evaluation were taken. Operating point C4 was measured before the investigation of the M2 parameter space was complete, as it was deemed more important to proceed quickly with in-situ measurements rather than wait for the full range of known operating points to be known. Operating point E3 was measured for the comparison of materials.

	A	B	C	D	E	F	G
1	T [C]	Summary Graph					t = 300 s
2	200			1		1	
3	180				1		
4	160		1	5		1	
5	140						
6	120						
7		50	150	300	450	600	P [N/cm^2]
8							
9	T [C]						t = 120 s
10	200			1		1	
11	180						
12	160			1		1	
13	140						
14	120						
15		50	150	300	450	600	P [N/cm^2]

Figure 39: Measurement points for the in-situ performance investigation of process parameters.

A single operating point was chosen to compare the different materials used in M2, M3, M4, M5 and M6. Operating point E3 was chosen as a point that exhibits a good transfer quality for each set of materials (see chapter 6).

7.2 Statistical Evaluation: Results and Discussion

Figure 40 shows the polarization curves for the five MEAs of the statistical evaluation. Only the portion of the polarization curve at outset of 1.5 A/cm^2 constant current is shown.

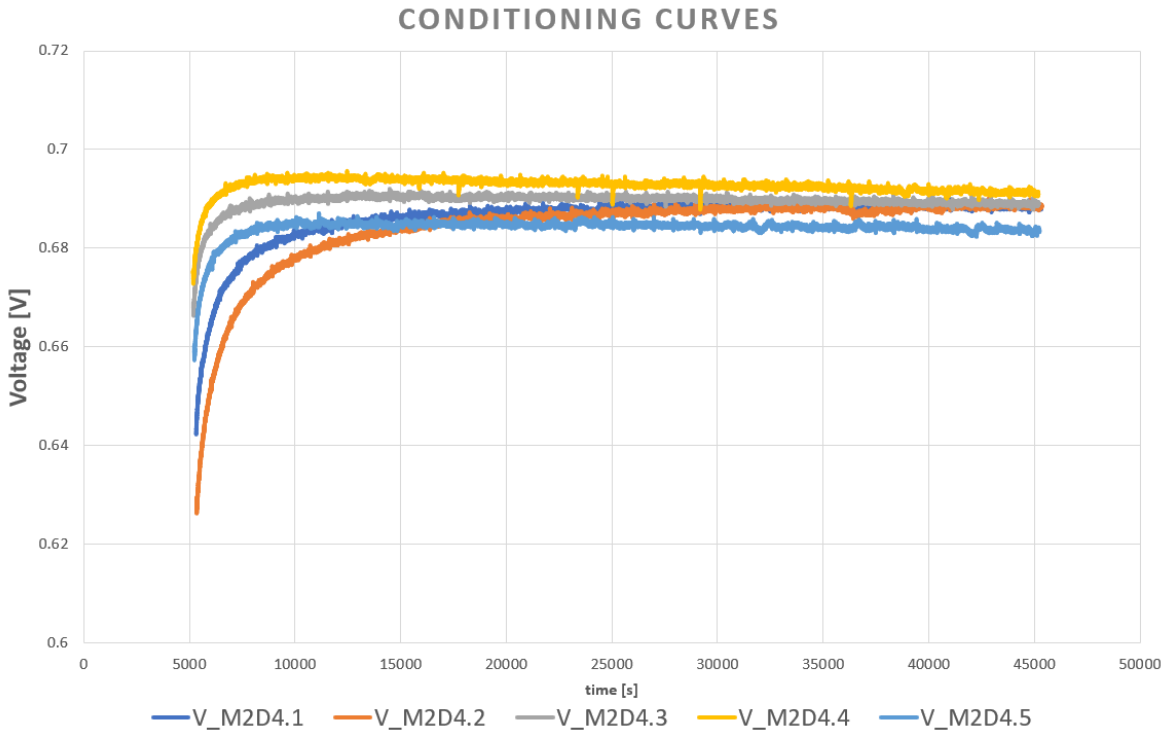

Figure 40: Polarization curves for the five statistical repeats at operating point M2D4.

Each of the MEAs shows the expected logarithmic increase initially, with most of the MEAs quickly assuming a steady level. The exception is M2D4.4, which shows a slight decrease in potential along the course of the conditioning. In this case the decrease is minor enough to not present a significant concern. The deviation of the final average conditioning values is around 8 mV. Looking at the initial behavior of the MEAs, there is a significant difference - M2D4.1 and M2D4.2 have a much slower increase in their voltage. This indicates a much smaller water uptake in the MEA. These two MEAs were produced several weeks before the later ones, so this could indicate a different initial humidification in the membrane, which is not stored under climate controlled conditions. It could also be an indication that the catalyst material these two MEAs were produced from had differences affecting the water uptake. These two MEAs were produced with cathode material from the batch with a measured I/Pt of 0.27, while the remaining MEAs used cathode material from the other batch, which had a measured I/Pt of 0.24 (see chapter 2.5.2).

Figure 41 shows the HFR and EIS resistance values for the MEAs in the statistical evaluation.

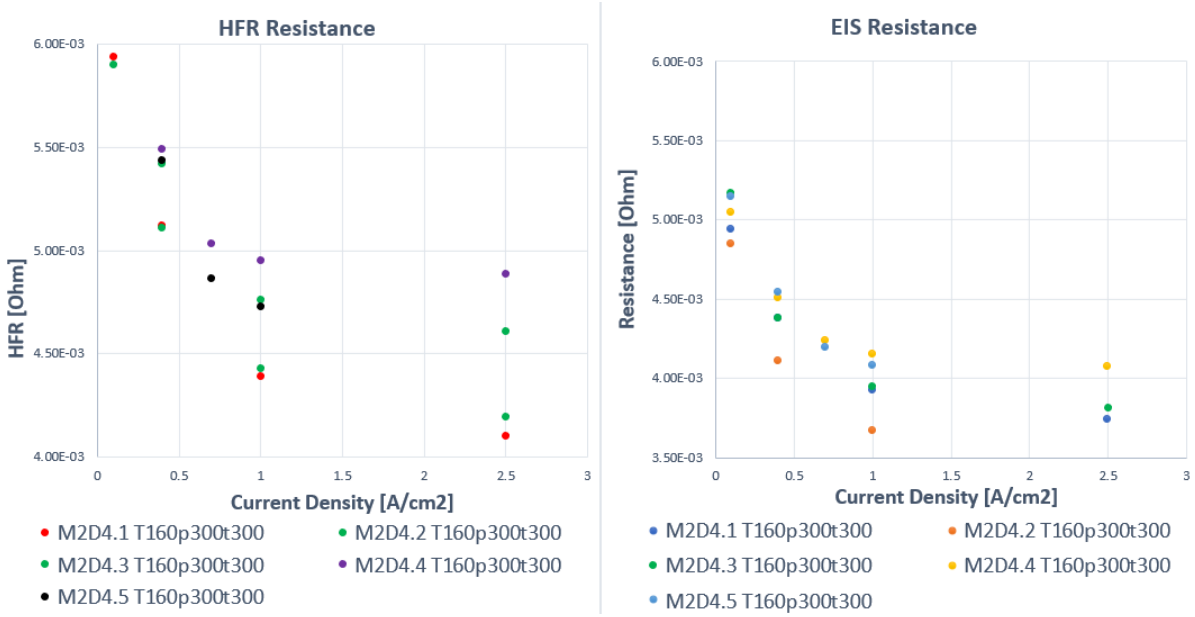

Figure 41: EIS and HFR resistance values for the statistical repeats.

This is a very high variance in the resistance as measured by EIS as well as HFR, showing that the resistance variance from all sources, including the specific sheet of the cathode, differences in the testing conditions, ambient humidity during assembly etc. is very high. Of note is that the order of the resistance is not constant between the two methods, which is particularly evident looking at the results for M2D4.1 (red) and M2D4.2 (green). The expectation is that there is a constant offset between the EIS and HFR resistances, which is not the case here. There may be a variation in the testing conditions between when the HFR and EIS measurements take place. Table 3 shows the average resistance at 1.0 A/cm^2 for both EIS and HFR measurements along with the standard deviation σ. The relative deviation is comparable, so it may be preferable to rely on HFR values as they can be recorded in parallel to polarization curve measurements.

Table 3: Average and standard deviation of the HFR and EIS resistance for the five statistical repeats at 1.0 A/cm^2.

[Ohm]	HFR	EIS
Average	4.65E-03	3.95E-03
σ	2.12E-04	1.66E-04
σ_rel	4.56%	4.20%

For the statistical evaluation, a reduced polarization curve was used, with measurements at 0.1, 0.4, 0.7, 1.0 and 2.5 A/cm^2. This is shown in Figure 42. Because these measurements were among the earliest taken for this thesis, the testing protocol was not fully complete for some measurements, which is why not all the MEAs have data points at 0.7 A/cm^2.

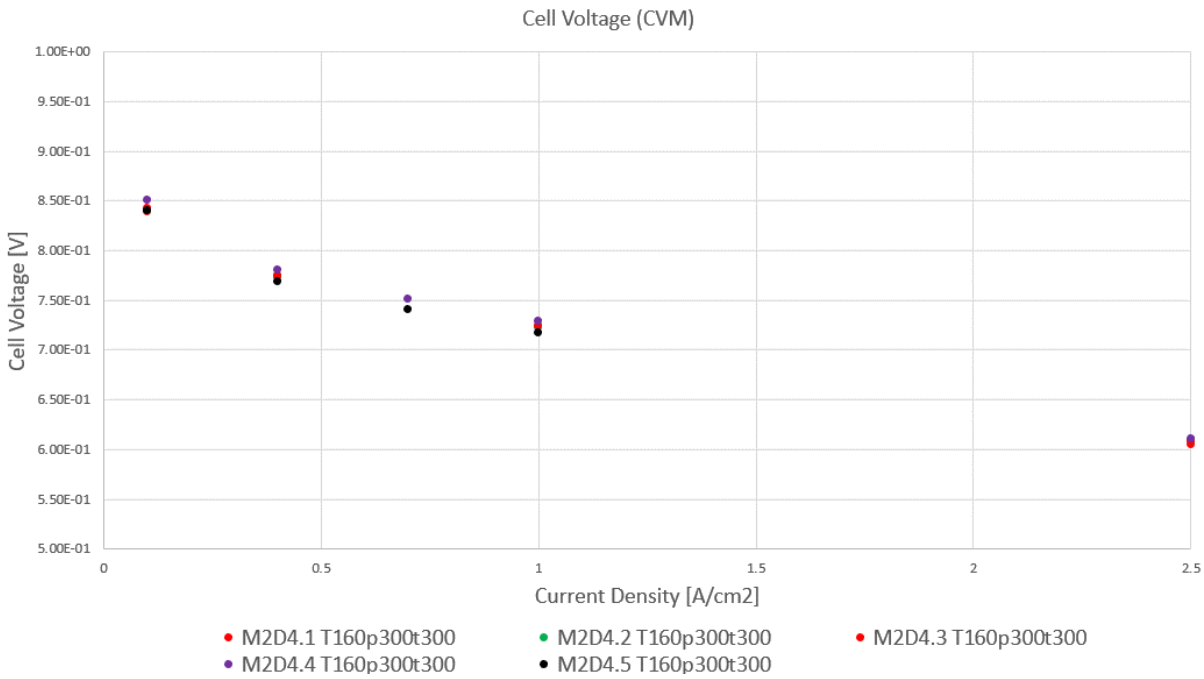

Figure 42: Reduced polarization curve for the statistical evaluation.

More information can be gained by looking at the three regions of the polarization curve. Compared to the resistance values, the polarization curve has a much smaller relative deviation, as seen in Table 4.

Table 4: Average and standard deviation of the polarization curve voltage for the five statistical repeats at 1.0 A/cm².

[V]	Voltage
Average	7.23E-01
σ	2.12E-04
σ_rel	0.03%

The kinetic point at 0.1 A/cm² shows a comparable deviation to the rest of the curve, indicating that a significant portion of the variance in the polarization curve comes from differences in the reaction kinetics. As the reaction kinetics are dominated by the cathode, this implies a variance in the behavior of the cathode material. The polarization curves are normalized to the kinetic point in Figure 43 to allow for a better evaluation of the ohmic and mass transport regions.

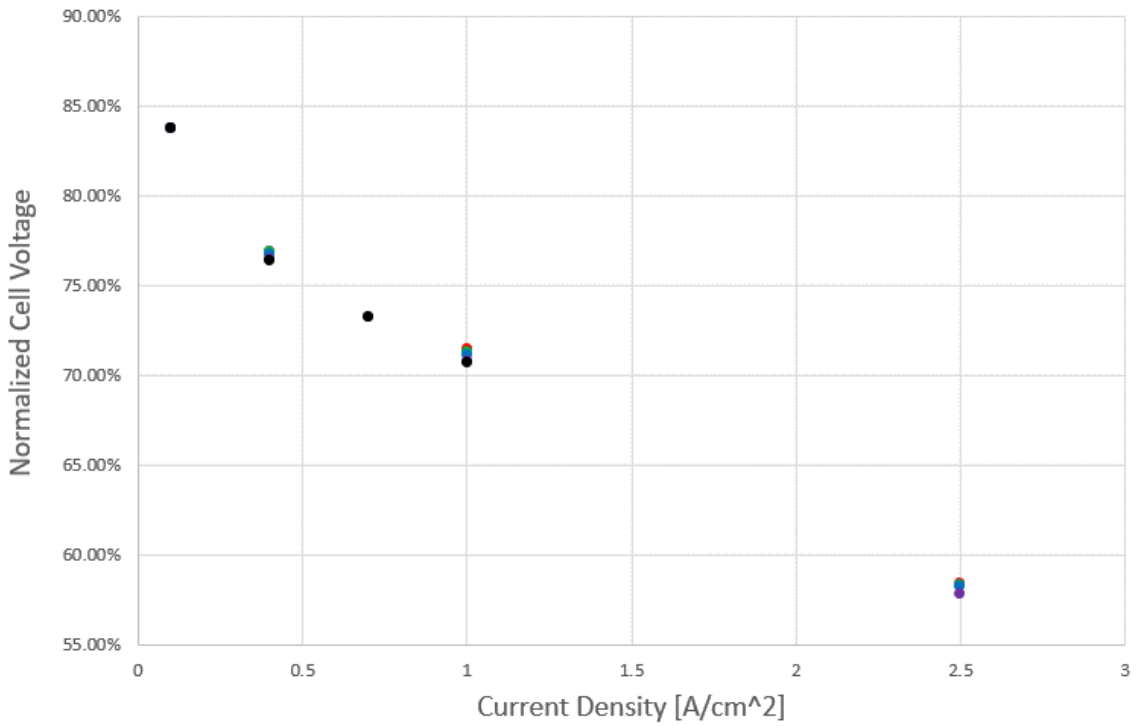

Figure 43: Reduced polarization curve for the statistical evaluation, normalized to the kinetic point.

Looking at 1.0 A/cm^2, it appears that the remaining deviation comes from the ohmic region. This is a combination of the resistances across the membrane, electrodes, gas diffusion layer and the various interfaces. Variations in the proton conduction resistance across the membrane correlate to differences in the hydration of the membrane, which could be explained by the differences in the water uptake behavior observed in the conditioning curves.

Overall, the polarization curve shows a much narrower deviation window than the HFR or EIS resistances, and the conditioning behavior suggests that we must consider differences in the water uptake between different MEAs.

7.3 Series Stack Performance: Results and Discussion

Figure 44 shows the conditioning curves for the MEAs in the series stacking experiment.

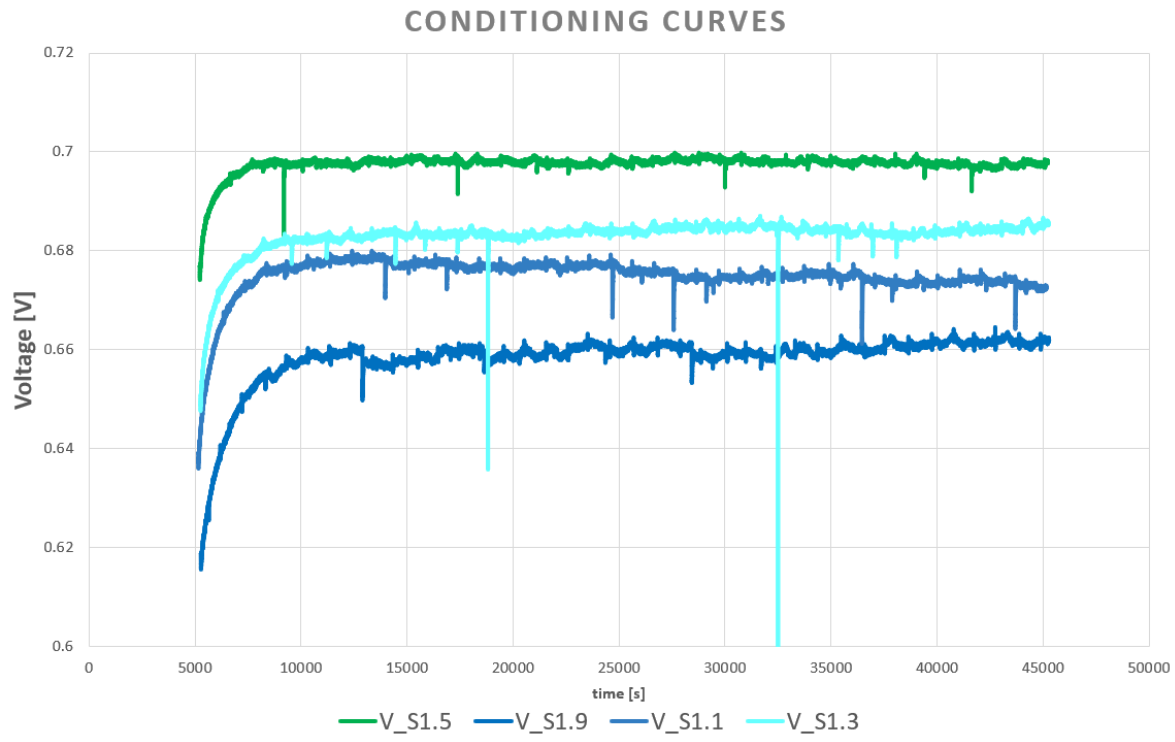

Figure 44: Conditioning curves for the series stack in-situ experiments.

All the curves reach a steady voltage, and all have a comparably rapid initial ascent of the curve. Of note is that the final voltage reached is highest for the central MEA, S1.5, and lowest for the outer MEAs, S1.1 and S1.9.

Figure 45 shows the HFR for the series stack.

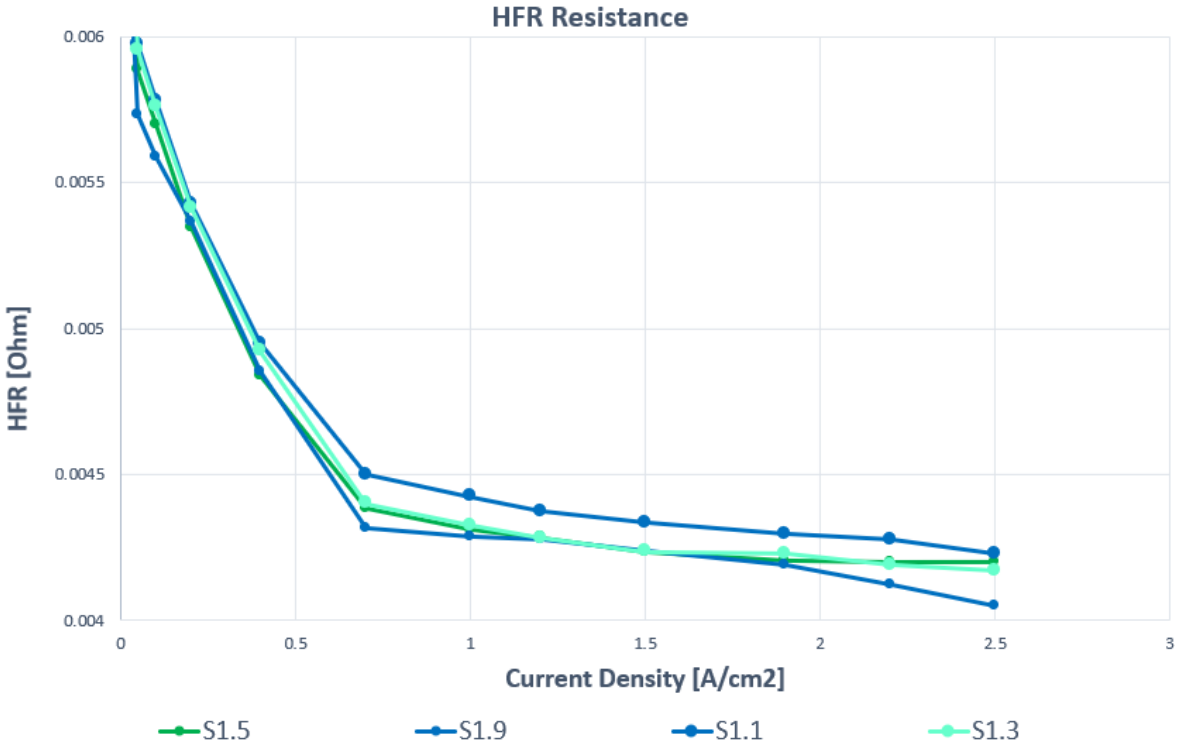

Figure 45: HFR for the series stack experiments.

The resistances are much closer than the resistances in the statistical evaluation. This is described numerically in Table 5. The series stacking experiment uses the same anode and cathode sheet for each MEA, so that any variations resulting from differences in the electrode material should be much smaller, even as the greater thermal resistance across the stack should result in a greater variety of transfer temperatures between the series stack MEAs. That we still get a smaller deviation suggests that the greatest source of error in the statistical evaluation may have come from inconsistencies in the electrode material. This reduced error makes it difficult to analyze the resistance values here. One point of interest is that besides the deviation, the average resistances are lower in this experiment than they were in the statistical evaluation.

Table 5: Average and standard deviation of the HFR for the five series stacking at 1.0 A/cm².

[Ohm]	HFR
Average	4.34E+00
σ	5.22E-02
σ_rel	1.20%

Figure 46 shows the polarization curves for the series stack experiment. Note that the OCV of MEA 9 is lower than the others, as this shifts that MEA down relative to the others. As the OCV is still well above 0.9, this does not indicate a tightness problem. Figure 47 shows the polarization curve normalized in the kinetic point.

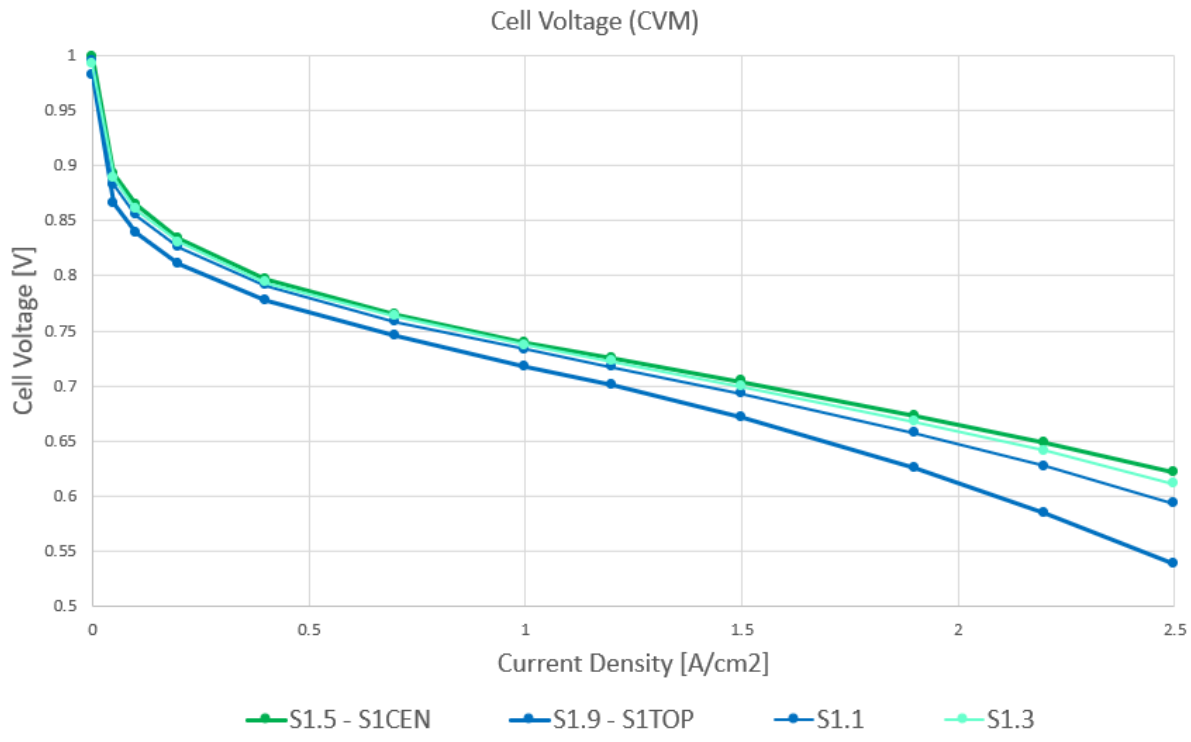

Figure 46: Polarization curve for the series stack tests.

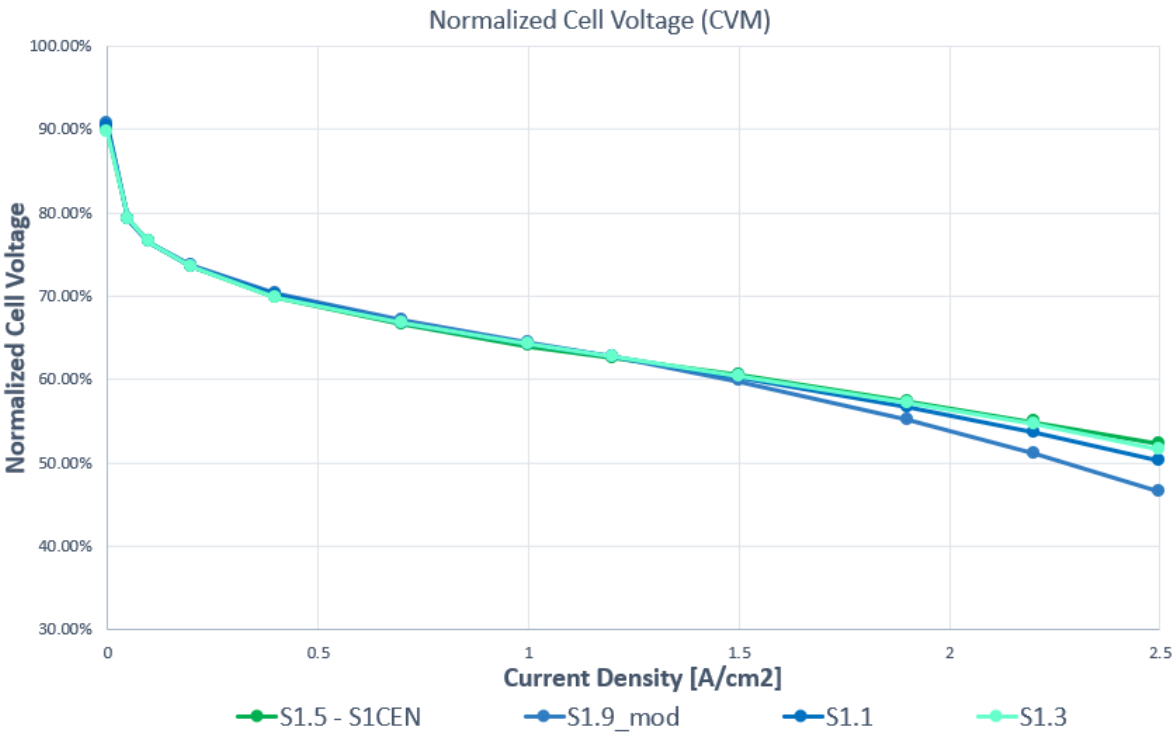

Figure 47: Normalized polarization curve for the series stack tests.

In the kinetic region and ohmic regions, these curves are very similar. It is in the mass transport region that the curves begin to divide, as is particularly clear in the normalized curve. The results show the greatest decrease in the mass transport region for the top MEA (S1.9) with some distance to the remaining three, of which the bottom MEA (S1.1) performs worst and the central MEA (S1.5) performs best. There appears to be a gradient by which the MEAs in the center, which face the greatest thermal resistance and thus have the slowest temperature response, perform the best in the mass transport region. This could be because the additional time spent at a higher temperature either affects the ionomer degradation or the state of hydration in the MEA. Another possibility is that the rate of change in temperature of the MEA is decisive. The glass transition of an ionomer is a complex phenomenon, which occurs here in a composite system with many components at high pressure. Many phase transitions are very dependent on the rate of change of temperature. If this is the case, then both the initial heating and final cooling cycles of the transfer process may present opportunities for tuning and optimization.

7.4 Processing parameters: Conditioning Curve Screening

For the investigation of the processing parameters, one of the repeated MEAs from the statistical evaluation must be chosen. The results of M2D4.3 were taken for this role as a collective median between the polarization and conditioning curves as well as the HFR and EIS resistances. The matrix shown in Figure 39 for the experiment overview then only uses a single result from the five in operating point D4.

Figure 48 shows the conditioning curves of these MEAs.

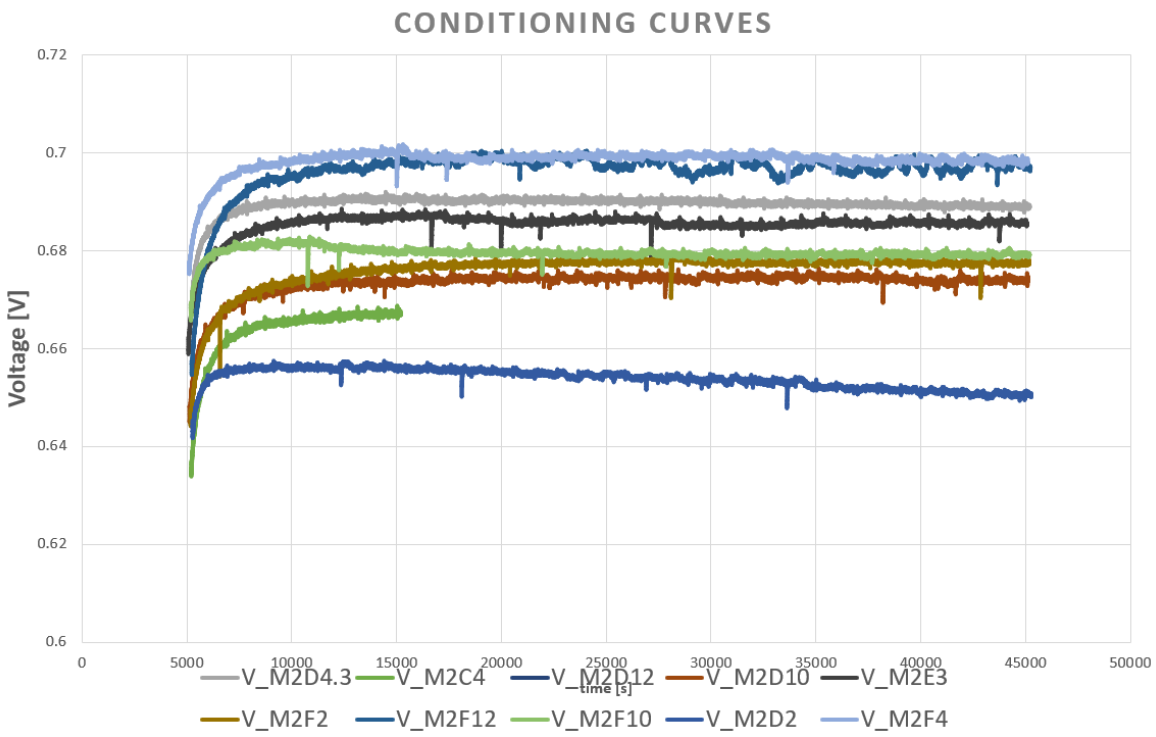

Figure 48: Conditioning curves of the MEAs used for the 2^k factorial investigation of process parameters.

The M2D12 MEA is a problem, as it sees no voltage increase, and instead a decrease, and does not reach a constant voltage. This may be because of physical damage to the MEA, during testing or storage. Of the other MEAs, M2D2 has a decrease in voltage along the conditioning. However, this is very slight, and M2F4 has high voltage fluctuations during the conditioning. This is not sufficient to screen out these results, however.

Figure 49 shows the EIS resistance data and Figure 50 the HFR data for the process parameter evaluation, with the higher time level presented on the left, and the lower time level on the right. The higher pressure level is colored blue and the lower pressure level green. The higher temperature level is the lighter shade, and the lower temperature level the deeper shade. Note that due to a problem with the testing equipment at the time of measurement, HFR data for M2F4 is not available.

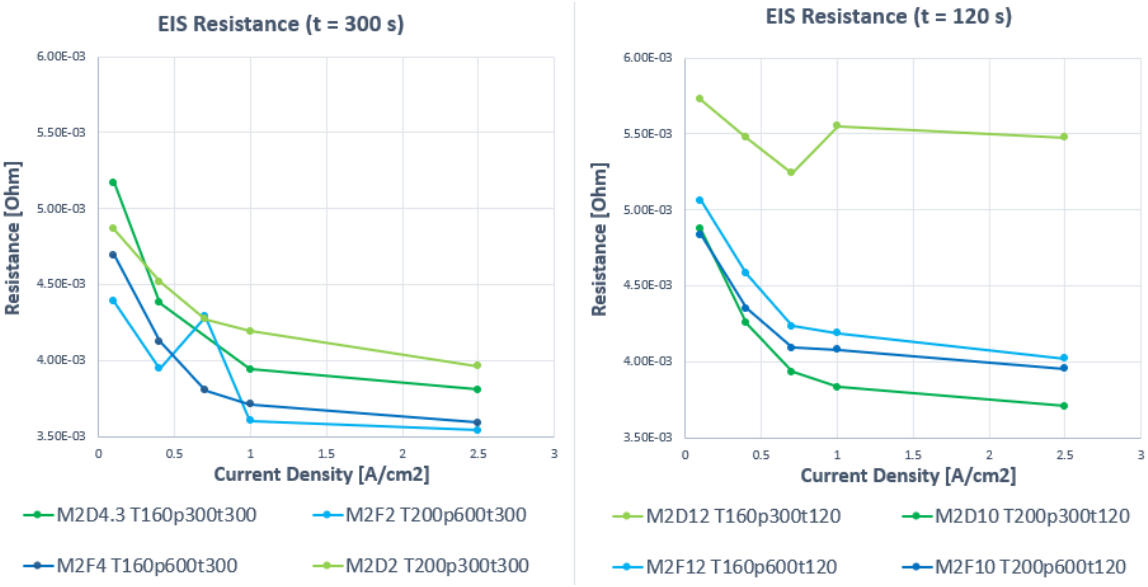

Figure 49: EIS resistance data for evaluating processing parameters.

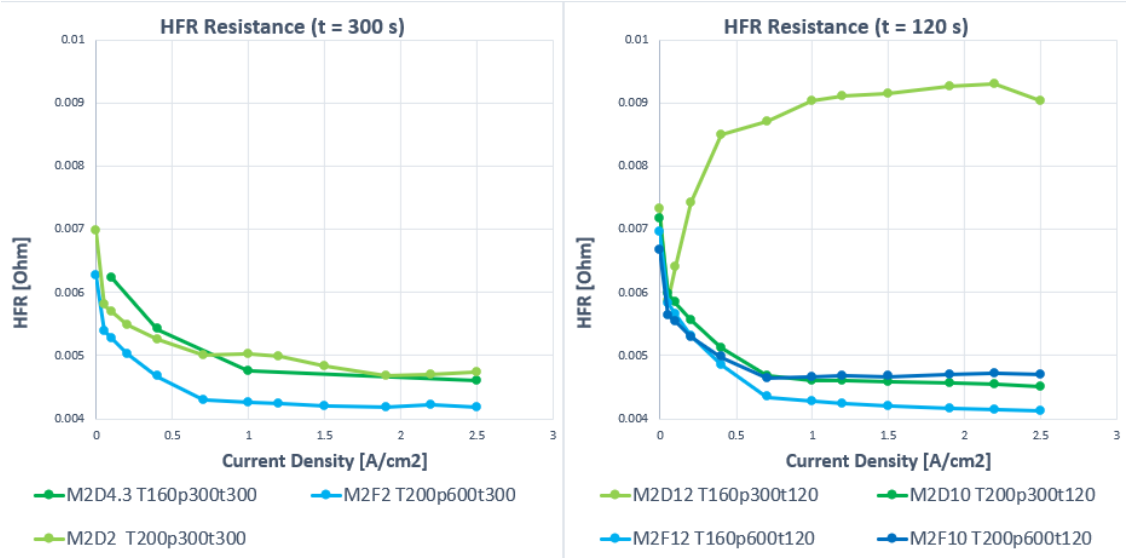

Figure 50: HFR data for evaluating processing parameters.

M2D12, the dark green curve at the t=120 s time level, is the MEA that was identified previously from the conditioning behavior as problematic. This is seen here again, as the EIS resistance is considerably higher than that of any of the other MEAs and shows an increase between 0.7 and 1.0 A/cm^2, which should not be the case for a properly functioning MEA, and the HFR values show an increasing resistance with current density. It is possible that some damage occurred between these measurements. The M2F2 MEA, light blue at the t = 300 s time level, also shows a jump. However, this is an isolated value and is more likely due to a change in testing conditions at the time of measurement.

Except for the faulty M2D12 MEA and the jump in the EIS curve for MEA M2F2, the curves look as expected. Resistance values are mainly useful here to give information on the ohmic region of the cell performance, so the resistance at 1.0 A/cm^2 is particularly interesting. The values, however, make it difficult to identify clear trends, particularly considering the high deviation found in the statistical evaluation, as the differences visible here are comparable in scale to those found in the statistical

repeats. The differences between the EIS and HFR curves is attributed to the difference in the testing history as they were not measured at the same time.

More information can be obtained from the polarization curves, which can be connected to the resistances as the slope of a polarization curve in the ohmic region corresponds to the resistance of the cell. It is useful to look at the variation of one parameter at a time. Figure 51 shows the polarization curves as the transfer temperature is changed. Each graph in the figure shows the lower transfer temperature (160 °C) in blue and the higher transfer temperature (200 °C) in green while keeping the transfer pressure and time constant. Note that some of the polarization curves were recorded before the testing protocol was fully established, and therefore have fewer recorded data points.

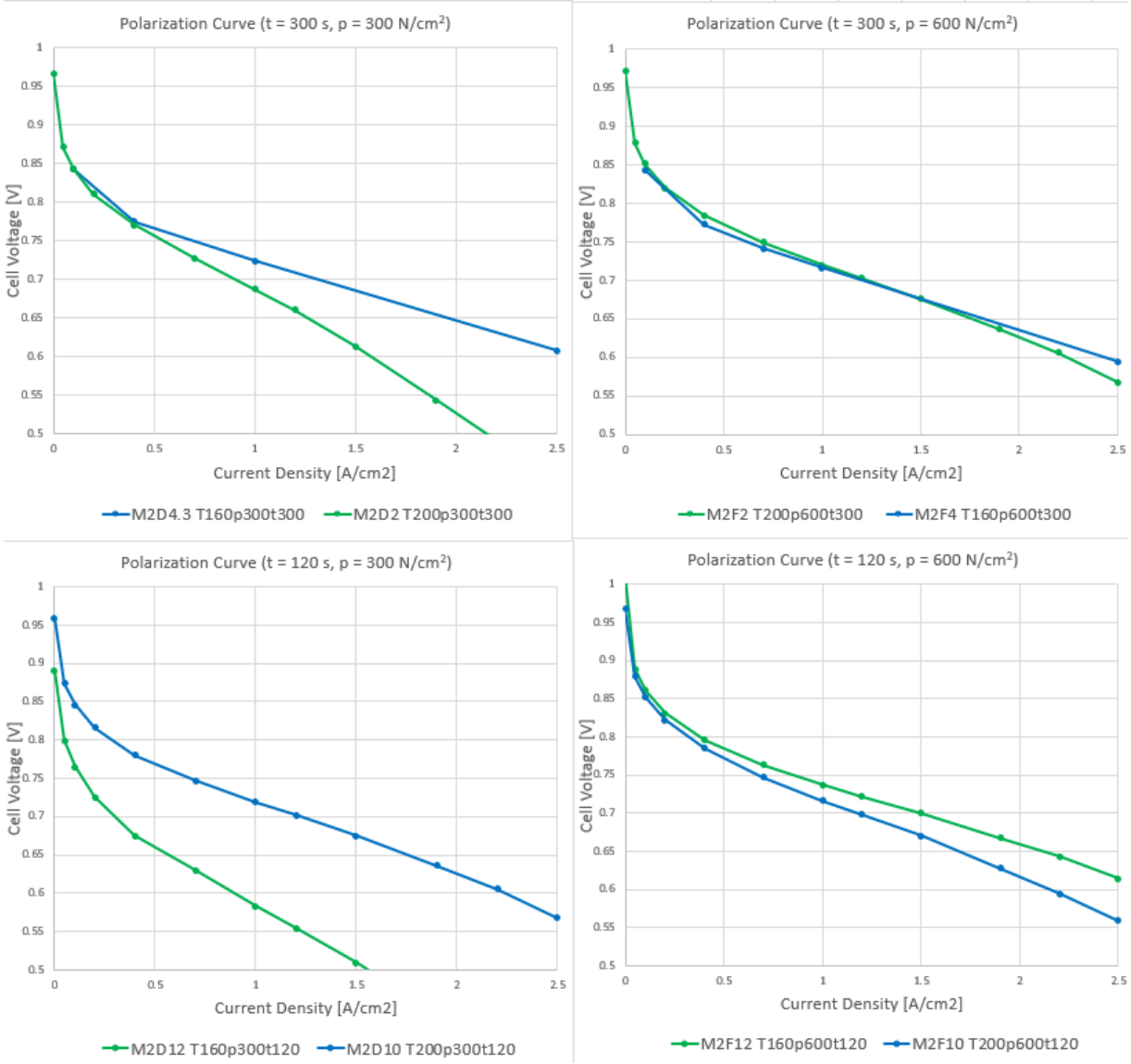

Figure 51: Polarization curves for the variation of transfer temperature.

M2D12 is the only polarization curve with an OCV below 0.9. This MEA was previously identified as faulty, and this low OCV indicates a 'tightness' problem where the MEA has excessive fuel crossover, supporting the idea that the MEA may have suffered minor damage. The other curves show a consistent trend where the MEA produced at higher temperature has a comparable kinetic performance to the MEA produced at lower temperature, which is expected as the kinetic region is mainly driven by cathode-side reaction kinetics and the electrodes are the same. There is a steeper

slope in the ohmic region around 1.0 A/cm^2, indicating worse performance here. This is particularly pronounced in the top left graph, where the MEAs are produced at the longer time level (300 s) and lower pressure (300 N/cm^2). Both graphs with MEAs processed at higher pressure show a much smaller difference in the ohmic region slope. This can be seen in the mass transport region as well, where the low time and pressure graph sees a much greater divergence than either of the graphs where the MEAs were produced at high pressure.

We can therefore conclude that, while there is a minimum to the transfer temperature below which the transfer is not complete, raising the temperature further does not improve results, and indeed seems to harm the performance of the MEA, either due to problems with ionomer degradation or hydration. This behavior seems to be reduced at higher pressures.

Figure 52 shows the polarization curves as the transfer pressure is changed. Each graph in the figure shows the lower transfer pressure (300 N/cm^2) in blue and the higher transfer pressure (300 N/cm^2) in green while keeping the transfer temperature and time constant.

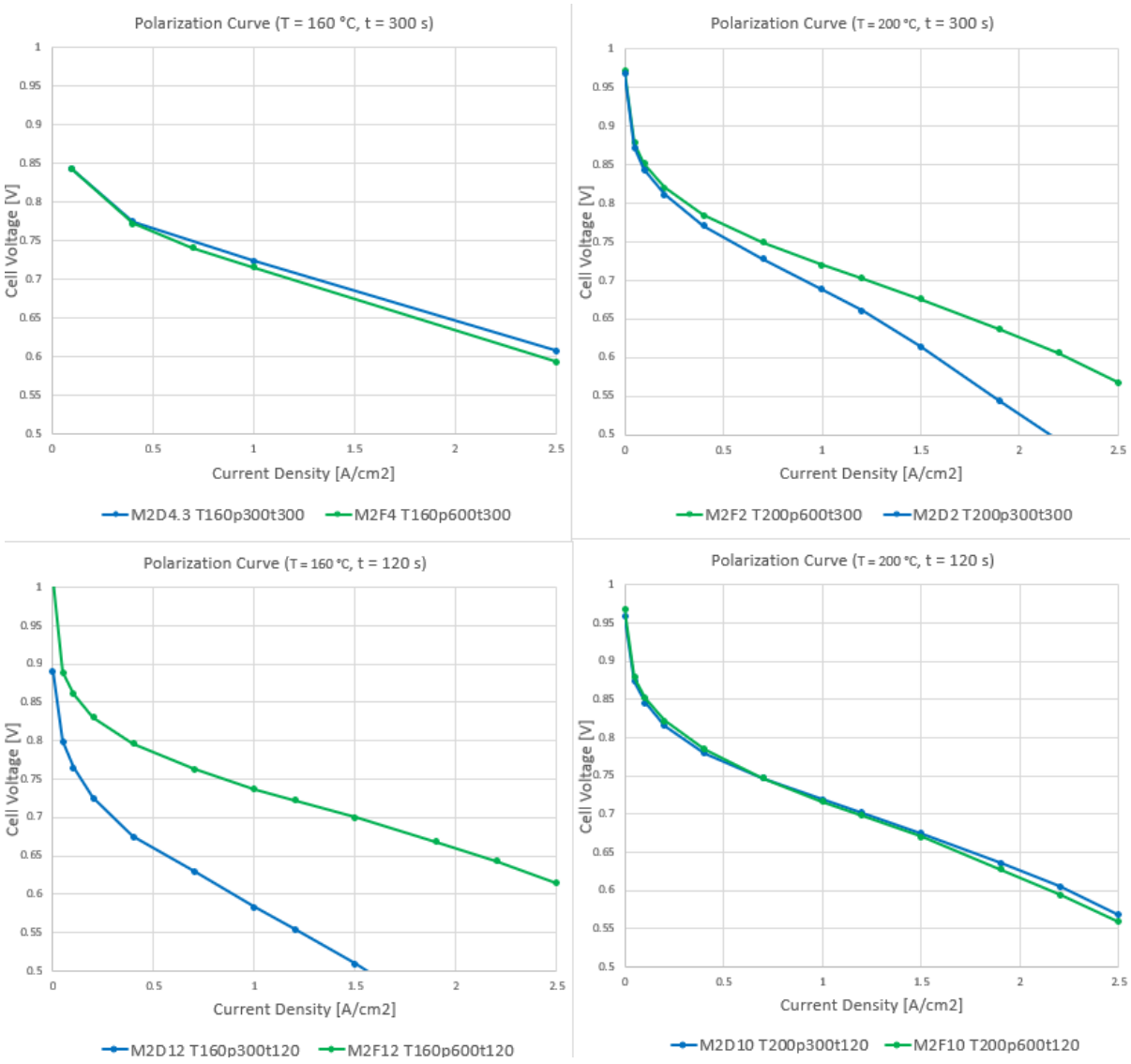

Figure 52: Polarization curves for the variation of transfer pressure.

The lower left graph is again not useful due to the faulty MEA M2D12. In all the other graphs, the kinetic region is very similar between the two pressures, as is expected. Two of the other graphs, at

the lower temperature and higher time level and at the higher temperature and lower time level, show very similar polarization curves across the kinetic, ohmic and mass transport regions. In the third, at the higher temperature and time levels, the polarization curve of the MEA produced under greater pressure shows better performance in the ohmic and mass transport regions, suggesting that the detrimental effects from the higher transfer temperature discussed earlier may have less of an effect at higher transfer pressure.

This is not sufficient to suggest that a higher transfer pressure is inherently beneficial to the performance of the MEA, but it does demonstrate that, in the pressure region examined here, a higher transfer pressure does not negatively impact the performance. Literature examining the transfer pressure up to 1000 N/cm^2 has found that the ohmic resistance continues to increase with higher pressures during transfer, but that this sees diminishing returns such that beyond 600 N/cm^2 the difference is negligible [10]. The behavior observed here seems to support that observation.

Figure 53 shows the polarization curves as the transfer time is changed. Each graph in the figure shows the lower transfer time (120 s) in blue and the transfer higher time (300 s) in green while keeping the transfer temperature and time constant.

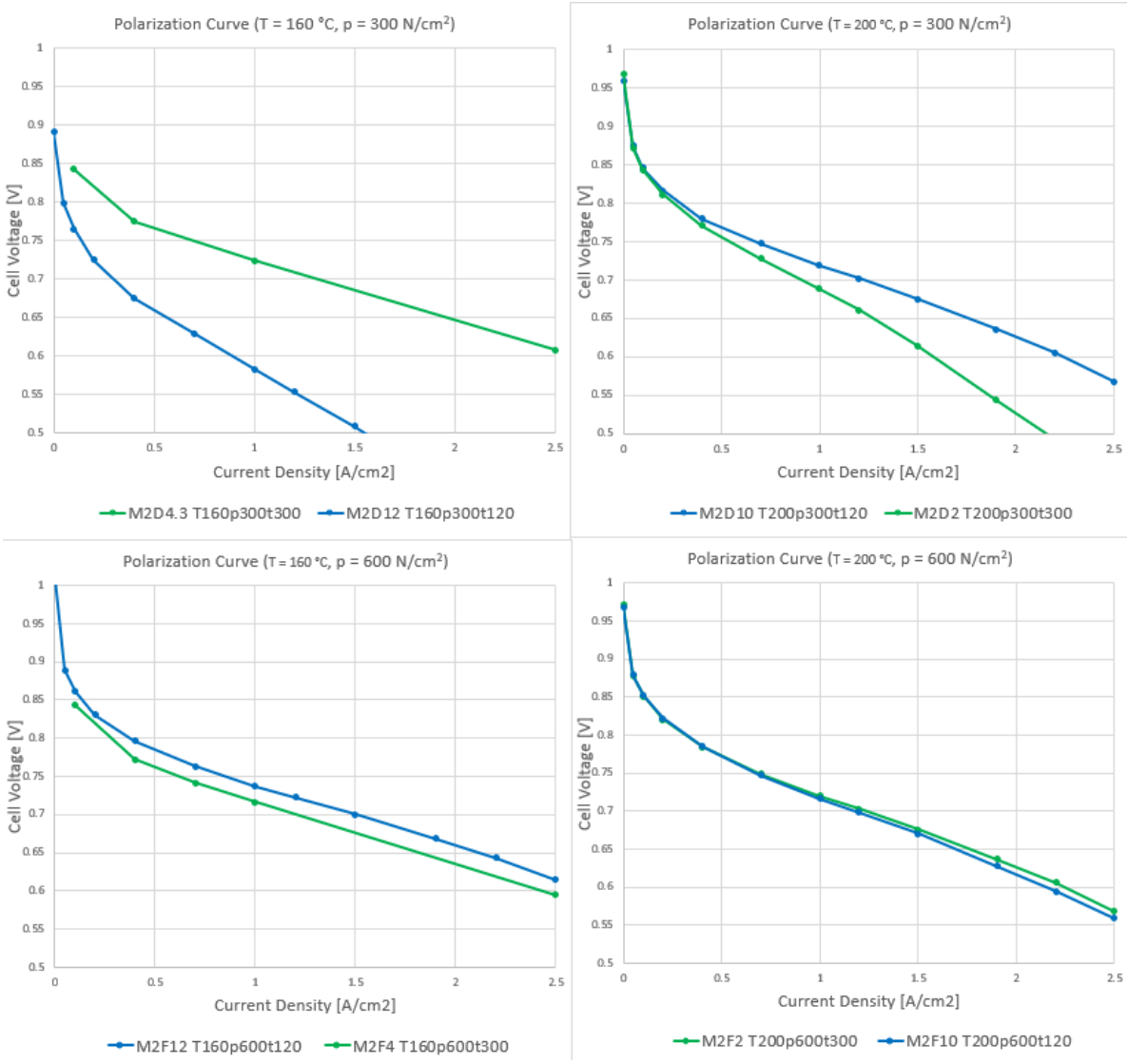

Figure 53: Polarization curves for the variation of transfer time.

An analysis of the transfer time must take into account the results from chapter 4.3, which shows that at the lower time level the set transfer temperature is only barely reached. Discounting the top left graph as it contains the faulty M2D12 MEA, it seems that the MEAs produced at higher pressure have very similar behavior. In the bottom right, the MEAs produced at high temperature and pressure have very similar polarization curves, particularly in the kinetic and ohmic regions. In the bottom left, at high transfer presure and lower transfer temperature, the MEA produced at a longer transfer time seems to show lower performance – this is , however, a straight shift downwards, suggesting that this is merely a difference in the OCV and tightness of the MEA, and the ohmic and mass transport behavior are very close. At high temperature and lower pressure, the polarization curves diverge in the ohmic and mas transport regions, showing a major effect of the processing time. Interestingly, it is the lower transfer time that provides better results. This speaks to effects from ionomer degradation or dehydration rather than an insufficiently developed interface, as in this case a longer transfer time should be beneficial.

Overall, the transfer time is difficult to analyze. It appears to be dependent on pressure, with higher pressure leading to closer results between the two time levels. It is clear that the lower time level can produce MEAs with comparable or superior performance to the higher time level, though the results from the parameter spacing suggest that the lower time level is less consistent, particularly at low temperatures which are prefered. This is easily explicable by the results from chapter 4.3, as the set temperature is only barely achieved at t = 120 s. A lower bound for the transfer time of 120 s can be established as this is the requisite time to reach the set temperature, and as some MEAs produced at this time level perform comparably to those transferred for 300 s, it can be concluded that the higher time level is over dimensioned. It may be worth investigating slightly longer times, such as t = 180 s, which may show more consistent results while cutting down on transfer time.

Overall, the best results (shown in Figure 54) were reached by M2F12 (blue, with a pressing temperature of 160 °C, a pressing time of 120 s and a pressure of 600 N/cm^2), M2F4 (green, with a pressing temperature of 160 °C, a pressing time of 300 s and a pressure of 600 N/cm^2) and M2D4 (red, with a pressing temperature of 160 °C, a pressing time of 300 s and a pressure of 300 N/cm^2). M2E3 (black, with a pressing temperature of 180 °C, a pressing time of 300 s and a pressure of 450 N/cm^2) is the operating point used when varying materials.

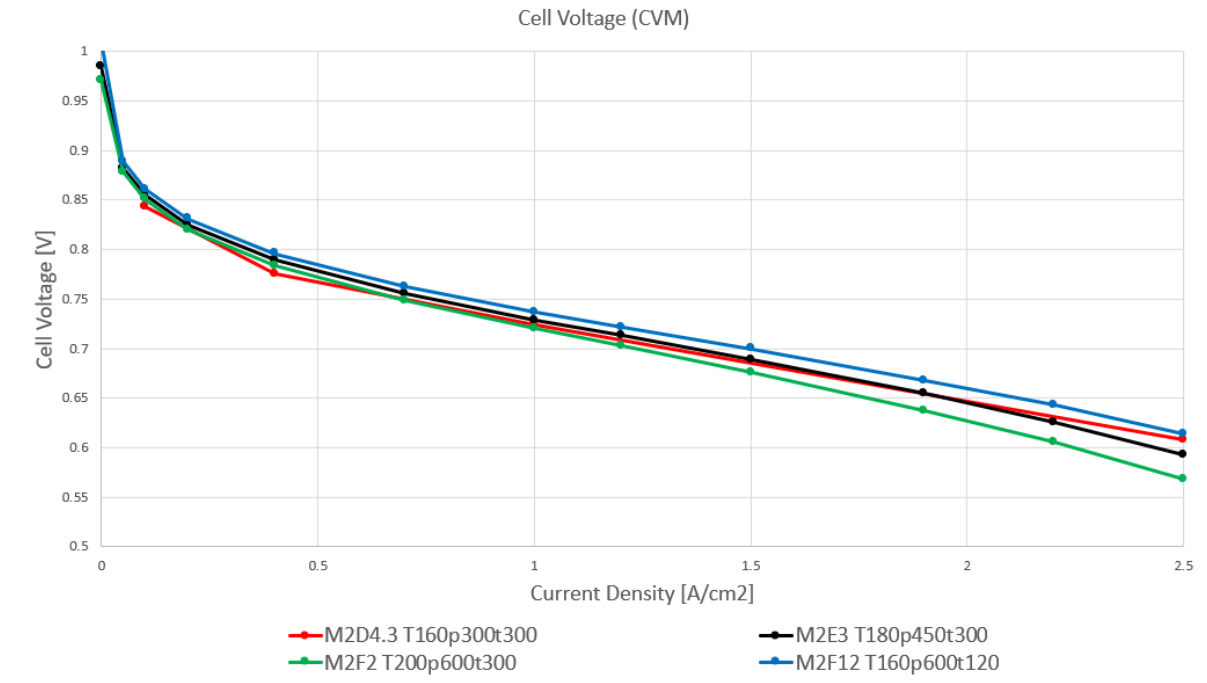

Figure 54: polarization curves of the best performing MEAs in the parameter spacing test.

The M2F12 and M2D4 operating points (red and blue) are the only points in the parameter spacing which show a full load point above 600 mV, while the M2F4 point (green) is only below this value due to a low kinetic performance which suggests a low catalyst utilization. The M2E3 point also shows quite good behavior, but despite a good value in the kinetic point has a full load point below 600 mV. This is an expected decrease in performance, given the previously discussed trends, but is a reasonable performance that can be used to rate different materials. Low catalyst utilization in M2F4 is a significant concern. However, the ohmic and mass transport behavior is very good, and this curve also reaches a comparable full load potential if it is normalized in the kinetic point. This indicates again that the temperature should not be above 160 °C, and further shows that both low and high pressure and low and high transfer time can be used to achieve good results. Unfortunately, reliable data from M2D12 is not available to confirm whether low time and low pressure together also provide a good result.

With the trend towards lower temperatures, a closer investigation of low-temperature transfers would be useful. The chapter 6 results show that for a longer transfer time, temperatures of 140 °C can achieve full transfer. Such temperatures should be investigated more closely; while lower temperatures show an improvement in cell performance, there may be a point at which temperatures below the glass transition can still achieve good transfer without forming a well-developed interface.

In summary, the process parameter variation finds that the transfer temperature should be near the glass transition, but not increased beyond it, in order to provide a good transfer result and performance. The pressure has a minimum value affected by the transfer temperature and time, but increasing the pressure beyond this does not seem to have a major effect on the performance. Both time levels have likewise given results with good performance. However, at the lower time level the set temperature is only barely reached. This suggests that the higher time level is over dimensioned. It may be prudent to investigate an intermediate time such as 180 s in order to ensure consistent and stable results.

7.5 Varying Materials: Results and Discussion

Figure 55 shows the conditioning curves for the MEA material variation. As described in chapter 7.1, these MEAs are all produced at operating point E3 (T = 180 °C, p = 450 N/cm^2, t = 300 s) with different materials. M2, M3, M4 and M5 use Supplier A anode and cathode material with membranes A, B, C and D respectively. M4E3_15mu has the same materials as M4 but uses a 15 micron version of membrane C instead of the 12 micron version. M6 uses membrane A and a Supplier A anode, but the in-house produced cathode 1.

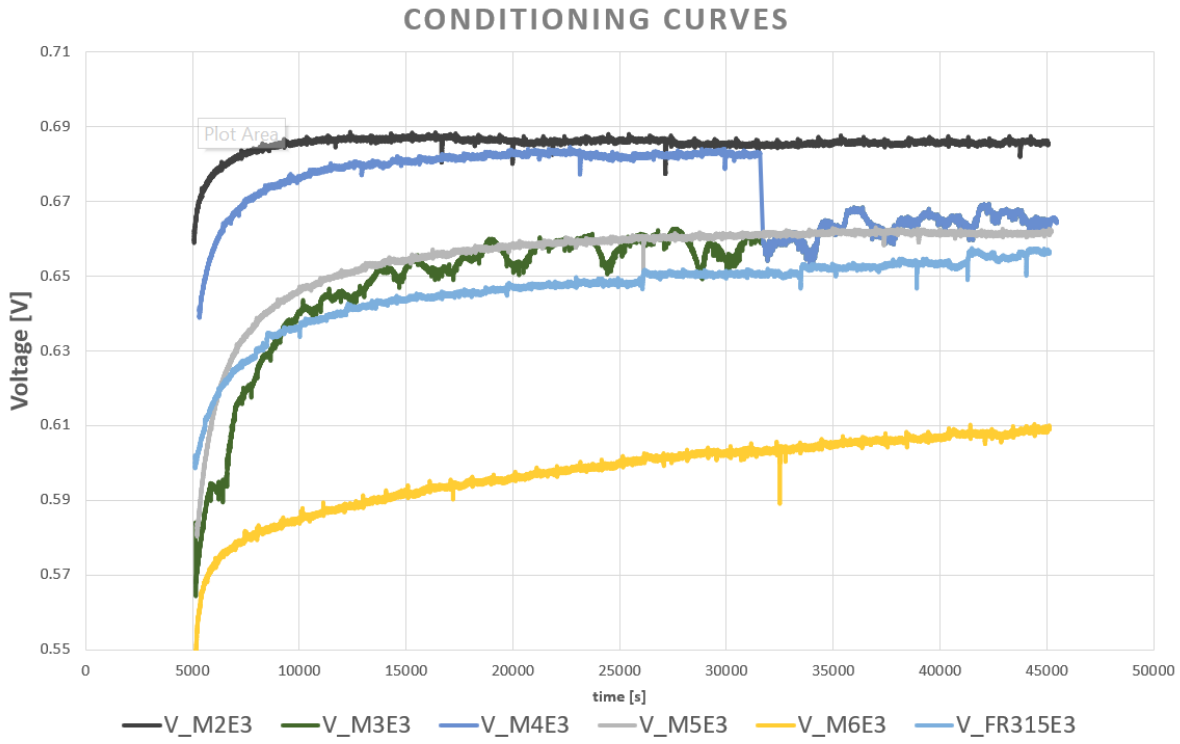

Figure 55: Conditioning curves for the material variation experiment.

Two MEAs stand out in the conditioning; M3E3, which shows high fluctuations in the voltage value but does not decrease, and M4E3, which initially looks stable but then drops and fluctuates significantly. M3E3 is likely fine; M4E3's behavior should be considered for the later analysis.

Figure 56 shows the EIS resistance and HFR for the MEAs.

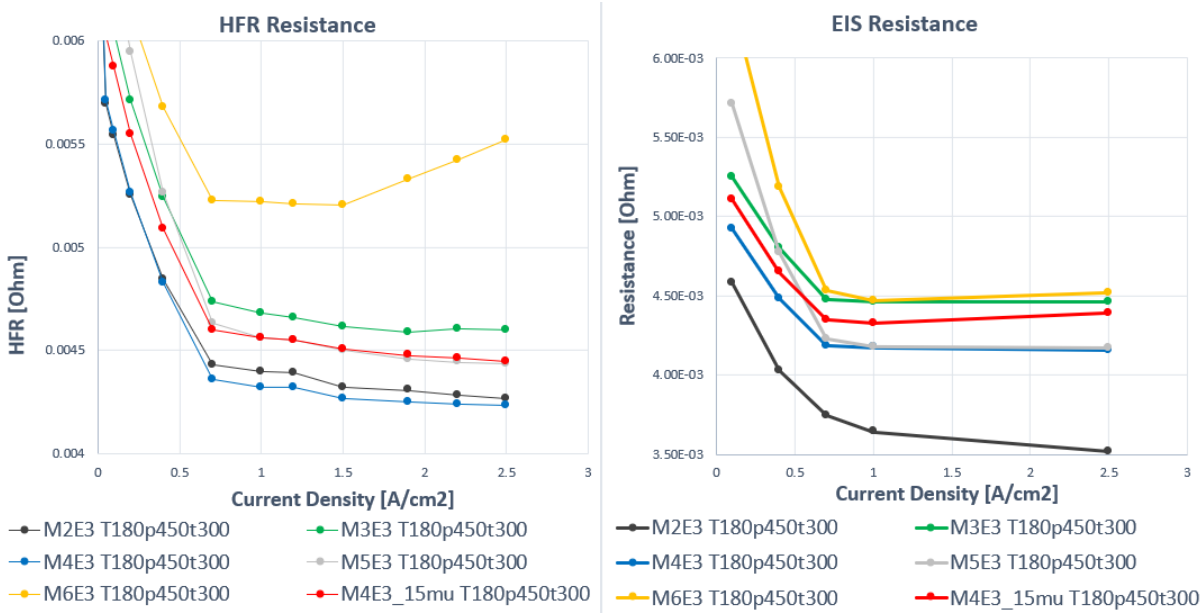

Figure 56: HFR and EIS resistance for the material variation.

The order of the resistance in the ohmic region remains roughly constant between EIS and HFR. Comparing this to Figure 56 shows that the order of the resistances corresponds to the order of the slopes in the ohmic region of the polarization curve, as is expected. Note that the HFR values are recorded at the same time as the polarization curve and correspond to the ohmic-region slopes more closely. This is most clearly observed in the black and yellow lines. The difference is due to the EIS measurement being affected by the test history of the MEA.

Figure 57 shows the polarization curve for the material variation, Figure 58 shows the polarization curve normalized to the kinetic point (0.1 A/cm^2).

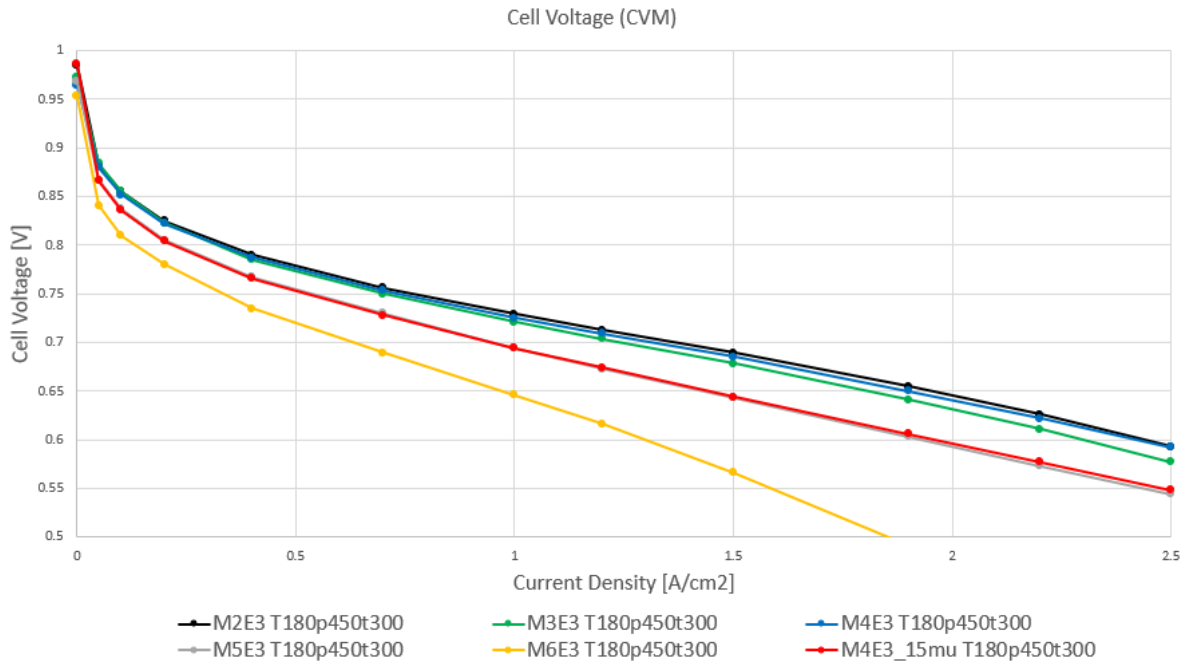

Figure 57: Polarization curves for the material variation experiment.

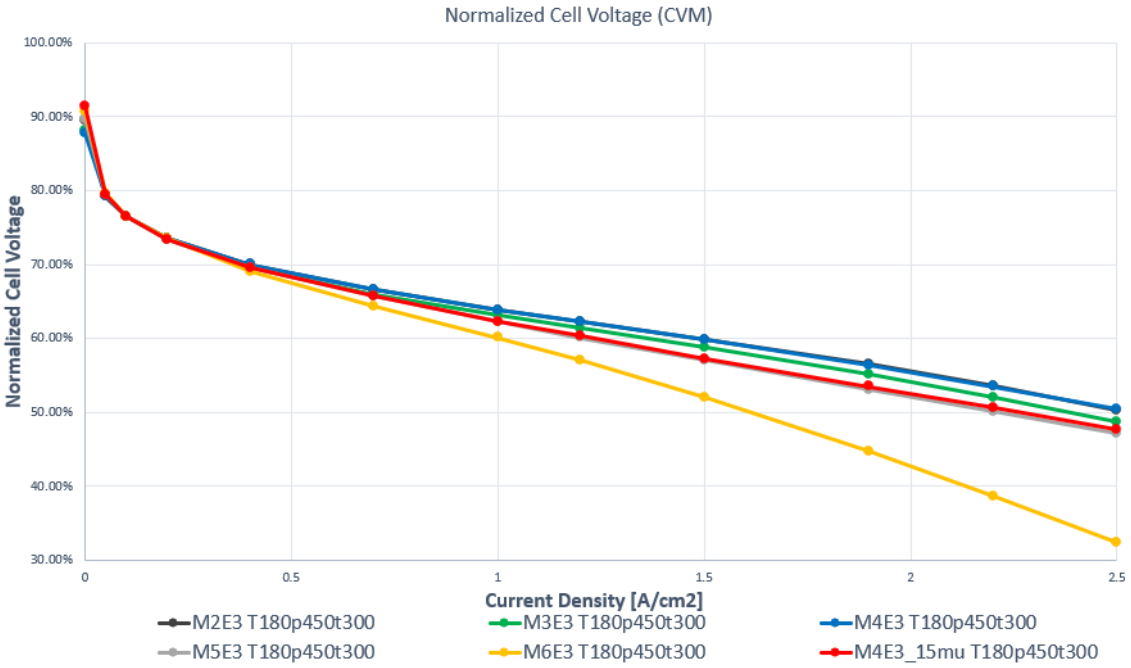

Figure 58: Normalized polarization curves for the material variation experiment.

M2, M3 and M4, which use supplier A anode and cathode with different PFSA membranes (A, B and C respectively) show very similar polarization curves. In the kinetic region, the behavior is nearly identical, which is expected as this region is defined by the cathode rather than the membranes. In the ohmic region where the membranes dominate, the curves remain similar, although M3 (membrane B) has a steeper gradient than M2 (membrane A) and M4 (membrane C) and a slight divergence in the mass transport region. This is explicable from the membrane thicknesses and side chain lengths, as membrane B has a thickness of 15 microns compared to 12 microns for membranes A and C (see chapter 2.5.1) and has long side chains while membranes A and B have medium and short side chain lengths respectively. Short side chain PFSA ionomers have higher proton conductivities compared to long side chain ionomers because the density of ionic groups relative to the molecular weight is higher.

The results for M5E3, which uses the hydrocarbon-based proton exchange membrane D, show slightly worse ohmic and mass transport properties compared to the PFSA membranes but is overall quite comparable. This is particularly evident in the normalized polarization curve. Given how new HC PEMs are compared to PFSA membranes, the fact that this membrane is comparable to conventional PFSA membranes is a very promising result for the technology and shows that HC PEMs are now a serious contender in the proton exchange membrane market. Continuing to monitor the development and testing the performance of new HC PEMs as they come to market may then be crucial to improving the performance of fuel cells. It would also be interesting to investigate the interactions of HC PEMs with PFSA ionomers in the electrodes, as this may cause interface resistances that may contribute to the ohmic behavior seen here.

The 15 micron version of membrane C (M4E3_15mu) shows significantly worse performance compared to the other PFSA membranes. This is particularly clear in the kinetic point, despite the high OCV, which shows a very low catalyst utilization. The ohmic behavior is also worse than membrane B, which is unexpected because membrane B has long side chains and the same thickness while membrane C is a short side chain ionomer that is more conductive. Comparing this result to its 12

micron sister membrane, M4E3, also shows a poor result. This result is unexpected and should be statistically validated for confirmation.

In conclusion, material variation has shown expected results for the three main PFSA membranes, except for the 15 micron version of membrane C which requires confirmation. The hydrocarbon-based membrane D showed a marginally worse performance compared to the PFSA membranes, but is overall comparable in performance, which shows a rapid maturing of this technology. The in-house cathode results were less impressive, showing a low maturity which is particularly evident in the kinetic point.

The yellow M6E3 curve, using membrane A and the in-house produced cathode 1, performed significantly worse than all other MEAs in the kinetic, ohmic and mass transport regions. This is especially evident when compared to the black M2E3 curve, which uses the same membrane such that only the cathode is different. This electrode has a very low performance and requires significant improvement. The low kinetic point in particular shows a very low catalyst utilization. In chapter 7.6, a further study of in-house electrodes is conducted.

7.6 In-house Electrodes: Results and Discussion

A further study is conducted using in-house electrodes with varying dispersion energies applied to the ink used for the cathode following the thesis work of E. Ulberstad [9]. The same anode, anode 1, is used for each MEA and the cathode is varied between cathode 2 (blue, with a total dispersion energy of 200 kWs), cathode 3 (green, with a total dispersion energy of 50 kWs) and cathode 4 (red, with a total dispersion energy of 10 kWs). The electrodes are described in further detail in chapter 2.5.2.1.

The MEAs were produced at operating point E3, with T = 180 °C, p = 450 N/cm^2 and t = 300 s using membrane A. No EIS data was gathered for these MEAs. Multiple polarization curves with different operating conditions were recorded. However, in this thesis only the polarization curves under normal operating conditions (see chapter 2.4.3) are considered. Each MEA has two such polarization curves. The tests were conducted in a 25 cm^2 subscale test setup under anode/cathode stoichiometric excess of 3.0/3.6, which is different from the test setup (chapter 2.4.3) used for all other MEAs in this thesis.

The conditioning curves for the three in-house MEAs are shown in Figure 59 alongside a supplier electrode reference in black.

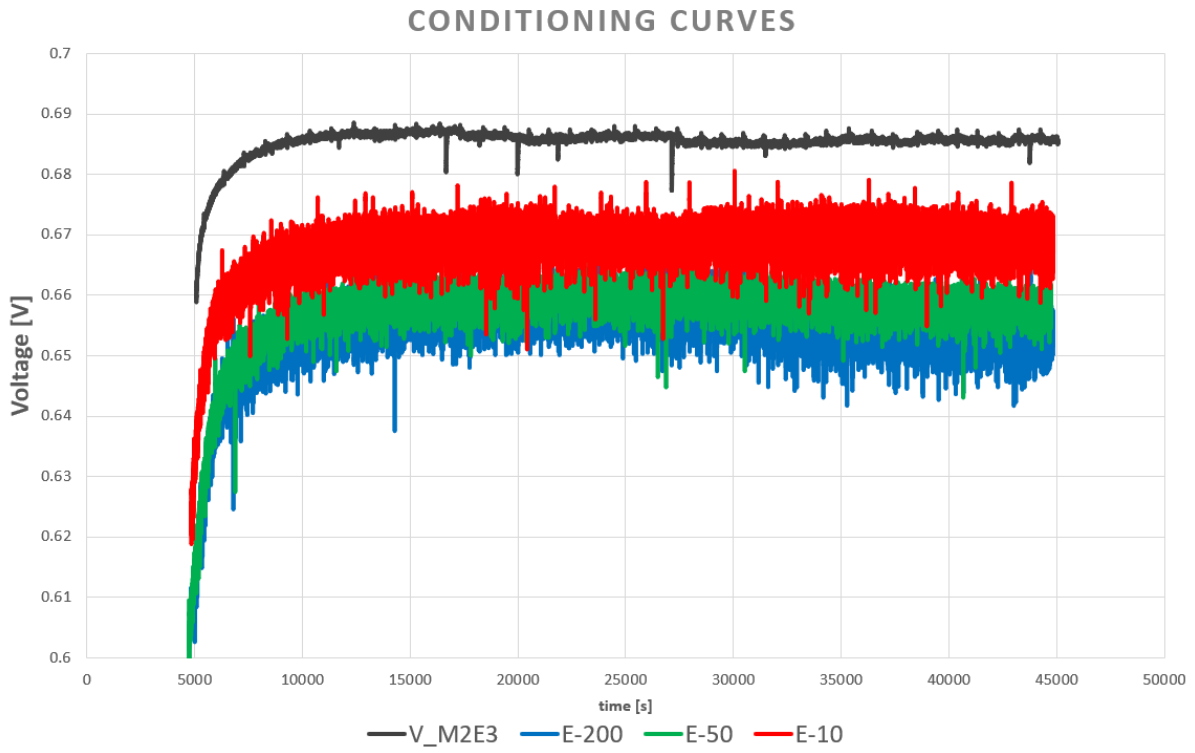

Figure 59: Conditioning curves for the in-house electrode MEAs with 10, 50 and 200 kWs dispersion energy input.

This curve shows a large amount of noise for all the in-house electrode MEAs, though it is not clear if this is an effect from the electrodes or the testing setup. A moving average method can be used to remove the noise. This is shown in Figure 60.

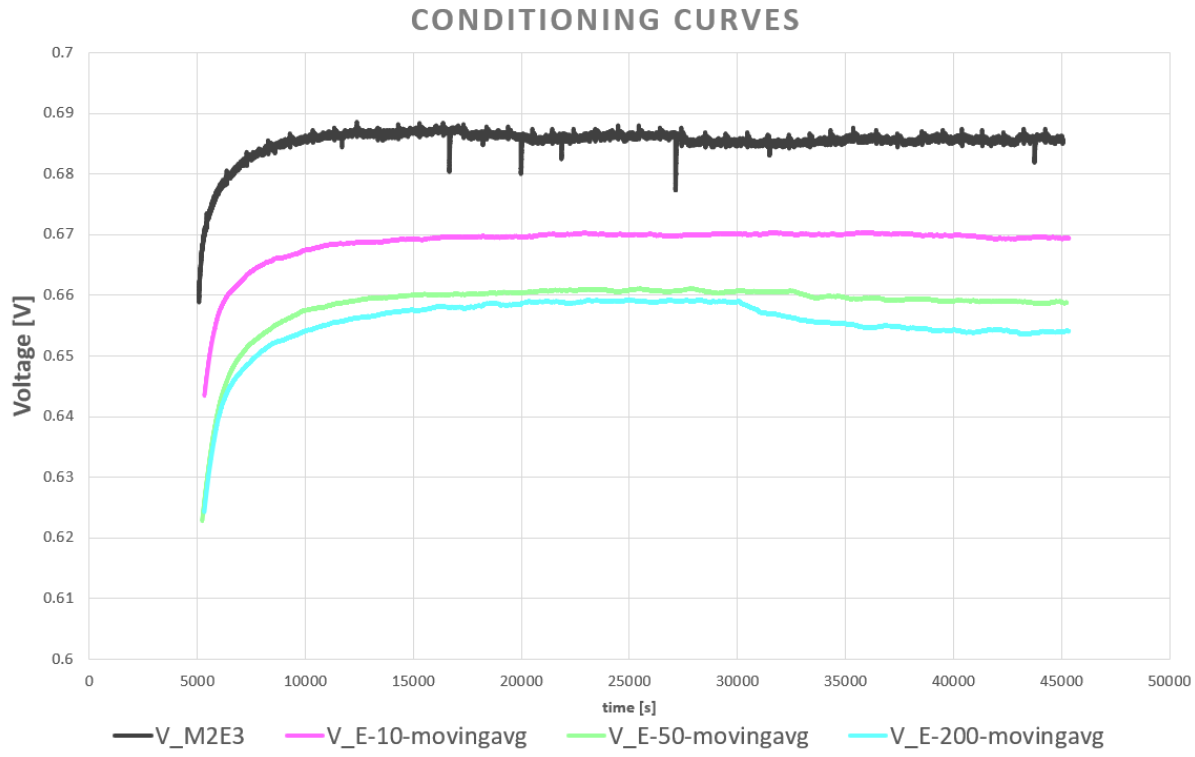

Figure 60: Conditioning curves for the in-house electrode MEAs with the noise removed.

All the curves have a comparable initial increase rate, which shows a comparable water uptake behavior for each of the electrodes. Each of the MEAs quickly reaches a stable level. However, the 200 kWs MEA sees a drop down before restabilizing. This is concerning, but the restabilization allows the data to still be used.

Figure 61 shows the HFR curves for the in-house electrode MEAs. The supplier electrode reference is again included in black.

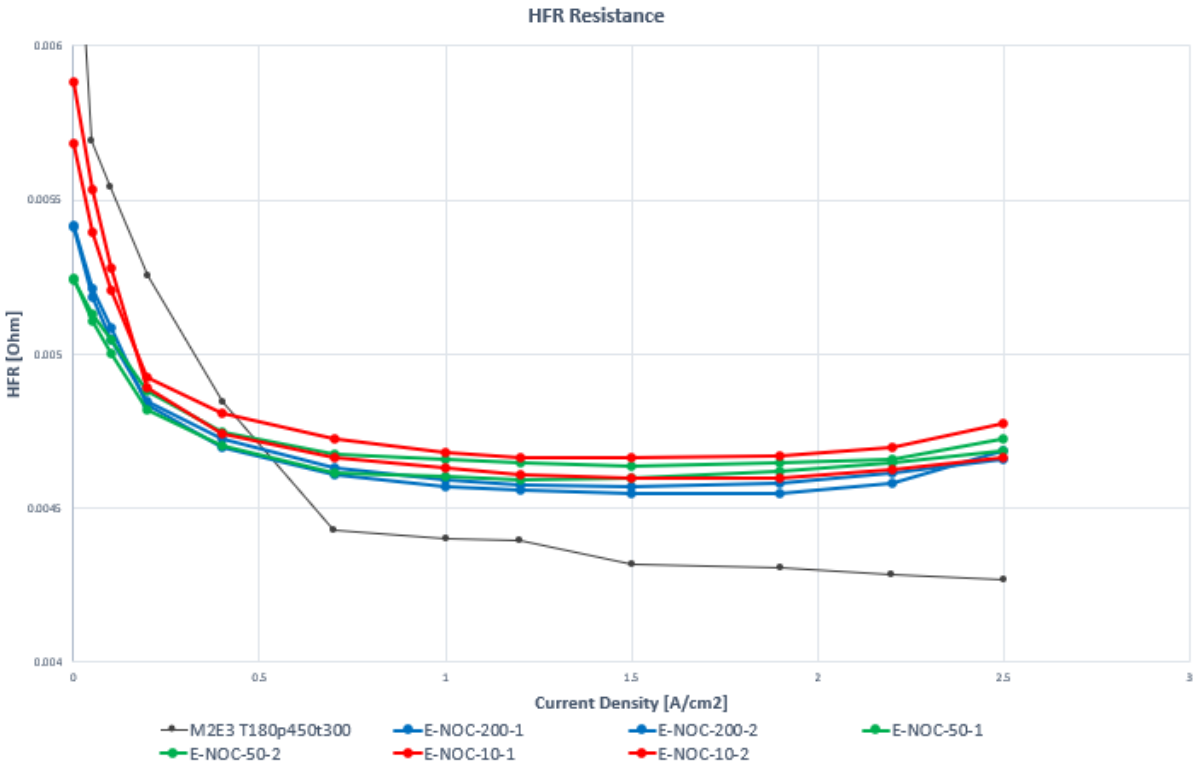

Figure 61: HFR curves for the in-house electrode MEAs.

All the MEAs reach a stable resistance, that is higher than the reference, while also showing very coherent, similar values and trends. There is an indication of a trend of increased resistance with lower dispersion energy, but the data is too close for a conclusion. Of note is the increase in the resistance value at high current density observed in all the MEAs, which indicates a drying out of the anode. This suggests mass transport problems in the electrodes.

The polarization curves for the in-house electrode MEAs are shown in Figure 62.

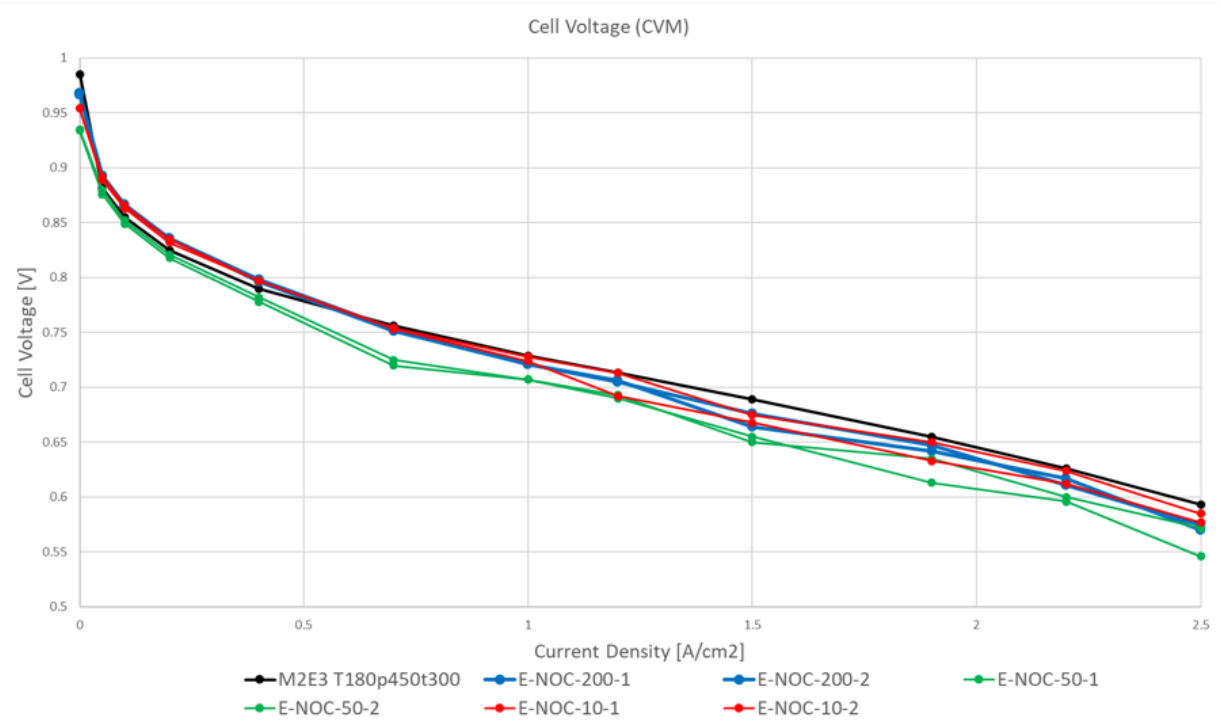

Figure 62: Polarization curves for the in-house electrode MEAs.

These polarization curves show a significant amount of noise compared to the reference, which is either due to a low electrode maturity or fluctuations in the testing conditions. The 50 kWs dispersed MEA performs comparably to the reference electrode in the kinetic point, while the 10 and 20 kWs MEAs perform better. This is very promising for catalyst utilization; however, it does not show an improving trend with increased dispersion as expected. This may be due to a variety of factors, including the relatively high amount of catalyst used in the electrodes, changes to electrode morphology as described in the 'annealing' change (chapter 5), and the high level of noise observed in the polarization curves.

In order to better observe the ohmic and mass transport regions, the polarization curve is normalized in the kinetic point (Figure 63).

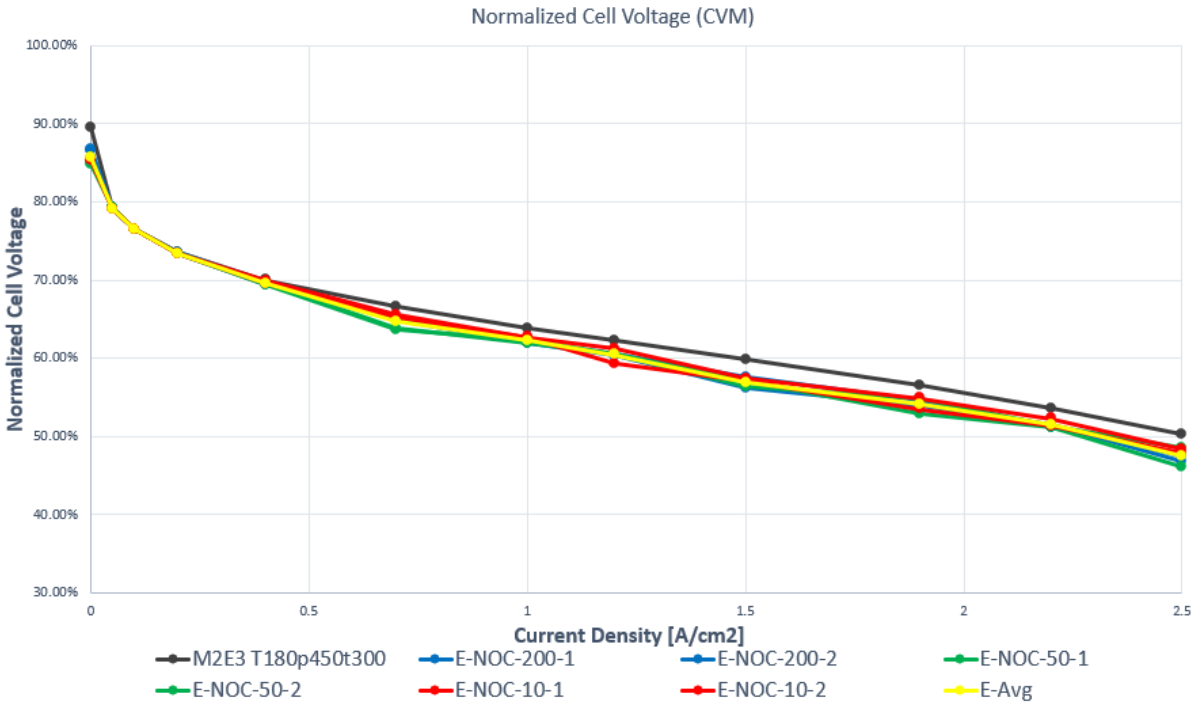

Figure 63: Normalized polarization curves for the in-house electrode MEAs.

The normalized polarization curve shows little difference in the ohmic region between the three different dispersion levels of the MEA cathodes. Such differences seem to be smaller than the noise in the polarization curve. What is clear is that the ohmic slope of the in-house electrode MEAs is steeper than the reference, i.e., the ohmic performance is worse. This performance is expected from the higher HFR resistance values of the in-house electrode MEAs.

Overall, in-house electrode production can produce functional electrodes, but significant refinement is still needed to improve performance and reliability.

8 Conclusion

In this thesis, the available set of transfer parameters was established for several materials and performance trends within those dimensions was explored. The decal transfer setup was refined, and a better understanding of the internal pressure distribution and temperature profile of the was reached, which is vital knowledge for understanding the transfer and performance behavior of the MEAs. A proof of concept was made for a series stacking approach to increase MEA production volume, with successful results. Initial observations of the glass transition temperature were, which are vital to understanding the effects of the transfer temperature on the MEA performance. While many questions remain, these experiments can serve as the foundation for further inquiries.

The analysis of transfer quality and the analysis of performance for MEAs with different processing parameters have shown that temperature has the greatest impact on MEA performance, with a required lower bound for a successful transfer which seems to be related to the glass transition temperature and diminishing performance at higher transfer temperatures. The transfer pressure also seems to have a temperature-dependent lower bound, but higher pressures in the analyzed range seem to have little impact on performance compared to the temperature. Because the higher time level is shown to be over dimensioned since high performances have been reached at both time levels, it may be prudent to investigate an intermediate time such as 180 s in order to ensure consistent and stable results. A significant achievement for further work is the establishment of a method for reliably obtaining a full transfer of the MEA in the decal transfer process.

The material variation has shown that the in-house catalyst production still requires improvement, and that hydrocarbon PEMs are approaching the performance levels of PFSA membranes. The performance of the PFSA membranes A, B and C also followed expectations, except for the 15 micron version of membrane C which showed unusual results in need of statistical verification.

Hopefully, this thesis has provided insight into many factors affecting the decal transfer process, particularly the effects of the processing conditions, and can serve as a foundation to continue improving MEAs and fuel cells in service to a clean energy future.

9 Outlook

The work in this thesis should serve as a foundation to unlock more research and answer more questions so that MEAs and fuel cells can continue to develop and improve. This outlook serves to discuss effects seen in the thesis and how they might be investigated further, and to discuss other ideas that could not be investigated in this study.

The annealing behavior of electrodes, described in chapter 5, is not well understood and may be crucial for the electrode preparation and quality. The observed behavior indicates that it may be very important to view catalyst preparation and the decal transfer process together rather than as separate processes as the structure of the electrode seems to undergo a significant change. The introduction of a heat treatment between the catalyst drying and decal transfer processes should be investigated, and in-situ performance measurements conducted to better understand this behavior.

The results of this thesis indicate that the glass transition is a vital part of the decal transfer process. As such, the glass transition behavior of the ionomers should be much more closely investigated. Note that the phase change behavior likely involves complex interactions that differ across the MEA. Such an investigation may need to include elements of composite theory to account for interactions with the catalyst particles, which may also be connected to changes in the ECSA. It is also possible that the heating and cooling rates in the decal transfer affect the glass transition behavior and subsequent MEA performance. This possibility is supported by observations in chapter 7.3, where the performance of the MEA differs during the series stack test, as the central MEAs see a higher heat transfer resistance and subsequently lower heating and cooling rates.

The interactions of different types of ionomers may be worth investigating, particularly the interaction between PFSA ionomers and hydrocarbon based ionomers. Of particular interest is whether the interface resistance changes when different types of ionomers are used in the electrodes and membranes. Literature shows that hydrocarbon based ionomers are rapidly approaching the performance levels of PFSA ionomers [11], which the results in chapter 7.5 corroborate. Understanding the behavior of HC ionomers in general and in conjunction with established PFSA ionomers will likely be even more critical as these technologies develop.

The results in chapters 4.4 and 7.3 show that the series stacking approach is a viable concept, which has major implications for a final commercial MEA production procedure. While a roll-to-roll process is typically seen as a ‘holy grail’ for such production, a more refined series stacking method could allow for sufficient capacity in a ‘batch’ method to support commercial production. Such a batch method would require significant further development, however.

While many questions remain around the decal transfer process, this thesis has established a method and transfer parameter set for reliably achieving a good transfer result with a variety of different materials. If high-performance in-house electrode production can be achieved, PowerCell might be able to begin moving towards full scale stack testing with in-house produced MEAs, which would be a significant milestone and allow for the early testing of in-house MEAs in a near-commercial environment. This sort of prototype testing could then provide valuable feedback regarding the requirements for both electrode and MEA research.

Some ideas could not be investigated in this thesis due to constraints on time and materials. The type of decal substrate used in the transfer has a major impact on the transfer, which was not investigated in this thesis. The same type of decal substrate (glass fiber reinforced PTFE) was used in every test.

There are many ways in which the decal substrate can affect the transfer behavior. The surface and adhesion properties of the decal substrate affect the coating and should also affect the 'release force' for removing the decal substrate after transfer, which may impact the transfer space and quality of the MEA. This could be investigated using the water surface contact angle and the adhesion force of different decal substrates. The contour of the decal surface may also be relevant. The glass fibers in the decal substrate used in this thesis introduce a 3-dimensional surface to the electrode and MEA, and residual electrode can remain stuck in the valleys of the decal. This does not appear to significantly affect the pressure distribution, however. A rigorous comparison to other, flat decal substrates may be useful. The physical properties of the decal substrate may also be interesting to investigate but are unlikely to have a significant effect relative to the employed transfer pressures. Considering rigid crystalline decal substrates such as highly polished silicon could be interesting but challenging to implement due to the brittleness of such materials.

In this thesis, all performance tests were conducted under normal operating conditions (see chapter 2.4.3). Previous work at PowerCell has explored other testing conditions at higher and lower humidity, but these have not been comprehensively studied at different operating points [4]. As the operating conditions significantly impact the hydration state of the MEA, running such experiments would be particularly useful for comparing different membranes.

Besides the glass transition, the thermal degradation of the ionomers could be a relevant quantity to investigate. For this, thermogravimetric measurements may be useful. It is also possible that temperatures are reached that are not sufficient to cause degradation but are sufficient to change the polymer cross linking structure. This would require mechanical testing to verify.

The effects of testing history and the behavior over time of the MEAs performance were not investigated in this thesis, however the difference between EIS and HFR measurements indicate that they are significant. Understanding these effects would contribute to understanding the behavior over time and enable a better understanding of the differences between different results, especially in the recorded resistances.

The compression force of the cell was not considered in this thesis but may also have some significance.

The effects of different catalyst loadings and I/Pt ratios of the cathode on the performance and transfer behavior of the MEA present a valuable target for investigation. Such an investigation could be complicated by the low maturity of the in-house electrode production. Acquiring the capability to reliably produce electrodes with a higher performance should be the priority here. Investigating the particle size distribution in the catalyst ink through methods such as FTIR may help in this regard.

Different processing parameters may influence the ECSA of the electrodes and influence agglomerates.

The current conditioning procedure occurs in-situ for over 12 hours. This is problematic as it requires every measurement to take place overnight and effectively limits the number of performance measurements that can be conducted to one per day. The purpose of the conditioning is to introduce water to the membrane, activating the proton conductivity. If the conditioning time could be reduced sufficiently or conducted ex-situ, the testing capacity could double. This could be achieved by optimizing the current conditioning protocol. Most MEAs reach stable conditioning in less than 3 hours, showing that in most cases the current protocol is vastly over-dimensioned. Another method would be to conduct a portion of the conditioning ex-situ, by exposing the MEA to water prior to testing. This has been demonstrated using pressurized steam [12], as well as water at various

temperatures. Investigating a pre-conditioning protocol would require further insights into the Schröder paradox as it applies to ionomer water uptake in liquid and gas forms [13]. Such a procedure would be immensely useful for PowerCell.

A novel method of improving MEA performance is to engineer the interface between electrode and membrane. This can be achieved by adding a micro structured pattern to the membrane or electrode, introducing an increased concentration of ionomer in the catalyst near the membrane (ionomer gradient), introducing a gradient in the catalyst loading, engineering the porosity of the membrane, using hydrophilic additives to help engineer hydration levels in the MEA, and through ionomer infiltration from the membrane into the catalyst layer [14] [15] [16]. Such methods should not be a priority at PowerCell, however, until in-house electrodes with good performance can be made consistently.

Bibliography

[1] IPCC, "Synthesis Report of the IPCC Sixth Assessment Report (Summary for Policymakers)," IPCC, 2022.

[2] K. Jack, "How much do we know about the development impacts of energy infrastructure?," 29 Mwarch 2022. [Online]. Available: https://blogs.worldbank.org/energy/how-much-do-we-know-about-development-impacts-energy-infrastructure#:~:text=Energy%20infrastructure%20may%20contribute%20to,may%20constrain%20output%20when%20unavailable..

[3] J. Vernes, The Mysterious Island, Pierre-Jules Hetzel, 1874.

[4] S. A. OGU-EGEGE, "Fuel Cell Membrane Electrode Assembly - Fabrication and Characterization," *Politecnico di Torino,* 2022.

[5] SpecialChem SA, "Glass Transition Temperature," 10 May 2023. [Online]. Available: https://omnexus.specialchem.com/polymer-properties/properties/glass-transition-temperature#:~:text=The%20Tg%20for%20most%20synthetic%20polymers%20lies%20between%20170K%20to%20500K..

[6] Cadence Design Systems, Inc., "Understanding Resistor Behavior at High Frequencies," 08 May 2023. [Online]. Available: https://resources.system-analysis.cadence.com/blog/msa2021-understanding-resistor-behavior-at-high-frequencies.

[7] L. H. W. W. X. G. J. C. S. L. L. B. K. Tong Lin, "Prediction of high frequency resistance in polymer electrolyte membrane fuel cells using long short term memory based model," *Energy and AI,* 2021.

[8] Gamry Instruments, "Basics of Electrochemical Impedance Spectroscopy," 8 May 2023. [Online]. Available: https://www.gamry.com/application-notes/EIS/basics-of-electrochemical-impedance-spectroscopy/.

[9] E. Ulberstad, "Investigation on effect of dispersion methodology on PEMFC catalyst ink and resulting electrode structure," Chalmers University of Technology, Gothenburg, 2023.

[10] X. P. G. X. L. &. W. J. Liang, "A modified decal method for preparing the membrane electrode assembly of proton exchange membrane fuel cells.," *Fuel,* 2015.

[11] H. K. C. M. L. V. S. &. B. M. Nguyen, "Fully hydrocarbon membrane electrode assemblies for proton exchange membrane fuel cells and electrolyzers: An engineering perspective," *Advanced Energy Materials,* 2022.

[12] B. P. Anderson.USA Patent US 20060105214A1, 2006.

[13] Y. C. W.-Q. T. Lei Chen, "Schroeder's paradox in proton exchange membrane fuel cells: A review," *Renewable and Sustainable Energy Reviews,* 2023.

[14] M. K. M. V. S. Z. R. &. T. S. Breitwieser, "Tailoring the Membrane-Electrode Interface in PEM," *Advanced Energy Materials,* 2017.

[15] Y. Q. D. Y. P. P. L. &. L. X. Wan, "Design and optimization of gradient wettability pore structure of adaptive PEM fuel cell cathode catalyst layer," *Applied Energy,* 2022.

[16] Y. C. G. F. R. &. C. T. Xu, "Effects of various operating conditions and optimal ionomer-gradient distribution on temperature-driven water transport in cathode catalyst layer of PEMFC," *Chemical Engineering Journal,* 2023.

[17] Y.-K. T. Z. F. C.-C. L. S.-C. C. J.-M. L. R.-S. &. H. S.-F. Liao, "Extensively reducing interfacial resistance by the ultrathin Pt layer between the garnet-type solid-state electrolyte and Li-metal anode," *ACS Applied Materials & Interfaces,* 2021.

[18] B. S. &. K. Y. S. Pivovar, "The membrane–electrode interface in PEFCs," *Journal of the Electrochemical Society,* 2007.

[19] D. P. L. Y. P. L. W. &. L. X. Qiu, "Review on proton exchange membrane fuel cell stack assembly: Quality evaluation, assembly method, contact behavior and process design," *Renewable and Sustainable Energy Reviews,* 2021.

[20] M. S. R. D. N. &. S. A. Secanell, "Optimization of a proton exchange membrane fuel cell membrane electrode assembly," *Journal of the International Society for Structural and Multidisciplinary Optimization,* 2010.

[21] F. Q. X. C. J. &. W. H. Tan, "Effects of coupling agents on the properties of epoxy-based electrically conductive adhesives," *International Journal of Adhesion & Adhesives,* 2006.

[22] M. B. M. Z. R. &. T. S. Klingele, "Direct deposition of proton exchange membranes enabling high performance hydrogen fuel cells," *Journal of Materials Chemistry,* 2015.

[23] S. M. J. R. P. S. P. M. U. S. M. Min Wang, "Impact of Microporous Layer Roughness on Gas-Diffusion-," *ACS Appl. Energy Mater.,* 2019.

DEPARTMENT OF PHYSICS
CHALMERS UNIVERSITY OF TECHNOLOGY
Gothenburg, Sweden 2023

CHALMERS
UNIVERSITY OF TECHNOLOGY